Gabriel G. Vianna

Use of high-resolution satellite data to infer marsh zonation in rewilded salt marshes

2024

Gabriel G. Vianna

Use of high-resolution satellite data to infer marsh zonation in rewilded salt marshes

Master of Marine and Coastal Systems (MaCS)

Work performed under the supervision of: A. Rita Carrasco (CIMA/ARNET, University of Algarve) & Sónia Cristina (CIMA/ ARNET, University of Algarve)

2024

Declaração de autoria de trabalho

Declaration of authorship of work

Use of high-resolution satellite data to infer marsh zonation in rewilded salt marshes.

Declaro ser o(a) autor(a) deste trabalho, que é original e inédito. Autores e trabalhos consultados estão devidamente citados no texto e constam da listagem de referências incluída.

I declare I am the author of this work, which is original and unpublished. The sources consulted have been duly cited in the text and included in the list of references.

Copyright on behalf of Gabriel G. Vianna, and the University of Algarve

The University of Algarve reserves the right to, in accordance with the provisions of the Copyright Law and Code, archive, reproduce, and publish this work in any medium, as well as to disseminate this work through academic repositories and allow it to be copied and distributed for educational, research, and non-commercial purposes, while ensuring credit is given to the work's author and publisher.

Acknowledgements

I want to thank my supervisors, Ana Rita Carrasco and Sónia Cristina, for their patience and guidance while working on this thesis. Thank you, Planet®, for providing the images. I also appreciate all the volunteers in the fieldwork campaigns for taking the time to help with this work. Thank you, Professor Gustavo Baptista, from the University of Brasília (UNB), for helping me use the SuperDove imagery in the SNAP software. Thank you to my home family for always being supportive, even without being by my side. Lastly, I want to thank my girlfriend Nathalia Almeida for her support throughout this work.

Table of contents

List of Figures

List of Tables

List of Appendix

List of acronyms

d_{50}: Median diameter

EM: Expected maximisation

H_2O%: Water content

KD-KNN: KDtree K-nearest neighbours

KNN: K-nearest neighbours

LOI: Loss on Ignition

MD: Minimum distance

ML: Maximum likelihood

NIR: Near infra-red

OM: Organic matter

RF: Random Forest

RF-AC-EA: Random Forest classifications with a composite of data from all seasons, using the entire area of the salt marsh

RF-AC-PA: Random Forest classifications with a composite of data from all seasons, using the area close to the plots

RF-EA: Random Forest classifications of the entire areas of the salt marsh

RF-PA: Random Forest classifications of the plot areas

RMSE: Root mean squared error

ROI: Region of interest

Sumário

Os sapais são ecossistemas costeiros caracterizados pela vegetação tolerante a salinidade elevada. Estes ecossistemas prestam importantes serviços ecossistémicos, como a proteção costeira, a captura de carbono e o apoio à biodiversidade. No entanto, estes habitats estão ameaçados globalmente devido a atividades humanas e ao aumento do nível do mar. Os governos iniciaram esforços para restaurar ou renaturalizar os sapais. A renaturalização difere da restauração tradicional, pois permite que os processos naturais regenerem os ecossistemas com uma intervenção humana mínima. A renaturalização é normalmente feita através da remoção de diques ou da reintrodução de fluxos naturais de água.

Os métodos tradicionais de monitorização da vegetação, tais como levantamentos de campo, são frequentemente trabalhosos, demorados e limitados em extensão espacial. A deteção remota por satélite oferece uma alternativa poderosa para análise e gestão de áreas vegetadas, permitindo a aquisição de dados em grande escala, repetíveis e consistentes. Esta tese tem como objetivo utilizar imagens de satélite de alta resolução para estudar as variações sazonais e a zonação das plantas em dois sapais renaturalizados na zona lagunar da Ria Formosa, costa sul de Portugal. Foram aplicados diversos métodos de classificação supervisionados e não supervisionados, além de assinaturas espectrais para identificar as técnicas mais eficazes na análise destes ecossistemas e nas suas dinâmicas.

O estudo focou-se em duas áreas de interesse na Ria Formosa, na costa sul de Portugal, que foram anteriormente utilizadas para aquacultura, posteriormente renaturalizados após o rompimento de diques em Bias (2011) e Olhão (2017). Campanhas de campo foram desenvolvidas para recolher dados em vários setores sobre a vegetação ao longo das quatro estações do ano e sobre as características do sedimento (como o teor de matéria orgânica, tamanho dos grãos e conteúdo de água) ao longo da zonação dos sapais. Os setores foram distribuídos por toda a zonação do sapal, abrangendo o sapal alto, médio e baixo. Além dos setores, áreas cobertas por apenas uma espécie de planta (manchas) também foram analisadas.

Imagens de alta resolução da constelação de satélites SuperDove (3m) foram usadas para analisar os dois sapais renaturalizados. Vários tipos de classificação de imagem foram utilizados, incluindo métodos de classificação supervisionada (Random

Forest, K-nearest neighbours, KD-tree K-nearest neighbours, Maximum likelihood, e Minimum distance) e de classificação não supervisionada (Expected maximization Cluster e K-means cluster). O objetivo principal das classificações de imagem é encontrar o(s) método(s) de classificação de imagem com melhor desempenho na identificação de espécies vegetais, visando a analise da zonação das plantas nos sapais e variações sazonais. Além das classificações de imagem, foram adquiridas assinaturas espectrais de várias áreas dos sapais renaturalizados, juntamente com a percentagem da cobertura das diferentes espécies de plantas dentro da área analisada e amostras de sedimento. Essa análise visava descobrir a influência da mistura das espécies de plantas e das características do sedimento (como o teor de matéria orgânica, o tamanho dos grãos e o conteúdo de água) na assinatura espectral.

Este estudo atingiu com sucesso o seu objetivo de identificar a classificação mais eficaz para analisar variações sazonais e de zonação em sapais renaturalizados, com o Random Forest emergindo como a classificação com melhor desempenho. As metodologias de classificação mais eficazes foram baseadas no Random Forest aplicadas à área total dos sapais (RF-EA e RF-AC-EA). A classificação RF-EA mostrou melhor desempenho para análises sazonais, enquanto RF-AC-EA destacou-se como a mais adequada para análises da zonação das plantas de sapal. Porém, este trabalho não conseguiu encontrar uma ligação precisa entre as variações na mistura de espécies vegetais e as variações na forma da assinatura espectral, apenas encontrando a sua influência geral. A influência do tamanho dos grãos e o conteúdo de água foi observada na assinatura espectral, principalmente nas variações ao longo da zonação das dos sapais. Observou-se que as áreas com maior conteúdo em areia terão assinaturas espectrais com valores de refletância maiores, principalmente nas bandas próximas do infravermelho.

Sendo a primeira vez que as imagens de satélite SuperDove foram utilizadas em sapais renaturalizados, as metodologias empregues neste estudo revelaram-se eficazes para análise e potencial monitorização destes ecossistemas. Elas apresentam várias vantagens em comparação com outros métodos, tais como extensas campanhas de trabalho de campo. Primeiro, as classificações de imagens obtidas pelo Random Forest permitiram realizar uma análise sazonal ao longo de um ano com menos de 15 campanhas de campo. A redução do número de campanhas de campo resulta numa diminuição significativa dos custos em programas de monitorização, além de libertar tempo para a análise dos dados. Além disso, o presente estudo mostrou que usando imagens de satélite

multiespectrais do SuperDove, a classificação de imagens supervisionadas denotou resultados satisfatórios com alta precisão (acima de 50%) e diminuição dos erros.

As limitações do estudo incluíram a necessidade de um trabalho de campo estendendo a análise para mais de um ano, para ter uma melhor análise das variações sazonais. Além disso, seria benéfico aumentar o de número de setores por campanha de campo, aumentando o número de dados a serem usados na classificação. O uso de formas mais estáveis de capturar as fotografias do campo, como drones, aumentaria a precisão e reduziria o tempo de edição de fotos. A análise espectral também foi limitada devido à insuficiência de dados; a utilização de imagens hiperespectrais de satélite ou de radiómetros hiperespectrais de campo permitiria obter mais informações a nível espectral. Porém, esses métodos tem a desvantagem de ter um custo elevado.

A tese desempenhou um papel essencial no avanço de investigações futuras ao utilizar imagens de satélite SuperDove para identificar os métodos mais eficazes na análise de sapais renaturalizados. A alta resolução de 3m destes satélites provou ser suficiente para criar imagens de classificação altamente precisas. A análise das assinaturas espectrais de diversas misturas de espécies de plantas e as características dos sedimentos podem ser utilizadas como um primeiro passo para futuros esforços de monitorização ambiental mais detalhados e escaláveis. As abordagens deste trabalho estabeleceram as bases para estudos futuros, com o objetivo de refinar técnicas de classificação, otimizar a análise espectral e aplicar esses métodos a uma gama mais ampla de sapais renaturalizados em todo o mundo.

Palavras-chave: Sapais renaturalizados, Deteção remota, zoneamento de sapais, variações sazonais, gestão costeira, SuperDove

Abstract

Salt marshes are vital coastal habitats that provide ecosystem services such as wave and erosion protection and support economic activities like tourism and aquaculture. However, they are declining globally due to rising sea levels and human-induced degradation. To address this, governments are developing management plans for rewilding salt marshes, requiring a thorough understanding of their dynamics. With its high spatial and temporal coverage and cost-effectiveness, satellite remote sensing has become a valuable tool for analysing vegetated areas. This study employs high-resolution satellite imagery (3m) from the Planet Labs' SuperDove constellation to analyse seasonal and zonation variations of plant species in salt marshes. The goal is to identify the methods with the best skill for analysing rewilded salt marshes through remote sensing and to understand how the mixture of salt marsh plants and sediment characteristics influence the spectral signatures in these habitats. Two rewilded salt marshes in the Ria Formosa lagoon on the southern coast of Portugal were analysed, producing classification maps and extracting spectral signatures for each site across the seasons. The most effective classification method was Random Forest (RF), a supervised classification method. RF proved effective in analysing zonation and seasonal variations in both salt marshes. However, the results on the correlation between the mixture of plant species and spectral signatures were not satisfactory due to factors like plant height and age also influencing the reflectance values. The influence of the sediment characteristics, mainly water content and median diameter, was found, particularly in which zonation of the salt marshes had the highest reflectance values. A successful first step was reached by finding the most suitable method to analyse the variations in these areas. However, more in-depth studies are necessary to see the impact of the mixture of plant species on the spectral signature.

Keywords: Rewilded salt marshes, remote sensing, salt marsh zonation, seasonal variations, coastal management, SuperDove

1. Introduction and objectives

1.1. Introduction

Salt marshes are coastal vegetated ecosystems distributed worldwide in sheltered intertidal areas (Blount et al., 2022). Their main characteristic is the presence of plants with resistance to high salinities. These areas can provide many ecosystem services such as materials and food (Gu et al., 2018; Himes-Cornell et al., 2018), tourism (Gu et al., 2018; Hyland, 2002), coastal protection and erosion control (Gu et al., 2018; Shepard et al., 2011) and carbon sequestration (Alongi, 2020; Barbier et al., 2011; Duarte et al., 2005; McLeod et al., 2011). Salt marshes enclose varying vegetation zones inside of them due to the exposure to the tides (Eleuterius & Eleuterius, 1979), meaning that each zonation has different characteristics, such as having different plant species (Beeftink, 1996.; Caçador et al., 2007; Silvestri et al., 2005; Woerner & Hackney, 1997) and sediment characteristics (Contreras-Cruzado et al., 2017). Many countries understand the ecological value of these habitats and try to protect those ecosystems by creating protected areas or rewilding damaged ones; however, they first need to understand the processes occurring in them (Spencer & Harvey, 2012). The traditional methods of monitoring vegetation, such as ground-based surveys, are often labour-intensive, time-consuming, and limited in spatial extent. Satellite remote sensing provides a powerful alternative for vegetation analysis and management, as it can capture large-scale, repeatable, and consistent data (Blount et al., 2022). Even with this emerging tool and its advantages, few papers still use satellite remote sensing to analyse rewilded salt marshes.

This master thesis is a contribution to the project RestLands – Tracking ecogeomorphic changes in Restored wetlands (PLAN ID: 705677), with support from Planet (https://www.planet.com). The thesis aims to analyse two rewilded salt marshes on the south coast of Portugal using high-resolution satellite imagery from the SuperDove constellation of microsatellites from Planet. To achieve this, both supervised and unsupervised classification methods were applied to determine the technique with the best skill for visualising the seasonal and zonation variations of the rewilded salt marshes. Together with the multiple image classification methods, the spectral signature of various locations throughout the salt marshes was acquired, aiming to see the influence of the mixture of plant species in the spectral signature. In addition to the analysis of the mixture

of plants, the influence of the sediment characteristics in the spectral signature was also analysed. The main characteristics of the sediment (organic matter content, water content, and median diameter) were calculated, and their influence on the spectral signature was analysed.

1.2. Motivation for the topic

Satellite remote sensing tools are increasingly used to analyse the importance of salt marshes, including mapping their evolution and vegetation cover (Blount et al., 2022; Eastwood et al., 1997; Laengner et al., 2019; Reschke & Hüttich, 2014; Wu, 2018), and biodiversity (Guo et al., 2017; Meiman et al., 2012). These studies utilise this tool to quickly analyse large areas, which provides rapid insights into the status of the ecosystems (Blount et al., 2022). However, there is a lack of studies examining rewilded salt marshes and their variations using satellite remote sensing.

Since the SuperDove constellation is relatively new (launched in 2015), few studies use these images to study salt marshes. Similarly, few studies use multispectral satellite images to analyse the spectral signature of plant species and sediment. Since using the high-resolution satellite images from SuperDove can be valuable for analysing vegetated areas, testing the best methods for analysing rewilded salt marshes with them is essential.

1.3. Objectives

The primary goal of this project is to compare different classification methods/algorithms to determine the most effective approach for studying the seasonal variations and zonation of plant species in two rewilded salt marshes. The secondary objective is to examine how the combination of plant species and sediment characteristics affects the spectral signature of different salt marsh areas and identify any potential patterns. Lastly, this project aims to be one of the first steps for analysing these rewilded ecosystems using satellite remote sensing from Planet, aiming to improve these methodologies for management purposes, enabling quicker and more cost-effective analyses of these areas.

2. Review of the state of the art

2.1. Natural salt marsh

Salt marshes are distributed worldwide from the Arctic to the subtropical latitudes in sheltered intertidal areas (Blount et al., 2022), mostly abundant in temperate zones (Mcowen et al., 2017). They are characterised by periodical inundations of vegetated areas (Blount et al., 2022) and shaped due to a wide range of relationships between biological and physical mechanisms (Blount et al., 2022; D'Alpaos & Marani, 2016; D'Alpaos, 2011; Marani et al., 2006). They are of great importance for coastal communities due to them providing multiple ecosystem services, such as carbon sequestration (Chmura et al., 2003; Duarte et al., 2013), water filtering (Nelson & Zavaleta, 2012), habitat and nursery grounds (Irmler et al., 2002), and erosion protection (Bouma et al., 2014; Carrasco et al., 2021; Temmerman et al., 2013; Vuik et al., 2016).

The spatial distribution of the vegetation inside salt marshes is separated into zones, each with its plant species and geological and physicochemical characteristics. The zonation of the plants inside the salt marshes is highly influenced by factors such as salinity, pH, oxygen, and nutrient concentrations and by the tides (Beeftink, 1996.; Caçador et al., 2007; Moffett et al., 2012; Silvestri et al., 2005; Silvestri & Marani, 2004; Woerner & Hackney, 1997). The main vegetation zones are the tidal flat (with almost no species and constantly flooded), the low marsh (flooded at a high tide), and the high marsh (above the high tide).

Salt marshes are subject to seasonal variations, having seasonal patterns in, e.g., the biophysical properties of plant species (such as above- and below-ground production and biomass, and plant stem stiffness) (Dame & Kenny, 1986; Vernberg, 1993), time of occupancy of organisms (such as the utilization of the marsh during the summer when young stages feed within an estuary) (Vernberg, 1993), an sediment accretion (with large accretion in summer and erosion during winter) (Richard, 1978); They are also subject to these seasonal variations due to the annual biological cycle, adapted to the variations in tidal range that occur over a spring–neap cycle and annually (Mudd et al., 2010; Townend et al., 2011), also existing evidence suggesting that marshes respond to the lunar nodal tidal cycle (18.6-year period), with biological growth being enhanced and mineralogical

sedimentation reduced during phases of amplified tidal range and vice versa during the phases of suppressed tidal range (French, 2006; Townend et al., 2011).

2.2. Rewilded salt marsh

With the increase of anthropogenic pressures in salt marsh (Newton et al., 2020), there has been a loss of these environments in various areas (McLeod et al., 2011; Orson et al., 1985; Potts et al., 2014; Reed et al., 1999; Turner, 1990). Many countries have tried to attenuate/reduce those pressures by protecting salt marshes and rewilding or restoring already damaged areas (Mauchamp et al., 2002; Morris et al., 2004; Simenstad et al., 2006). The main difference between restored and rewilded areas is that restored areas focus on restoring the ecosystem to its previous conditions through direct human intervention, such as topography reconstruction, replanting of native species and hydrological adjustments (Mitsch & Gosselink, 2015). On the other hand, rewilding an area focuses on allowing natural processes to re-establish themselves with minimal human intervention, such as reintroducing water flows (without extensive efforts) or reducing human intervention (Hart et al., 2023; Perino et al., 2019).

There is a wide variety of methods to rewild saltmarshes and one of the most used ones is the removal or breaching of a dike (Billah et al., 2022; Burden et al., 2013, 2019; Crooks et al., 2002; French et al., 2007; Wolters et al., 2005), usually through the opening of an inlet to let water enter an area and naturally recover the ecosystem (Leachtenauer et al., 1998; Wolters et al., 2005); Dike breaching occurs in natural levees or constructed dikes (coastal defence structures) and can produce channel networks that have at least as much total channel surface area and length as those of reference natural tidal marshes, but the number of tidal channel outlets sites is about half that of reference marshes, which may reduce the access of fish (Hood, 2014). Other methods include grading an upland site to intertidal elevations, followed by a re-vegetation (Billah et al., 2022; Craft et al., 2003), Dispersion of sediment slurries (where dredged sediments are dispersed over the marsh surface) (Billah et al., 2022; Schrift et al., 2008; Slocum et al., 2005), construction of a culvert (Billah et al., 2022), and removal of invasive phragmites (Billah et al., 2022). Compared to natural salt marshes, the plant species in rewilded salt marshes experience lower competition, often resulting in high marsh species thriving in the low marsh areas at these sites (Muench & Elsey-Quirk, 2019).

To analyse the success of the restoration of salt marshes, first, key indicators and ecosystem attributes need to be analysed (Billah et al., 2022; Mcdonald et al., 2016), being the most studied indicators regarding species diversity the vegetation cover biomass (above and below ground) and stem density; regarding functional indicators, sediment organic matter, sediment carbon (%), and sediment nitrogen were the most used; and the main hydrological indicators were water surface salinity and temperature (Billah et al., 2022). Many studies have already analysed the responses of restored salt marshes, looking at the time required to achieve similar levels of the indicators compared to natural salt marshes (Billah et al., 2022; Craft et al., 2003; Nordström et al., 2014; Poppe & Rybczyk, 2021). A wide variety of methodologies are used to analyse salt marshes, but one emerging one is the use of satellite imagery.

2.3. Satellite remote sensing

Satellite remote sensing is a technique that acquires data through a sensor inside a satellite orbiting Earth (Blount et al., 2022). The use of satellite imagery for science has increased in the last decades, with the launch of different earth observation satellites missions such as Landsat (Goward et al., 2000; Hansen & Loveland, 2012; Phiri & Morgenroth, 2017; Tatem et al., 2008; Wulder et al., 2022), Sentinel (Phiri et al., 2020; Showstack, 2014), Superdove (Du et al., 2022; Niroumand-Jadidi et al., 2022; Zhang et al., 2022). Satellite imagery relies on surface reflectance, capturing the solar radiation that reflects from Earth into the satellites. The surface reflectance is divided into wavelength bands, ranging from visible light (red, green, and blue) to infrared. Other remote sensing methods exist, such as manned (aircrafts) and unmanned (unmanned aerial vehicle, or UAV) aerial photography (Farris et al., 2019; Krause et al., 2023; Pinton et al., 2021). Aerial photography has the advantage of having high resolution and the capacity for customisation based on user needs, including flight altitude, timing, and sensor types. However, this method has scarce global coverage, infrequent availability, and variable resolutions (Blount et al., 2022).

Each satellite mission has its own spatial and spectral resolutions. The spatial resolution refers to the size of the smallest object that the satellite sensors can detect. It is depicted in meters and is normally separated into high, medium, and low spatial resolution (Lu & Weng, 2007), being necessary for each study to choose the best option for their specific case; a high spatial resolution is needed for studies on a local scale, medium

resolution at a regional scale and low resolution at continental or global scale (Atkinson & Curran, 1997; Lu & Weng, 2007). The spectral resolution refers to the width of the spectral bands the sensor can detect and the number of such bands. There are two main spectral resolutions: the hyperspectral and the multispectral. Hyperspectral sensors capture a wide spectrum of light across numerous narrow bands, offering detailed spectral information for each pixel, while multispectral sensors capture data in fewer, broader spectral bands than hyperspectral (Awad, 2018; Govender et al., 2008). With the use of satellite imagery, the spatial and temporal analyses of physical, chemical, and biological processes became much more accessible and broader, opening the possibility for studies such as urban planning (Malczewski, 2004; Yeh, 1999), mapping hazards (Huabin et al., 2005; Jena et al., 2020), classification of vegetated area (Perumal & Bhaskaran, 2010; Sathya & Deepa, 2017; Xie et al., 2008).

2.4. The use of satellite image classification methods to analyse vegetated areas

One of the most used tools to analyse the evolution of vegetated areas is image classification methods. The image classification of vegetated areas involves using pattern recognition techniques, the spectral features of the satellite images, and empirical geographical knowledge to identify and extract various categories, such as land use types and vegetation species (Jiang et al., 2012; Xie et al., 2008). Image classifications can be categorised as semi-automatic (supervised classification) and automatic (unsupervised classification). Supervised classification consists of creating a set of classes in an image (also known as a training sample) and putting them into a software to train it to create correlations between these classes and the image (Olaode et al., 2014).

Some examples of commonly used supervised classification are the Random Forest (RF), K-nearest neighbour classifier (KNN), KDtree KNN classifier (KD-KNN), Maximum likelihood classifier (ML), and Minimum distance classifier (MD). RF generates multiple decision trees through ensemble learning based on the CART algorithm (Breiman, 2001; Iverson et al., 2008; Wei et al., 2022). The KNN classifies objects based on the closest training samples (Lowe, 2015; Sathya & Deepa, 2017). An object is classified by a majority vote of its neighbours, with the object being assigned to the class most common among its k nearest neighbours (Zhang et al., 2017). The KD-

KNN classifier uses a KD-tree, which is a binary tree that partitions the dataset with training samples sorted to the leaves of the tree (Cunningam & Delaney, 2021) to acquire better results but normally shows similar results to the KNN classifier (Hou et al., 2018). In the ML classifier, a pixel with the maximum likelihood (the posterior probability of a pixel belonging to a given class) is classified into the corresponding class (Perumal & Bhaskaran, 2010; Sathya & Deepa, 2017). In the MD classifier, any pixel in the scene is categorised using the distance between the data from the image and the means of the classes derived from the training samples, so the pixel is designated to the class with the shortest distance (Lowe, 2015; Perumal & Bhaskaran, 2010; Sathya & Deepa, 2017). The advantages and disadvantages of these methods can be seen in **Table 2.1**. Multiple misclassifications can occur after creating a supervised image classification, meaning a class would be assigned to an incorrect location. More training samples can be added to reduce these errors, especially in the locations where most misclassifications occur (Rummell et al., 2022). Eliminating noise and enhancing feature extraction with fusion techniques such as PCA can also help reduce classification errors (Ghassemian, 2016; Kumar et al., 2014; Qian et al., 2008). Optimising the classification model by tuning hyperparameters using advanced architectures like Convolutional Neural Networks (CNNs) can also reduce the number of misclassifications (Balarabe & Jordanov, 2024; Haffar et al., 2021).

Table 2.1. Comparison between supervised classification methods, adapted from Sathya & Deepa (2017).

ALGORITHMS	PROCESS	ADVANTAGES	DISADVANTAGES
MAXIMUM LIKELIHOOD (ML)	A pixel is classified into a corresponding class based on the maximum likelihood, which is the posterior probability of the pixel belonging to a given class (Sathya & Deepa, 2017).	1. Provides good separation from classes.	1. Requires well-trained training set. 2. Computationally intensive
MINIMUM DISTANCE (MD)	In this approach, each pixel within the scene is categorised by calculating the distance between the image data and the means of the classes derived from the training samples (Sathya & Deepa, 2017).	1. Fast execution. 2. All pixels are classified.	1. Fast execution 2. All pixels are classified

K-NEAREST NEIGHBOUR (KNN) & KD-TREE K-NEAREST NEIGHBOUR (KD-KNN)	For KNN, an object is classified by a majority vote among its k nearest neighbours, assigning it to the class most common among them (Sathya & Deepa, 2017). The KD-KNN classifier, which utilises a KD-tree to improve results, typically produces outcomes similar to those of the standard KNN classifier (Hou et al., 2018).	1. Low cost. 2. Effort for learning process.	1. Performance depends on the number of dimensions. 2. Computationally expensive to find the K neighbours when sample dataset is large.
RANDOM FOREST (RF)*	Random Forest (RF) employs a method of randomly and iteratively sampling data and variables to generate a large ensemble, or forest, of classification and regression trees. The classification output from RF is determined by the statistical mode of numerous decision trees, resulting in a more robust model than a single classification tree generated from a single model run (Breiman, 2001).	1. Robustness to outliers. 2. Ability to handle large datasets. 3. Estimating Feature Importance.	1. Long training time. 2. Computational Complexity.

* Information from advantages acquired from Rodriguez-Galiano et al. (2012) and disadvantages from Leistner et al. (2009).

Unsupervised classification automatically creates a set of classes without the necessity of the training samples (Olaode et al., 2014). Some examples of the most used unsupervised classification are the Expectation-Maximization cluster (EM cluster) and the K-means (Jung et al., 2014). EM cluster uses the expected maximisation (EM) algorithm for clustering data; this algorithm is an iterative method used to find maximum likelihood estimates of parameters in probabilistic models, particularly for models with latent variables (Dempster et al., 1977; Yang et al., 2013). K-means partitions a set of observations (in the case of remote sensing, the pixels) into a specified number, k, of clusters. In K-means classification, each pixel is assigned to the cluster with the nearest mean (Abbas et al., 2016; Gonzalez & Woods, 2018).

2.5. The use of satellite remote sensing in salt marshes

Satellite remote sensing offers a non-invasive and effective method to study salt marshes at various spatial and temporal scales. The main methods include optical remote sensing, Synthetic Aperture Radar (SAR), and LiDAR. Optical remote sensing utilises visible, near-infrared (NIR), and shortwave infrared (SWIR) bands to capture images of the earth's surface, making it useful in detecting vegetation health, species composition, and seasonal changes in salt marshes (Agrawal & Khairnar, 2019). Vegetation indices, such as the Normalized Difference Vegetation Index (NDVI) and the Enhanced Vegetation Index (EVI), are commonly employed to assess plant biomass and productivity (Dos Santos et al., 2019; Huete & Justice, 1999; Rouse et al., 1974).

SAR operates in the microwave region of the electromagnetic spectrum, enabling it to penetrate clouds and provide high-resolution images regardless of weather conditions or daylight (Singh et al., 2021). This method is useful in detecting hydrological changes and monitoring soil moisture levels in salt marshes (Grings et al., 2009; Lee et al., 2020). Its sensitivity to surface roughness and moisture content makes it an important tool for understanding the physical structure and inundation patterns of these ecosystems. Although more commonly associated with airborne platforms, spaceborne LiDAR is increasingly being used for high-resolution elevation mapping. LiDAR data can generate Digital Elevation Models (DEMs) that are used to study, for example, marsh topography, assess vulnerability to sea-level rise, and model tidal dynamics (Gesch, 2009; Goodwin et al., 2018; Raber et al., 2007).

While satellite remote sensing provides significant advantages for studying salt marshes, it also faces several challenges that limit its effectiveness, such as spatial resolution. Many satellite sensors have relatively coarse spatial resolution, which can be insufficient for capturing the fine-scale changes of salt marshes, such as the variations in vegetation and topographic features. Distinguishing between different species of salt marsh vegetation can also be difficult due to limited spectral resolution, and although hyperspectral sensors provide more detailed spectral information, they are not yet widely available on satellite platforms and can be expensive. Temporal resolution can be another issue, as salt marshes are dynamic environments that undergo rapid changes due to tidal cycles and seasonal variations (Richard, 1978; Townend et al., 2011; Vernberg, 1993). Thus, the frequency with which images are captured is often insufficient to monitor these

rapid changes effectively. Furthermore, the accuracy of optical remote sensing is often compromised by atmospheric conditions, such as cloud cover and water vapour, which can distort the satellite signal (Li et al., 2022; Shen et al., 2015). Another downside of satellite imagery is that some images (especially high resolution) are not open source (Malerba et al., 2023), making it challenging to obtain this data if the project does not have enough budget.

The future of satellite remote sensing in salt marsh research lies in addressing these challenges and expanding the scope of study to underexplored areas. Advances in sensor technology, such as developing new satellite sensors with higher spatial, spectral, and temporal resolution, will significantly enhance the ability to monitor salt marshes. For example, the launch of hyperspectral satellites, such as EagleEye (Cheng et al., 2024), will provide more spectral details, allowing for better discrimination of vegetation species and more accurate assessments of the health of these ecosystems. Applying machine learning algorithms to remote sensing data also holds great promise for improving the classification and interpretation of salt marsh features. Data fusion techniques that combine optical, SAR, and LiDAR data could lead to more comprehensive models of salt marsh dynamics (Allen et al., 2013). These methods are still in their early stages and represent a significant opportunity for future research. Lastly, another area that requires further study is the use of satellite imagery for rewilded salt marshes. Satellite imagery has been used to analyse the patterns and evolution of varying rewilded ecosystems such as forests, freshwater wetlands, drylands, chaparrals (shrub-dominated ecosystems), crops, and grasslands (Taddeo, 2022; Tang et al., 2019; Dronova et al., 2021), but there are still few studies regarding their use in rewilded salt marshes.

In conclusion, satellite remote sensing has revolutionised the study of salt marshes by providing tools for large-scale, long-term monitoring of these dynamic ecosystems (Klemas, 2013). However, challenges related to spatial, spectral, and temporal resolution and data integration and interpretation continue to limit its full potential. Future advancements in sensor technology, machine learning, and data fusion, combined with a focus on long-term monitoring and unexplored areas such as blue carbon and biodiversity mapping, will significantly enhance our understanding and management of salt marshes (Dat Pham et al., 2019; Klemas, 2013). Addressing these challenges and research gaps is essential for ensuring the resilience of salt marshes in the face of global environmental changes (Billah et al., 2022).

3. Methodology

3.1. Study Area

The two study areas are located on the south coast of Portugal (**Figure 3.1a**) inside the Ria Formosa Lagoon (**Figure 3.1b**). The Ria Formosa is an enclosed lagoon system, having six inlets that exchange water with the Atlantic Ocean; it is around 55 km long and up to 6 km wide, and the submerged area ranges from 53 km^2 at high-water and 14 km^2 at low water (Carrasco et al., 2021; Dias & Sousa, 2009). There are two types of salt marsh found inside the system: lagoon marshes, which are individual marsh bodies detached from the barriers, evolving depending on the morphodynamics of the tidal channel, and 'perched- or back-barrier marshes' which are marsh bodies in the lee of, and attached to, sandy barriers, evolving dependently on back-barrier sediment dynamics and marine barrier dynamics (e.g., overwash) (Carrasco et al., 2021). The tides are semi-diurnal and mesotidal, with a mean tidal range of about 2 m that can reach up to 3.5 m during spring tides (Blount et al., 2022; Carrasco et al., 2021). The average depth of the channels in the lagoon is 6 m, although most areas are less than 2 m deep (Carrasco et al., 2021; Salles et al., 2005). Shifts to inlet tidal prism, initiated mainly by the engineering works in Faro-Olhão Inlet, caused changes to the system over the last 70 years (Carrasco et al., 2021; Pacheco et al., 2010).

There are studies reporting the related evolution of barriers and inlets (e.g., Ferreira et al., 2016; Vila-Concejo et al., 2004, 2002), being the long-term retreat and growth of the lagoon marshes a direct response from natural processes and human interventions (Carrasco et al., 2021). No important inputs of fluvial water are found coming into the lagoon, and no input of coarse sediment. The sediment is mostly cohesive sediment, with fine sand and silt coming from the terrestrial margin as suspended load; a part of them is exported to the shelf during each tidal cycle and partly retained in intertidal flats and the salt marshes (Andrade et al., 2004). Vertical accretion in the Ria Formosa was estimated using empirical methods, estimating a 2 mm/yr as an upper limit for the current average sedimentation rate (Andrade, 1989; Carrasco et al., 2021). A wide variety of halophyte plant species exist in the Ria Formosa (Costa et al., 1996). The most frequent species are the *Spartina maritima*, *Sarcocornia perennis*, and *Puccinellietum convolutae* (Arnaud-Fassetta et al., 2006; Bertrand et al., 2003; Blount et al., 2022; Contreras-

Cruzado et al., 2017; Costa et al., 1996). On adjacent tidal flats, *Zostera noltii* is commonly found at times interspersed with colonising clumps of *Spartina maritima* and *Sarcocornia perennis* (De los Santos et al., 2022).

Since the Ria Formosa is a very important wetland area for the region, it has been a Natural Park since 1987 and is part of the Natura 2000 network, protected under the Ramsar convention (Cristina et al., 2019; Newton et al., 2003). Inside the system, many areas have been protected and are in the process of being rewilded. For this study, two rewilded salt marshes were chosen as the Regions of Interest (ROIs): Bias and Olhão. Both salt marshes were once enclosed and used for aquaculture. After a period of being abandoned, enclosing dikes were breached (dikes realignment), more precisely in Bias in 2011 (**Appendix A, Figure A1**) and Olhão in 2017 (**Appendix A, Figure A2**), to naturally let the system recover.

The first ROI rewilded salt marsh in Bias (**Figure 3.1c**) has an area of approximately 110km² and is divided into two areas (previously two aquaculture cells), each having at least one connection to the lagoon. The two rewilded salt marshes are of great importance for the local communities, being used, for example, for touristic activities and bivalve harvesting. The second ROI rewilded salt marsh in the city of Olhão (**Figure 3.1d**) covers an area of approximately 21km² and is directly connected to the lagoon. When comparing the two areas, the ROI in Bias is bigger, composed of older vegetation, and is more diverse in marsh vegetation species compared to the ROI in Olhão, which is much smaller and has a large part of its area covered with sand.

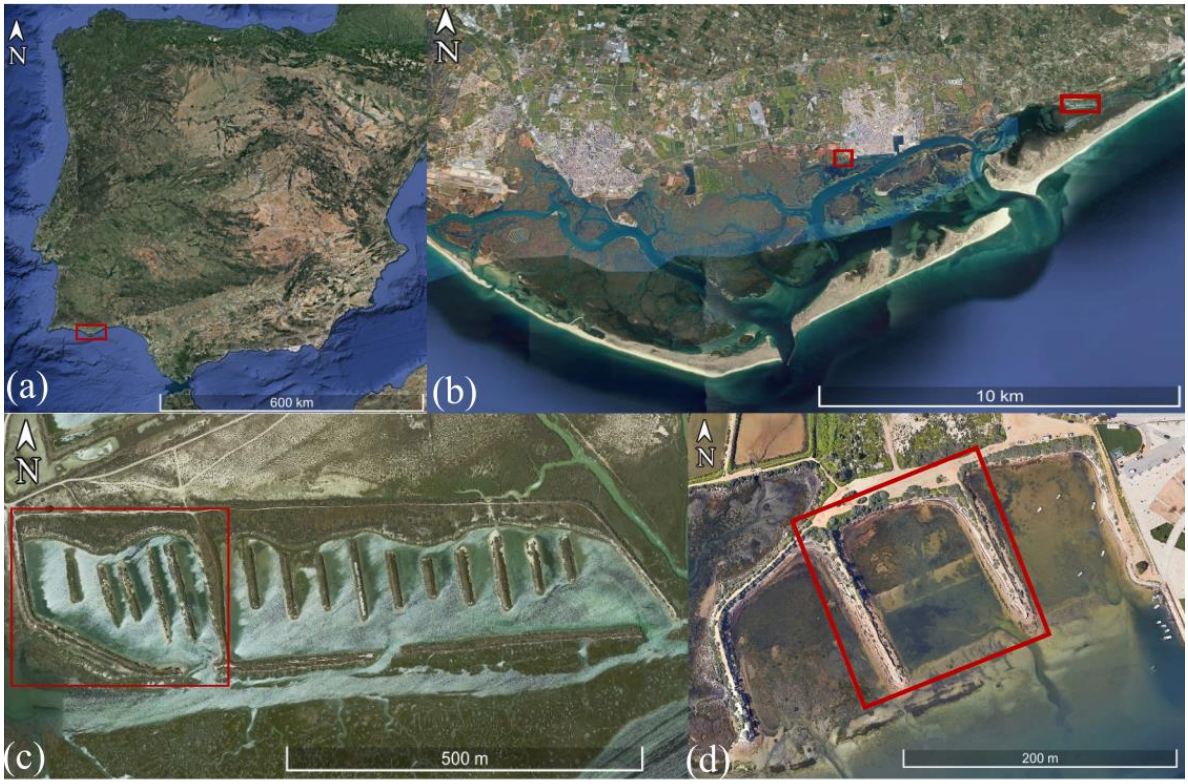

Figure. 3.1. a) Map of the Iberic peninsula highlighting the south of Portugal from (Google Earth image from 14/12/2015), **b)** map of Ria Formosa lagoon highlighting the location of the ROIs (red rectangle) (Google Earth image from 14/04/2022), **c)** map of rewilded salt marsh in Bias from (Google Earth image from 14/04/2022) with highlighted study area. The images used are from Google Earth PRO, 2023 and **d)** a map of a rewilded salt marsh in Olhão from (Google Earth image from 14/04/2022) with the area studied highlighted (red rectangle).

3.2. Fieldwork data collection

The fieldwork data collection comprised several campaigns between 2023 and 2024. The main objective of the fieldwork campaigns was to collect the distribution and location of plants throughout the salt marsh and characterise sediment properties. Data was collected in the four seasons to analyse the temporal variations in the vegetation pattern. Each field campaign was done at spring tide conditions during the morning, between 8:00h and 13:00h. Field campaign surveys took at least three days: two days to acquire data in Bias and another day for Olhão. All the surveys and further analyses were the same for each season. Existing data from previous research, such as drone images from the two ROIs, have been used to support the developed analysis and were acquired in April 2022 at low tide conditions. The drone was a Dji P4 with a Six ½.9" CMOS sensor, an RGB sensor for visible light, and five monochromatic sensors for multispectral

images. The drone images were used as a visual reference for the classification images to assess how well the classifications depicted the features of the salt marshes.

To characterise the current plant species distribution, multiple square 3x3 m plots (**Figure 3.2**) were deployed on each ROI (**Figure 3.3** for Bias and **Figure 3.4** for Olhão). These plots ranged from the high marsh to the tidal flat to fully cover the zonation of the salt marsh. After deployment, each plot was subdivided into four sub-sectors of 1.5x1.5m to facilitate the identification of plants and the upcoming capturing photos. The location of the plots took into consideration an area with high specific diversity, aiming to have a broad number of species inside of it, and were oriented northward to align with the pixels of the satellite images. The features collected ranged from plant species, soil (mudflat), ground (sand and artificial walking paths), and deposited dead *Zostera noltii*. Although *Zostera noltii* is dead vegetation, it was included in the tests because it occupies a broad area in the ROIs, especially Bias, influencing the classifications.

Figure 3.2. Photo of a plot taken during spring fieldwork in Bias.

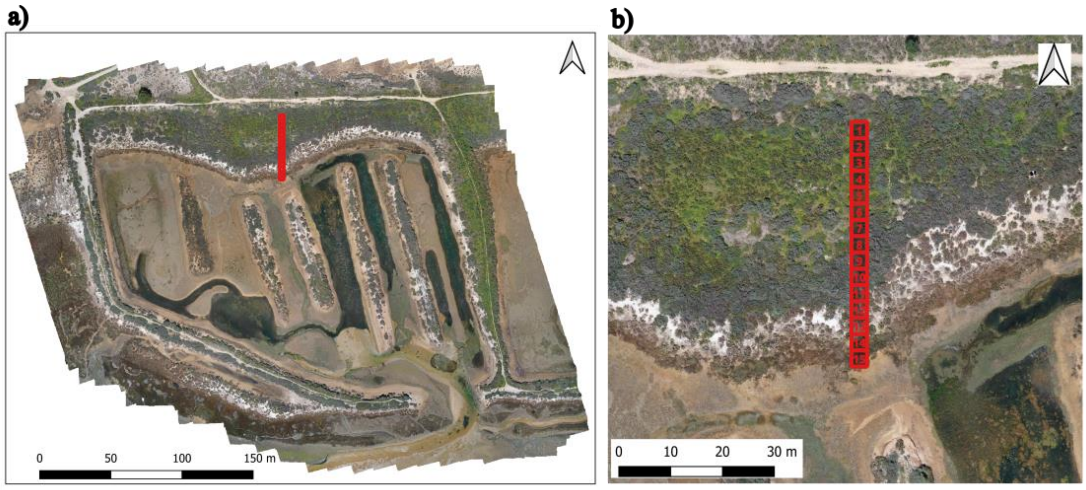

Figure 3.3. Location of the plots in the ROI of Bias, using the drone image (Dji P4) as a reference, with **a)** the entire ROI and **b)** the area close to the plots.

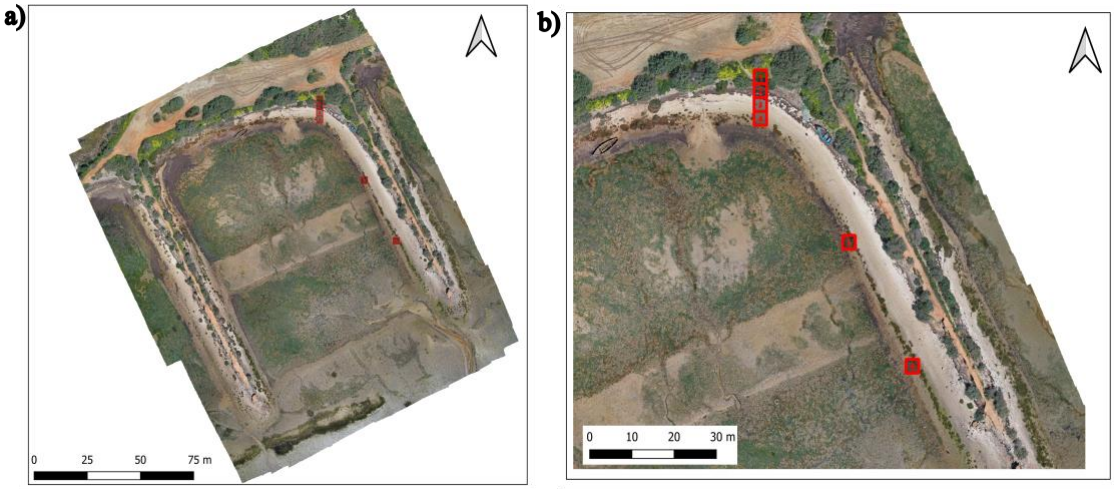

Figure 3.4. Location of the plots in the ROI of Olhão, using the drone image (Dji P4) as a reference, with **a)** the entire ROI and **b)** the area close to the plots.

After a plot was created, the coordinates of the sub-sector corners were taken using an RTK-DGPS (with a horizontal and vertical accuracy of 0.011 m and 0.017 m, respectively). Photos were collected for each sub-sector using a mobile phone connected to a selfie stick at a vertical distance of approximately 3m. The mobile phone position was zenithal, as upright as possible, to capture a "bird's eye view" photo (Guisado-Pintado & Jackson, 2020). In each sub-sector, an identification of the plant species inside of it was made using a plant species catalogue and plant identification applications such as PictureThis (https://www.picturethisai.com). For later validation of the location of those plants, drawings of the plants inside the plot were made in a logbook (**Figure 3.5**). Together with the plots, contours of specific plant species (patches) were located

throughout the rewilded salt marsh, using the RTK-DGPS to take coordinates of points around the species' patches.

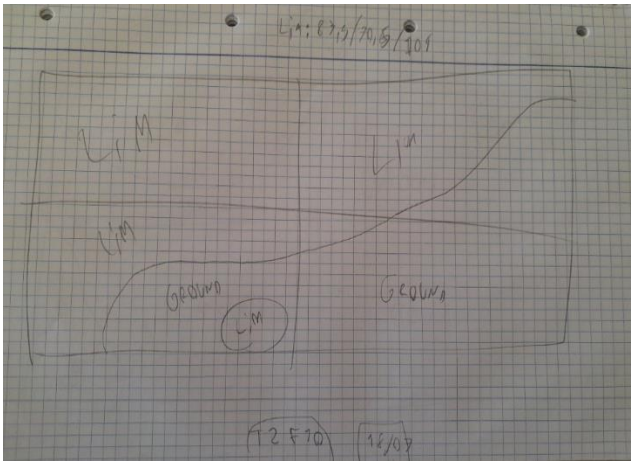

Figure 3.5. Photo of the logbook with a drawing of a plot.

Surficial sediment samples were also taken on the area of the plots in both ROIs using small syringes to characterise the sediment geochemistry signature. A total of 10 sediment samples were collected in Bias and 15 in Olhão. Even though there were only 6 plots in Olhão, more sediment samples were collected to complement the data. About 50 cm^3 of sediment was collected with plastic syringes, which were later placed in plastic cups, labelled and carried to the laboratory. The location where the sediment samples were collected can be seen in **Figure 3.6** for Bias and **Figure 3.7** for Olhão.

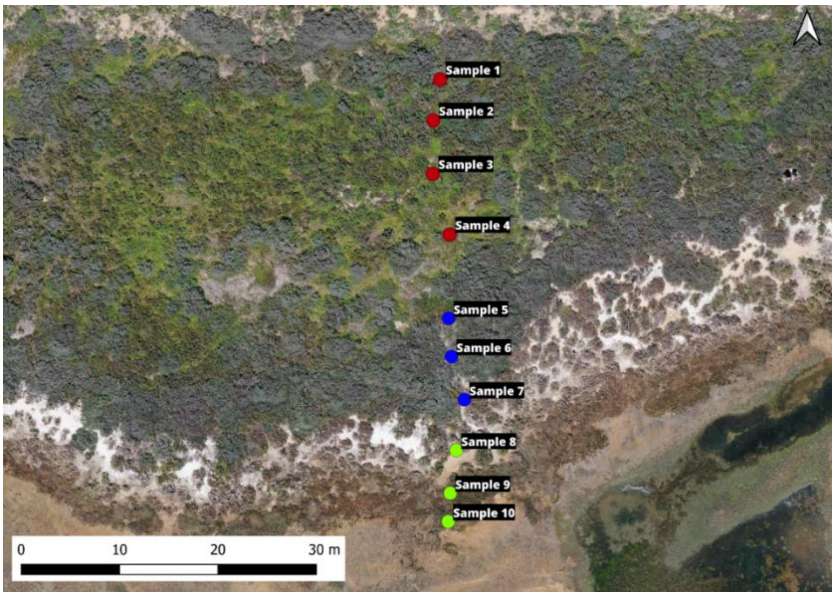

Figure 3.6. Location of the sediment samples throughout the ROI of Bias, having the samples 1 to 4 at the high marsh (red points), 5 to 7 at the medium marsh (blue points), and 8 to 10 at the low marsh (green points).

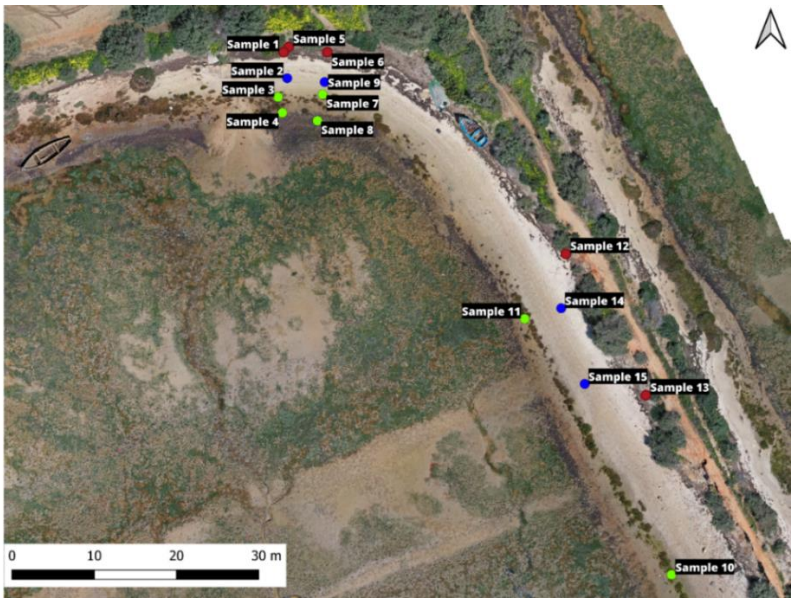

Figure 3.7. Location of the sediment samples throughout the ROI of Olhão, having the samples 1, 5, 6, 12, and 13 at the high marsh (red points), 2, 9, 14, 15 at the medium marsh (blue points), and 3, 4, 7, 8, 10, 11 at the low marsh (green points).

3.3. Fieldwork data handling

The vertical photos taken in the field from the plot sub-sectors were merged and edited into a single photo (**Figure 3.8**) using the GIMP software (Version 2.10.36) (see flowchart in **Figure 3.9**). Then, they were improved by removing shadows and any unnecessary objects, such as notebooks and people inside the photos (**Figure 3.9**). The fieldwork photos must match the point of view of the satellite images (horizontal), so they were edited to appear as horizontal as possible using the perspective tool in GIMP (**Figure 3.9**).

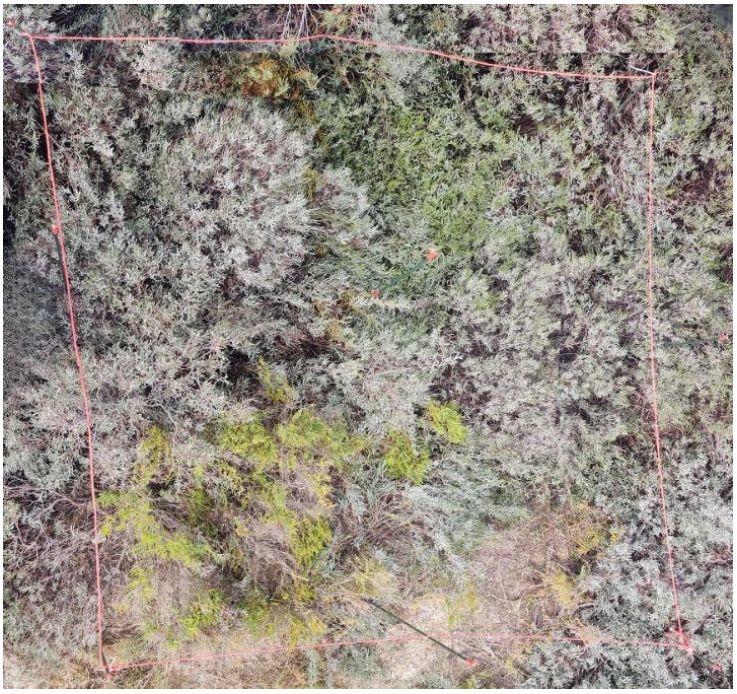

Figure 3.8. Fieldwork photos merged from the autumn campaign in Bias.

After editing the vertical photos, the RTK-DGPS coordinates from all points (sub-plot corners and plant patches) were turned into vector points in QGIS (Version 3.32.2) (**Figure 3.9**). Then, the vertical photos were georeferenced, using the corner of the sub-plots in the photos and the coordinate vector points in QGIS as a reference (**Figure 3.9**). The error from the georeferencing ranged from 0.26cm to 1.35cm.

Then, the contours of the plant species inside those sub-plot photos and plant patches were mapped based on changes in colour and texture in the pixels supported by the drawings made in the fieldwork logbook (**Figure 3.9**). These contours were used as training (spatial) samples for the supervised classification images.

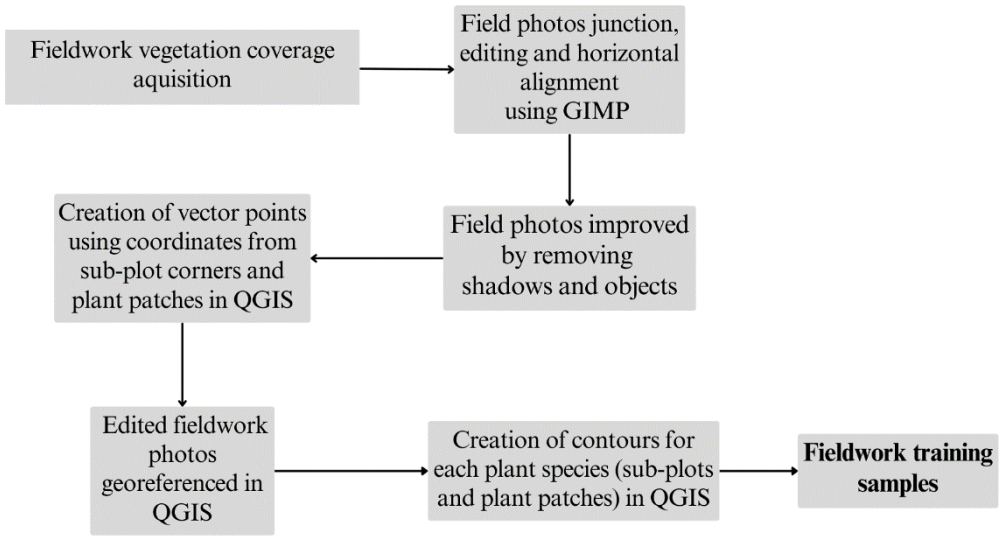

Figure 3.9. Flowchart of fieldwork data handling.

3.4. Laboratory sediment analysis

3.4.1. Sediment water content (H_2O%)

Sediment samples were prepared to analyse water content (H_2O%), organic matter content in %, and median sediment grain size diameter (d_{50}) (**Figure 3.10**). Firstly, the wet samples were weighed (wet weight), and then the sediment samples were dried in an oven at 60°C for approximately one week. After the evaporation of the water, the samples were weighed again (dry weight). By computing the weight difference, the H_2O% inside the sediment samples was calculated as the proportion of weight loss compared to the original weight (Castillo et al., 2010; Contreras-Cruzado et al., 2017). Then, the dry samples were separated in two, with half being transferred to a plastic container and the other half to a crucible.

3.4.2. Sediment organic matter (OM)

The organic matter content (OM) was estimated by the loss on Ignition method (LOI) (Carey et al., 2017; Craft et al., 1991; Heiri et al., 2001; Macreadie et al., 2013). The dry samples in the crucible were taken to a muffle furnace, increasing the temperature

to 450°C, then remaining at that temperature for 4 hours. The weight of destroyed organic matter was calculated as the proportion of weight loss before (dry weight) and after the muffle furnace (ash-free dry weight or AFDW) (**Figure 3.10**).

3.4.3. Sediment grain size distribution and median diameter (d_{50})

To assess the grain size distribution, the sediment plastic container samples were subject to a pre-treatment using 35% hydrogen peroxide (H_2O_2) for 2 to 3 days to destroy the organic matter (OM) (Allen & Thomley, 2004; Gray et al., 2010). After OM destruction, the coarse sediment fraction was sieved using a 2 mm sieve (with the aid of deionised water) to separate the sediment fractions above 2 mm (>2 mm) on the sieve and below 2 mm (<2 mm) (**Figure 3.10**). The sediment fraction >2 mm in the sieve was dried and weighed. The <2 mm sediment fraction remained steady for a few days to let the particles sediment. Once the <2 mm fraction was sedimented, the water was discarded, and a dispersant agent (Hexametaphosphate, 1g/L) was added to the sample to prevent flocculation. To determine the particle size distribution of the sediment fraction <2mm sample, a laser diffraction analysis was performed using a Malvern Mastersizer 3000 by measuring the angular variation of laser light intensity to determine grain size (Roner et al., 2016) (**Figure 3.10**). Values such as measurement time, stirring rate, and obscuration level were selected according to the sample composition. When using the equipment, the sediment in solution in the samples was slowly added to a container with a dispersant agent until an obscuration level between 5-15 %. Each sample was measured six times (around ten seconds each) with a background measurement time of 20 seconds. After the measurements, the sediment size values from both the coarse sediment fraction (>2mm sample that stayed on the sieve) and finer sediment fraction (<2mm from the Malvern) were then transferred to an Excel sheet to compute the clay and silt % and the median diameter (d_{50}) using GRADISTAT v.8.0 macro (Blott & Pye, 2001) (**Figure 3.10**). Results from the sediment analysis will complement the characterisation of the salt marsh zonation in the study sites and allows to decipher the influence of the sediment properties (H_2O%, OM, and d_{50}) on the spectral signature from the satellite images.

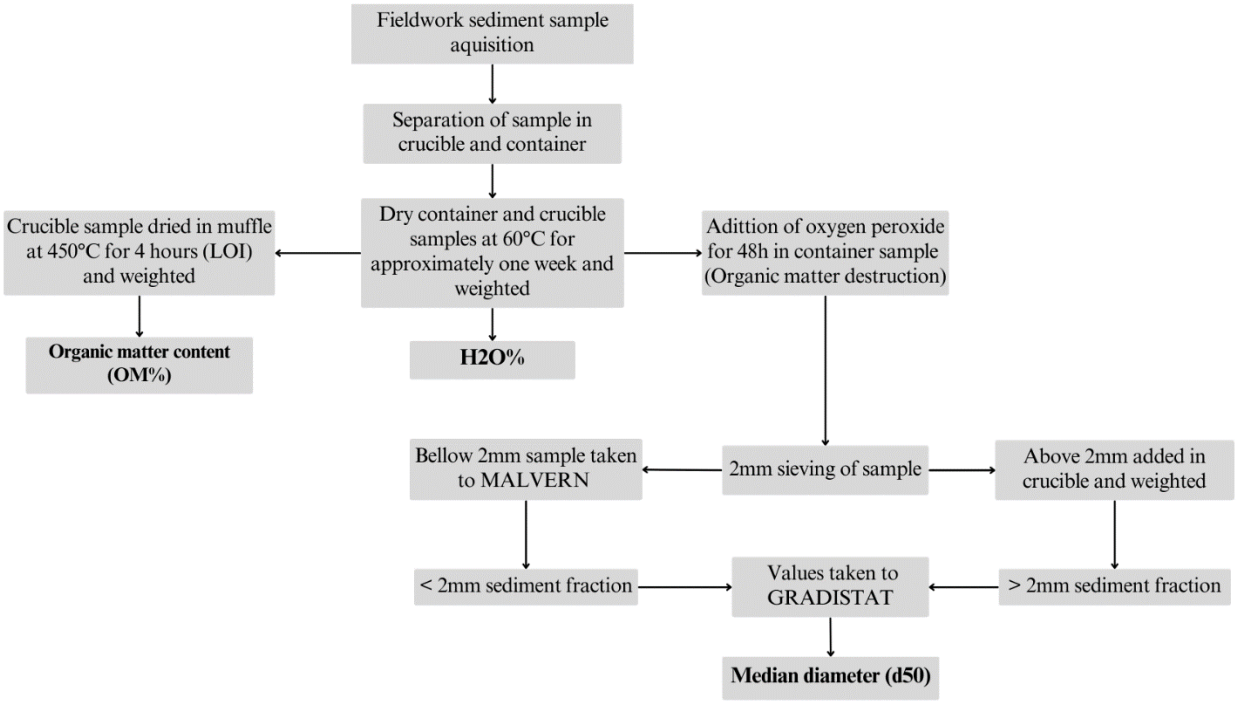

Figure 3.10. Flowchart of sediment analysis.

3.5. Satellite data processing

3.5.1. Satellite images and processing

The satellite imagery used for analysis was the SuperDove constellation of microsatellites from Planet LABS PBS. The SuperDove satellite images have eight spectral bands positioned between 400 and 900 nm (**Table 3.1**) with a resolution of 3m, meaning that each pixel has an area of 3x3 m (Du et al., 2022). The satellite images were downloaded from the Planet Explorer website (https://www.planet.com) and are aligned with the day closest to the fieldwork (**Table 3.2**), ensuring optimal conditions with minimal cloud cover in the ROIs. The images were downloaded as a ".tiff" in a composite format (meaning that they result from an overlap of images taken on the same day with a slight difference of time between them, assuring a better quality) and with harmonisation, providing data with a spectral response similar to Sentinel-2, making it easier to handle in the SNAP software (Version 9.0.0). The geolocation mean error of the SuperDove satellite image in Europe is approximately 8.2m (Wolfe et al., 2021), and the specific geolocation error of the study areas was of approximately 1m in Bias and Olhão. The

specific geolocation error for the study areas was assessed by comparing the SuperDove satellite images with the drone images, using specific landmarks, such as the artificial walk paths and plant species patches, to calculate the difference between the SuperDove satellite image and the drone image.

The satellite images were turned into subsets after being acquired to analyse only the ROIs, and then the image classification methods were tested in the SNAP software (Version 9.0.0). All the different supervised and unsupervised classifications were replicated in all four seasons to see the seasonal variations and zonation of the plant species.

Table 3.1. Bands and wavelengths from SuperDove satellite constellation (Planet, 2023).

Band	Name	Wavelengths (nm)
1	Coastal Blue	443
2	Blue	490
3	Green I	531
4	Green	565
5	Yellow	610
6	Red	665
7	Red Edge	705
8	NIR	865

Table 3.2. Dates of the retrieved SuperDove satellite images for both ROIs.

	Dates	
Season	**Bias**	**Olhão**
spring	24/06/2023	09/04/2024
summer	16/07/2023	11/06/2024
autumn	28/10/2023	20/10/2023
winter	31/01/2024	24/01/2024

3.5.2. Unsupervised classifications

Two unsupervised classification methods were tested: the EM cluster and the K-means cluster. The images were created and compared to determine the model skill to predict the variability of the vegetation in both ROIs, replicating them in all seasons. After choosing the method with the best skill for the analysis, a colour pallet was created. The pallet of colours for the classes shows the different vegetated areas with various green colours, soil classes with brown, water classes with blue, and ground paths with yellow. These steps were then replicated in all four seasons to see if this methodology can clearly show the seasonal variation and the variations in the zonation of both ROI's.

3.5.3. Supervised classifications

Five supervised methods were tested: RF, KNN, KD-KNN, ML, and MD (see flowchart in **Figure 3.11**). After choosing the model with the best skill to predict the variability of the vegetation in all stations, the classification was done only for the area where the plots were deployed (PA). Afterwards, a classification of the entire area of the ROIs (EA) was created (**Figure 3.11**).

The next step was to create a new set of images with the composite of all the data collected throughout all fieldwork campaigns (AC) (**Figure 3.11**). The plant species contours from spring were added to the summer data, creating one classification image (spring + summer data); after that, this composite of data would also have the data from autumn added, creating a second image (spring + summer + autumn data). Lastly, this second composite of data would have the winter data added, having, in the end, the third image with the plant contours acquired in the fieldwork from all the campaigns. This progressive composite of data was conducted for both the areas close to the plots (AC-PA) and for the entire areas (AC-EA) of both salt marshes to see how the cumulative effect of field data influences the quality of the classification. The composite of data considers that the location of the plants barely changed throughout the year. This methodology cannot be used to analyse the seasonal variations since it uses data from all the seasons, but it can be used to analyse the overall zonation of the plant species.

Since the supervised classification had ground-truth data from the plant species (training samples), the colour manipulation of the labelled classes tried to closely depict the colours from the plant species or their specific features, such as choosing the label colour purple for the *Limoniastrum monopetalum*, a plant species with purple flowers (**Appendix B, Table B1**). In certain instances, the colour representation of specific labelled categories was given a random colour label. For example, Sarcocornia perennis, typically green with red/orange parts during spring (**Appendix B, Table B1**), was assigned a labelled class with the colour blue. This was done to enhance the visualisation of the plant species, as most of them are predominantly green.

To determine the classification error compared to reality, the accuracy and root mean squared error (RMSE) were acquired (**Figure 3.11**). The accuracy is the ratio of correct predictions (when a prediction from the classification matches the actual class, or ground truth) to the total number of predictions. The RMSE represents a single value that summarises the average error between predicted ($\hat{y}_i$) and actual values (y_i) divided by the number of samples (**N**), providing insight into the proximity of the predictions to the true outcomes (**Equation 1**). The analysis of these values aimed to find the method with the highest accuracy percentages and lowest RMSE values, which would be the most precise method. The values come as an output from the SNAP software when creating the classification images.

$$\mathbf{RMSE} = \sqrt{\sum_{i=1}^{N} \frac{(y_i - \hat{y}_i)^2}{N}} \qquad \textbf{(Equation 1)}$$

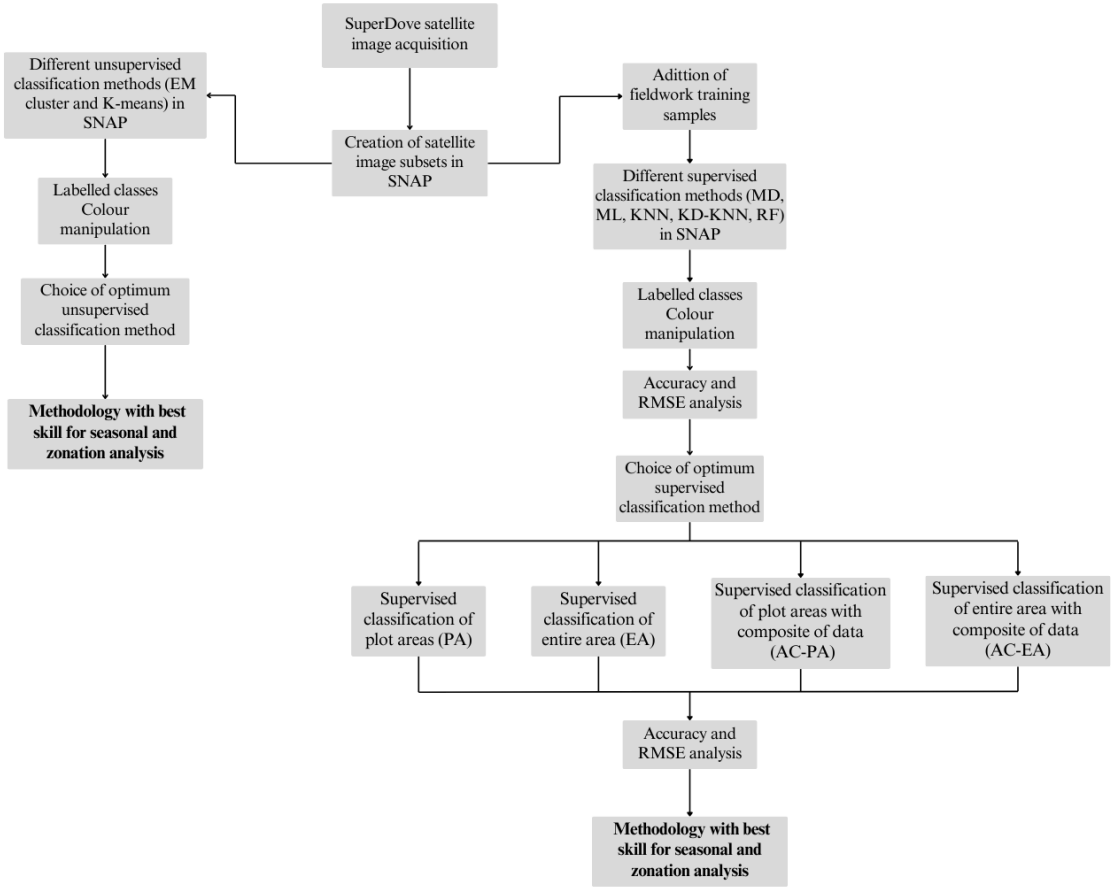

Figure 3.11. Flowchart of satellite data processing.

3.5.4. Spectral signature

The SuperDove satellite images were used to extract the spectral signature from the salt marsh vegetation inside the plots. The eight bands from the satellite image (**Table 3.1**) depict the visible light spectrum, ranging from Blue (443nm) to Near-infrared (865nm). The reflectance values from the SuperDove images are scaled by 10000 to reduce error (Vazir, 2021), so the values were divided by 10000 to depict the original reflectance values.

The spectral signatures were measured in heterogeneous locations, characterised by a high diversity/mixture of plant species (within the plots) and homogenous locations containing a single marsh plant species (additional plant species patches). The spectral signature values were extracted from the pixel centres of the satellite image using the SNAP software. Together with the spectral signatures, the percentage of plant species

inside the pixels was calculated in all seasons. These percentages were calculated using the pixel where the spectral signature was extracted as the total area. The contours of the plant species were used to calculate the percentage of each plant species inside the pixel using the field calculator in QGIS. These values were then compared to the spectral signatures to observe the influence of each plant species on the spectral signature.

4. Results

4.1. Analysis of sediment characteristics in the studied sites

Looking at the sediment analysed in the ROI of Bias (**Figure 3.6**), the values of H_2O% are lower and d_{50} higher in the high marsh (samples 1 to 4, **Figure 4.1**), decreasing the values of d_{50} and increasing H_2O% advancing into the lower marsh (samples 8 to 10, **Figure 4.1**). When looking at the organic matter content (OM), the obtained values do not vary considerably throughout the zonation, having their highest value closer to the low marsh.

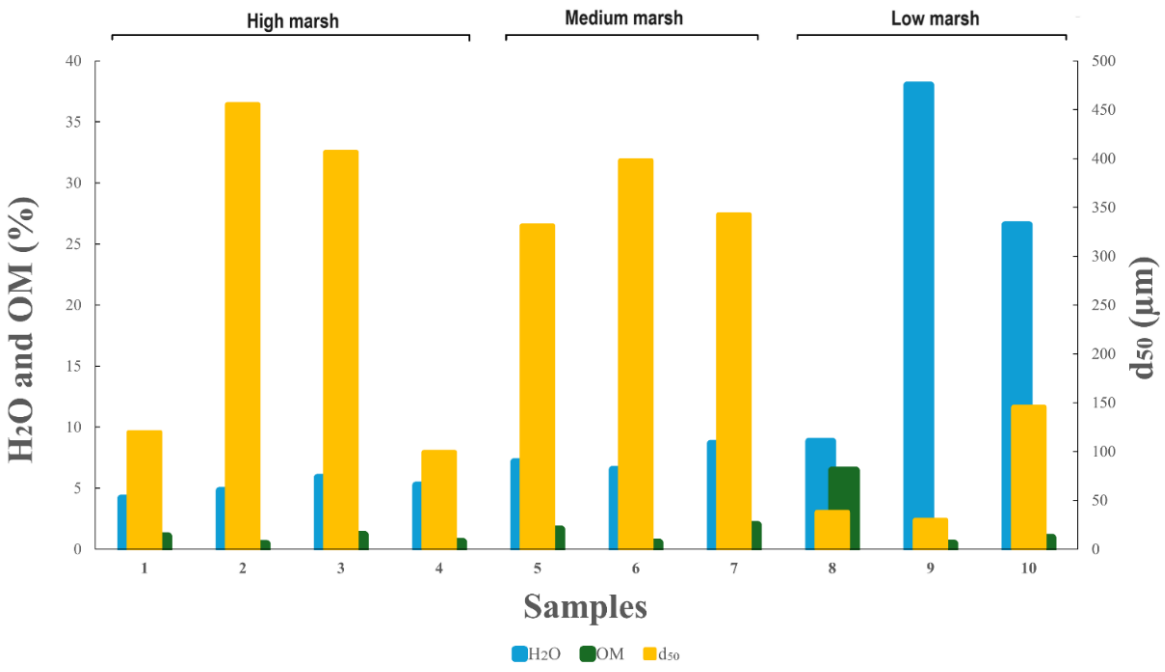

Figure 4.1. Grain size and sediment geochemical properties in Bias rewilded salt marsh, namely d_{50}, water content (H_2O%), and organic matter (OM), from the high marsh towards the low marsh.

When analysing the sediment in Olhão, a lack of pattern can be seen since only 9 out of the 15 samples cover the full zonation of the salt marsh (**Figure 3.7**). The high marsh showed high d_{50} values (between 300 and 350 µm) and low percentages of H_2O% (**Figure 4.2**). In the medium marsh, the values of d_{50} have a higher variation, with an increase in the percentage of H_2O%. Lastly, in the low marsh, the H_2O% is considerably higher, with, in general, lower values of d_{50} compared to the high marsh. OM values in Olhão were considerably low compared to Bias, having its highest values, close to 1% of OM, in the low marsh. All the values in the medium and low marsh do not have a pattern, possibly due to these areas still being in development since the rewilding process in Olhão is relatively recent, starting in 2017.

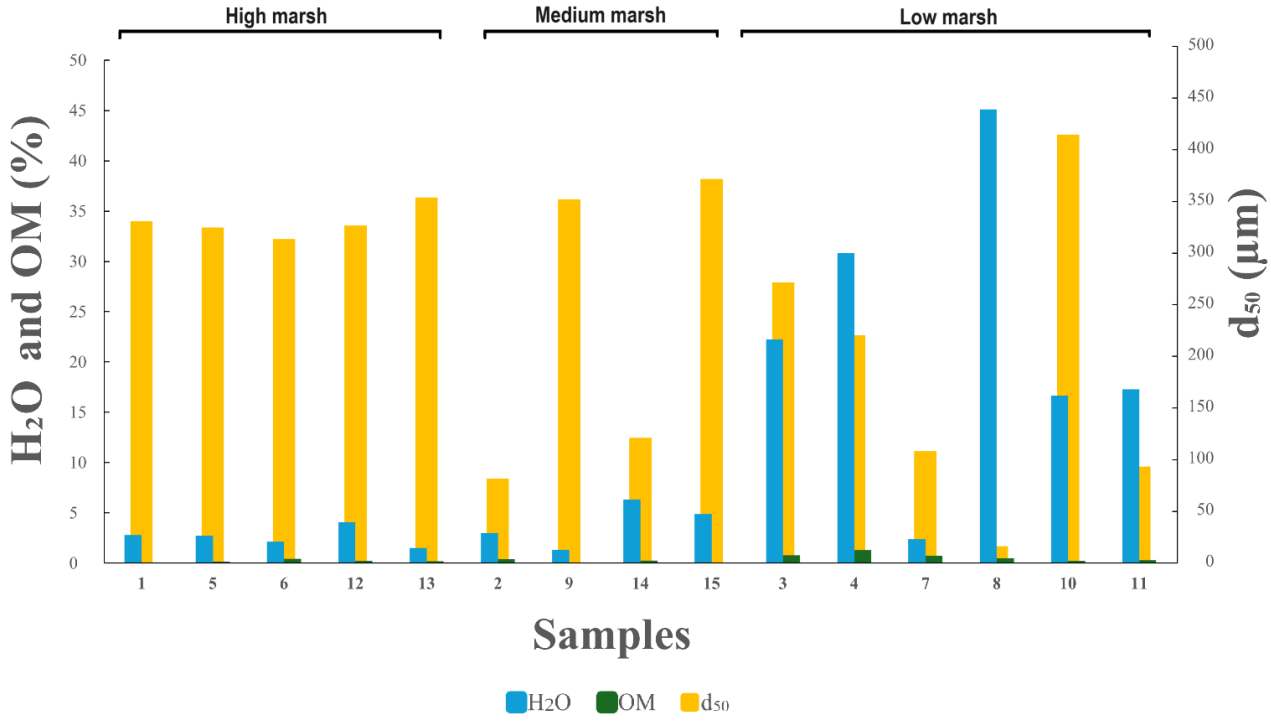

Figure 4.2 Grain size and sediment geochemical properties in Olhão rewilded salt marsh, namely d_{50}, water content (H_2O%), and organic matter (OM) in the sediment of Olhão, being the samples separated by the zonation in the salt marsh.

4.2. Unsupervised classifications

4.2.1. Comparison of unsupervised imagery methods

When comparing the results of the selected methods for unsupervised classification, the EM clustering (**Figure 4.3c** and **Figure 4.4c**) and K-means clustering (**Figure 4.3d** and **Figure 4.4d**) exhibit minimal differences in the distribution of the

classes. The differences mainly arise from the increased number of layers of vegetated classes in certain areas of the EM cluster images, such as the vegetated regions in the bottom left of the image in Bias (**Figure 4.3c**). While Bias exhibited these slight discrepancies between the two methods, the class variations were less pronounced in Olhão.

Since the unsupervised classifications cannot classify to the species level, the classes were labelled only with the main features of the salt marsh (vegetated areas, ground soil, and water). Even though it could not classify to the species level, the unsupervised classifications managed to depict different classes of vegetated areas. Given the similarity between the two classifications in capturing the seasonal variations of plant species, the EM clustering method was selected because it was slightly more consistent within the images.

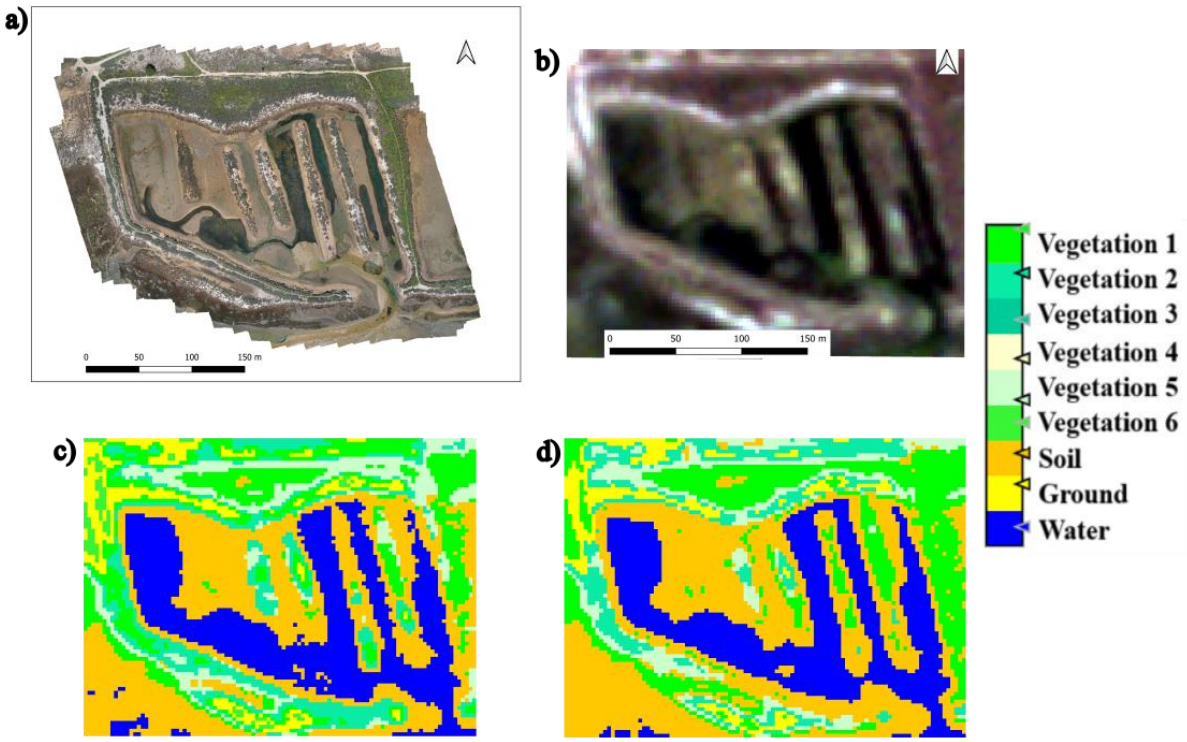

Figure 4.3. Comparison between unsupervised classifications derived from the spring fieldwork campaign in Bias. To facilitate comparison, panel **a)** presents a DJI P4 drone image, and panel **b)** displays the SuperDove satellite image from spring. The classification outputs include **c)** an EM cluster classification and **d)** a K-means cluster classification.

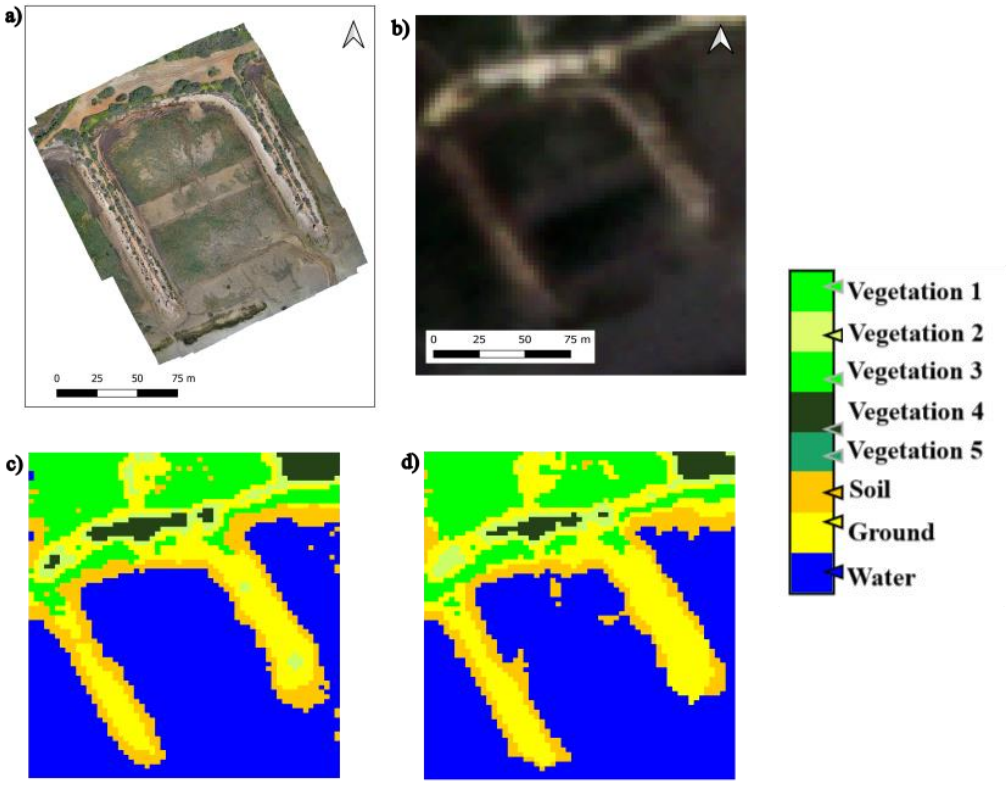

Figure 4.4. Comparison between unsupervised classifications derived from the spring fieldwork campaign in Olhão. To facilitate comparison, panel **a)** presents a DJI P4 drone image, and panel **b)** displays the SuperDove satellite image from spring. The classification outputs include **c)** an EM cluster classification and **d)** a K-means cluster classification.

4.2.2. Analysis of Expected Maximization cluster (EM cluster) imagery classifications

The unsupervised classification using the EM cluster for Bias (**Figure 4.5**) and Olhão (**Figure 4.6**) identified nine and eight classes, respectively. Since the unsupervised classification does not rely on training samples, it could not achieve species-level classification, only classifying broader vegetated areas and the main features of the salt marshes. However, the seasonal variation in vegetation is evident, as reflected in the changes among the identified vegetation classes. One example is the appearance of vegetation 6 in Bias in winter (**Figure 4.5f**) or the variations of the ground class in Olhão, increasing in spring and autumn and decreasing in summer and winter (**Figure 4.6**). Due to the inherent limitations of the EM clustering method of classifying up to the species level, visualising the variation of plant species is not feasible. This emphasises the need for more precise methods, such as supervised classifications.

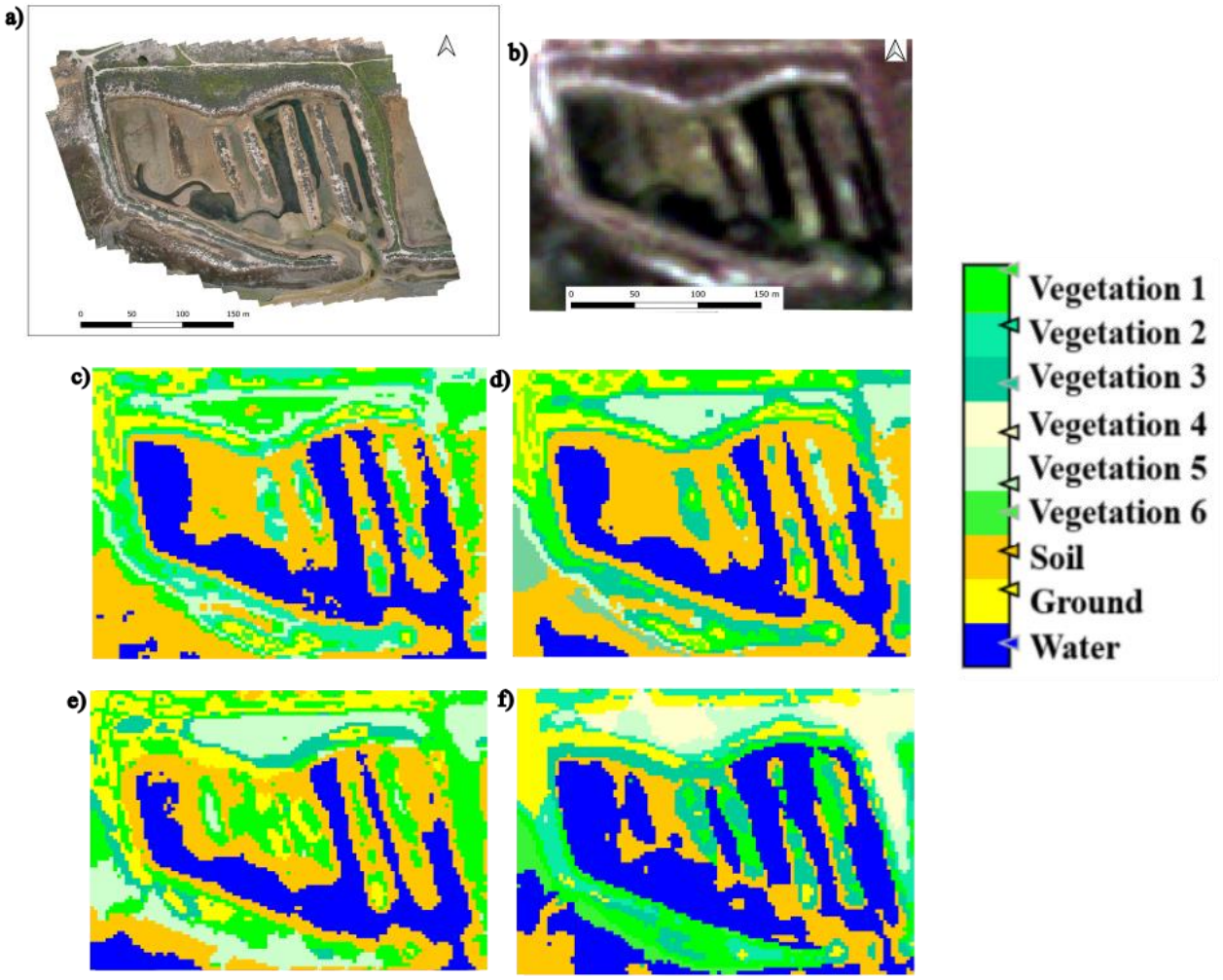

Figure 4.5. Unsupervised EM cluster classifications for the Bias rewilded salt marsh. To facilitate comparison, panel **a)** presents a DJI P4 drone image, and panel **b)** displays the SuperDove satellite image from spring. The EM cluster classification outputs include the **c)** spring, **d)** summer, **e)** autumn, and **f)** winter images.

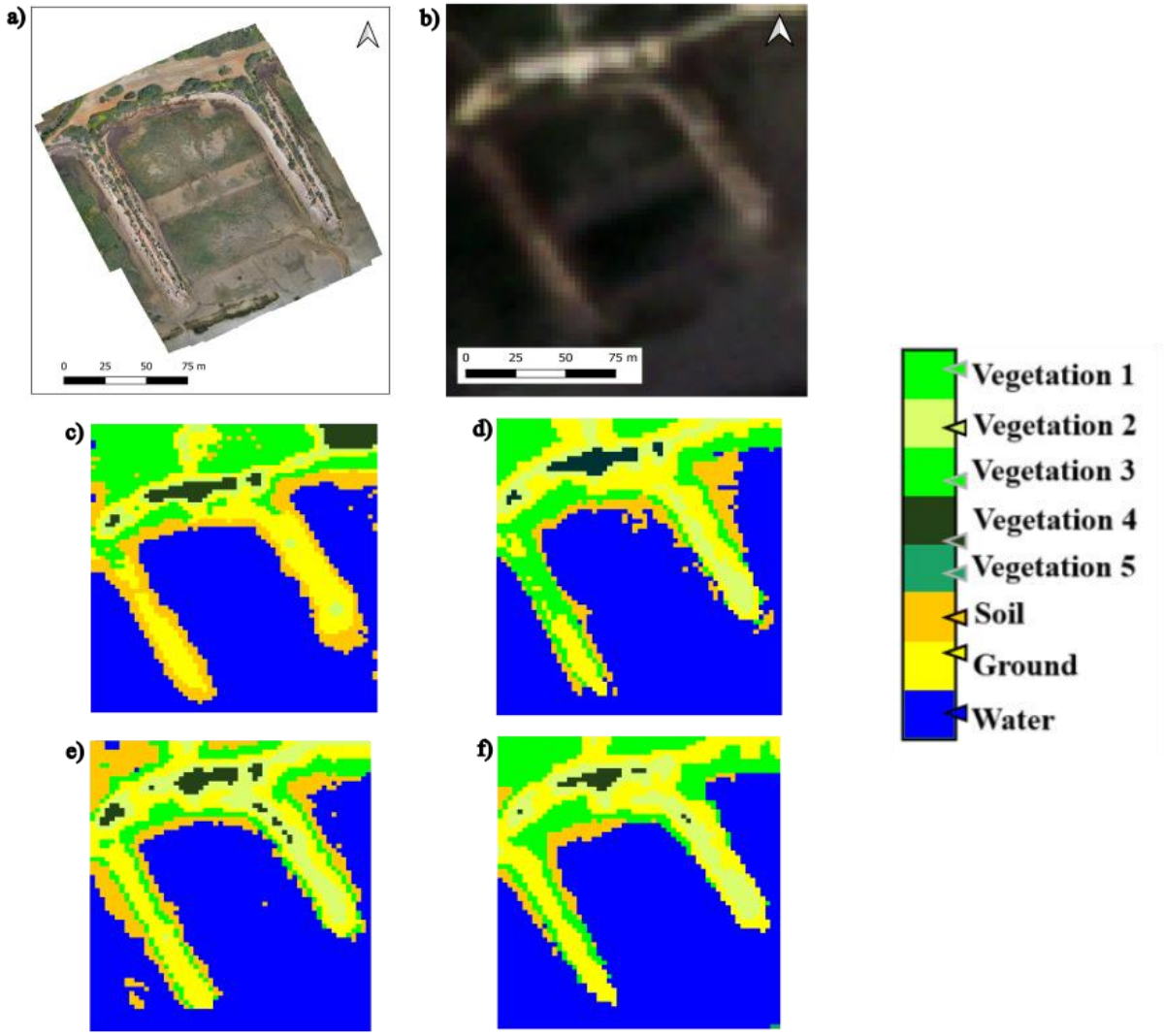

Figure 4.6. Unsupervised EM cluster classifications for the Olhão rewilded salt marsh. To facilitate comparison, panel **a)** presents a DJI P4 drone image, and panel **b)** displays the SuperDove satellite image from spring. The EM cluster classification outputs include the **c)** spring, **d)** summer, **e)** autumn, and **f)** winter images.

4.3. Supervised imagery classification

4.3.1. Analysis of the supervised imagery classifications

The RF classification method outperformed the other supervised methods, i.e., it had a better approximation between the output classified image and fieldwork data (**Figure 4.7g** and **Figure 4.8g**). It correctly portrayed most of the salt marsh zones and other natural/human features present in the area, such as the flooding zones, artificial walking paths, and vegetated areas, and most plant species are classified in their correct zonation.

The other classification methods, KNN (**Figure 4.7c** and **Figure 4.8c**), KD-KNN (**Figure 4.7d** and **Figure 4.8d**), and MD (**Figure 4.7e** and **Figure 4.8e**), provided less accurate imagery classifications for the plant species, particularly for the low marsh plant zonation. Plant species from the low marsh, such as *Sarcocornia perennis* (light blue class - **Figure 4.7** to **Figure 4.16**) and *Salicornia ramosissima* (light pink class - **Figure 4.7** to **Figure 4.16**), are depicted in the high/medium marsh in all the previously mentioned classification methods, aside from RF (**Figure 4.7g** and **Figure 4.8g**). Lastly, the ML (**Figure 4.7f** and **Figure 4.8f**) did not classify most of the pixels, only having three labels in Bias (Ground, *Limoniastrum monopetalum*, and water) and two in Olhão (Ground and *Limoniastrum monopetalum*). With those results, the RF was selected as the preferred supervised method for subsequent analyses.

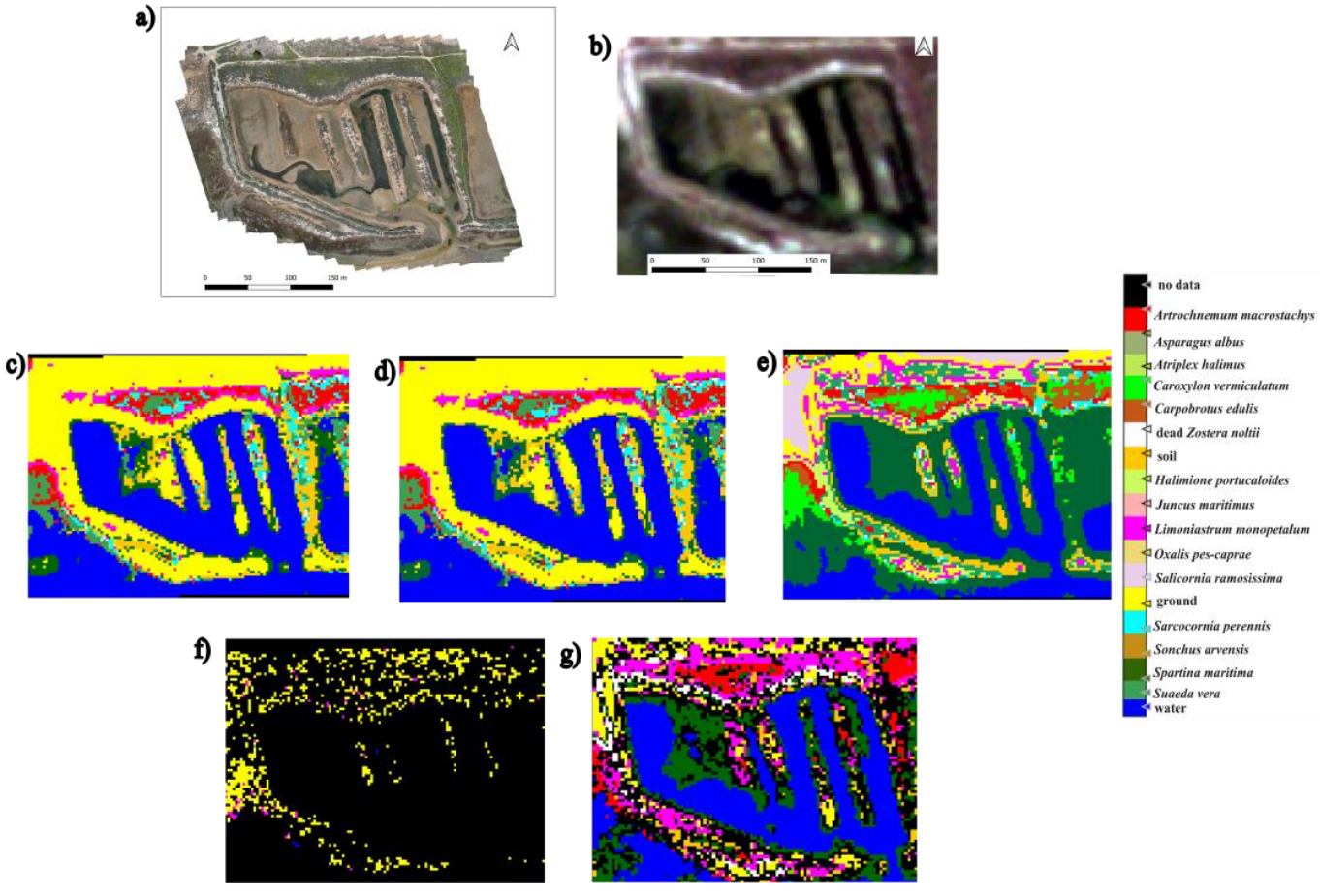

Figure 4.7. Comparison between supervised classifications derived from the spring fieldwork campaign in the Bias rewilded salt marsh. To facilitate comparison, panel **a)** presents a DJI P4 drone image, and panel **b)** displays the SuperDove satellite image from spring. The classification outputs include a **c)** KNN classification, **d)** KD-KNN classification, **e)** MD classification, **f)** ML classification, and **g)** RF classification.

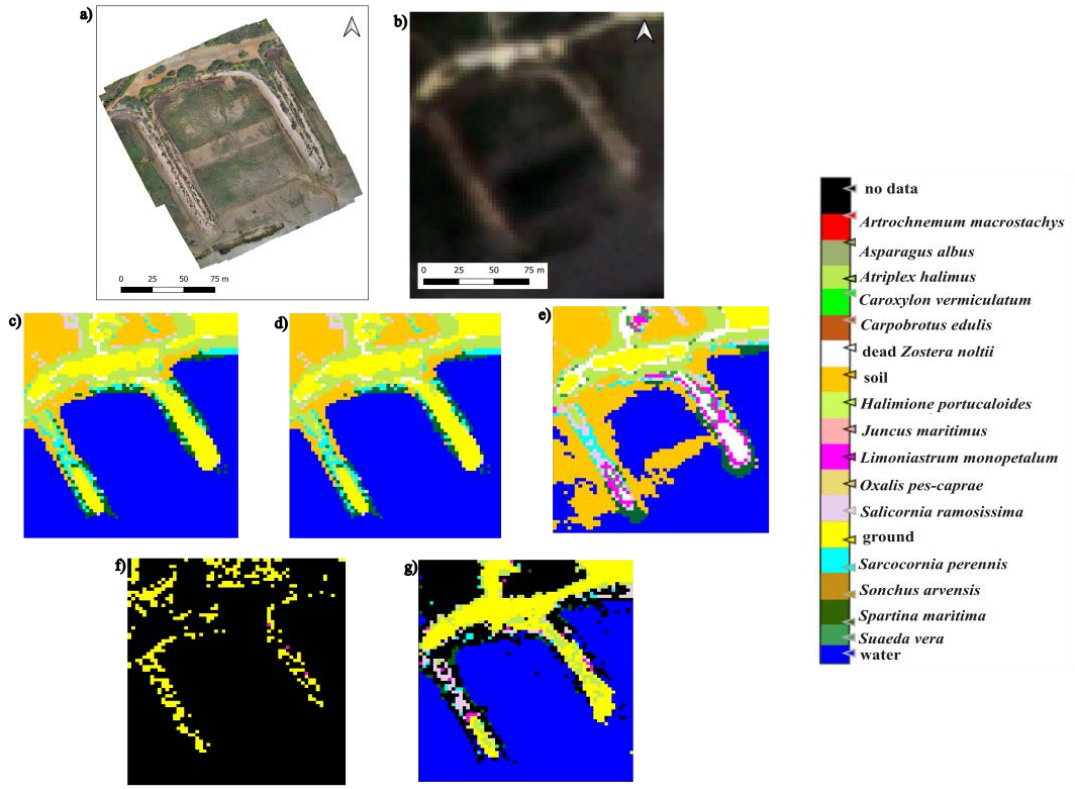

Figure 4.8. Comparison between supervised classification methods derived from the spring fieldwork campaign in the Olhão rewilded salt marsh. To facilitate comparison, panel **a)** presents a DJI P4 drone image, and panel **b)** displays the SuperDove satellite image from spring. The classification outputs include a **c)** KNN classification, **d)** KD-KNN classification, **e)** MD classification, **f)** ML classification, and **g)** RF classification.

4.3.2. Random Forest imagery classifications using the plot areas (RF-PA)

During fieldwork, 17 distinct plant species and other features, such as soil and water, were identified and used as training samples in Bias (**Appendix B, Table B1**). However, the produced RF classification images of the area close to the plots (RF-PA) portrayed only five classes in the spring (**Figure 4.9c**), seven classes in the summer (**Figure 4.9d**), eight classes in the autumn (**Figure 4.9e**), and ten classes in the winter (**Figure 4.9f**). The RF-PA classification was unable to accurately differentiate the zonation of plant species, with high marsh species such as *Limoniastrum monopetalum* (represented by the pink class - **Figure 4.7** to **Figure 4.16**), *Artrochnemum macrostachys* (red class - **Figure 4.7** to **Figure 4.16**), and *Caroxylon vermiculatum* (green class - **Figure 4.7** to **Figure 4.16**) (**Appendix B, Table B1**) being misclassified as low marsh species (**Figure 4.9c, Figure 4.9e,** and **Figure 4.9f**). A significant number of species identified during fieldwork within

the plots were not correctly classified by the RF methods, likely due to an insufficient number of training samples for the algorithm. Additionally, the spatial resolution of the satellite imagery, with each pixel representing a 3x3m area, may have contributed to the difficulty in accurately classifying individual plant species in areas with high species diversity and overlap.

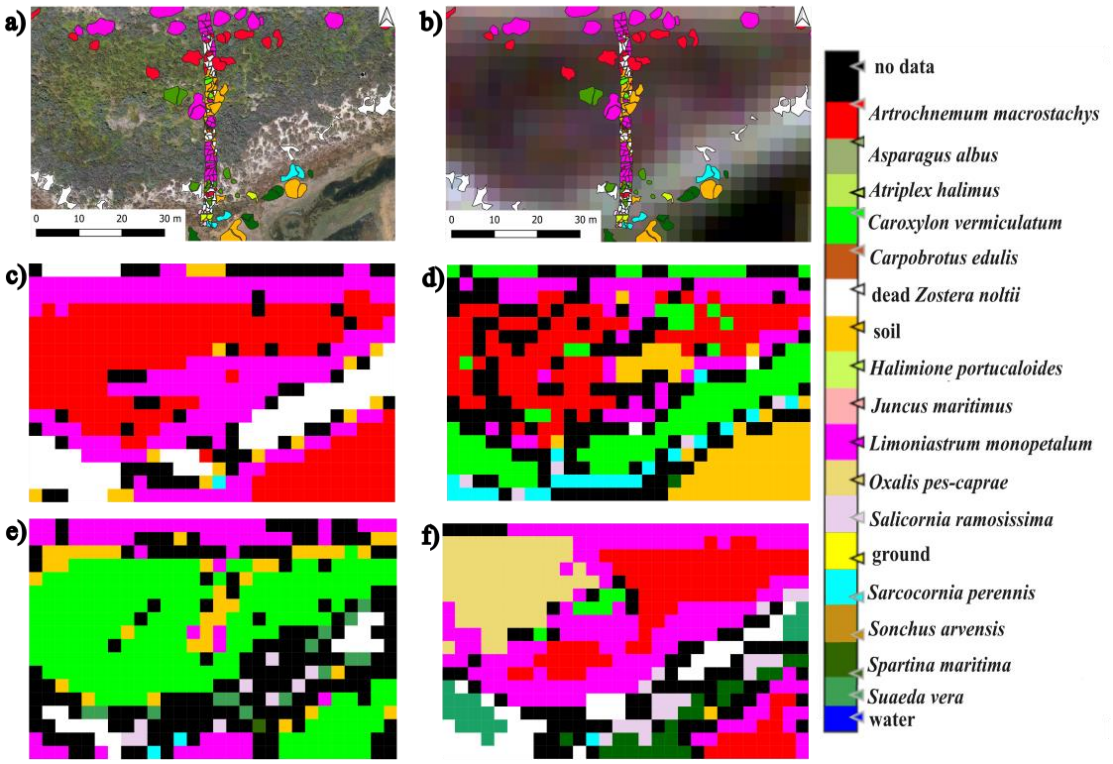

Figure 4.9. Supervised RF-PA classifications for the Bias rewilded salt marsh. To facilitate comparison, panel **a)** presents a DJI P4 drone image, and panel **b)** displays the SuperDove satellite image from spring. The RF-PA classification outputs include the **c)** spring, **d)** summer, **e)** autumn, and **f)** winter images.

In Olhão, 13 plant species and other features were identified during fieldwork and used as training samples (**Appendix B, Table B1**). The obtained RF-PA classifications resulted in five classes in spring (**Figure 4.10c**), nine classes in summer (**Figure 4.10d**), seven classes in autumn (**Figure 4.10e**), and four classes in winter (**Figure 4.10f**). The produced classifications could not accurately reproduce the vegetated areas and frequently led to misclassification of the plant species in the incorrect zonation of the salt marshes. For instance, in autumn (**Figure 4.10e**), the RF-PA classification incorrectly assigned *Caroxylon vermiculatum* (green class - **Figure 4.7** to **Figure 4.16**) to the low marsh zone.

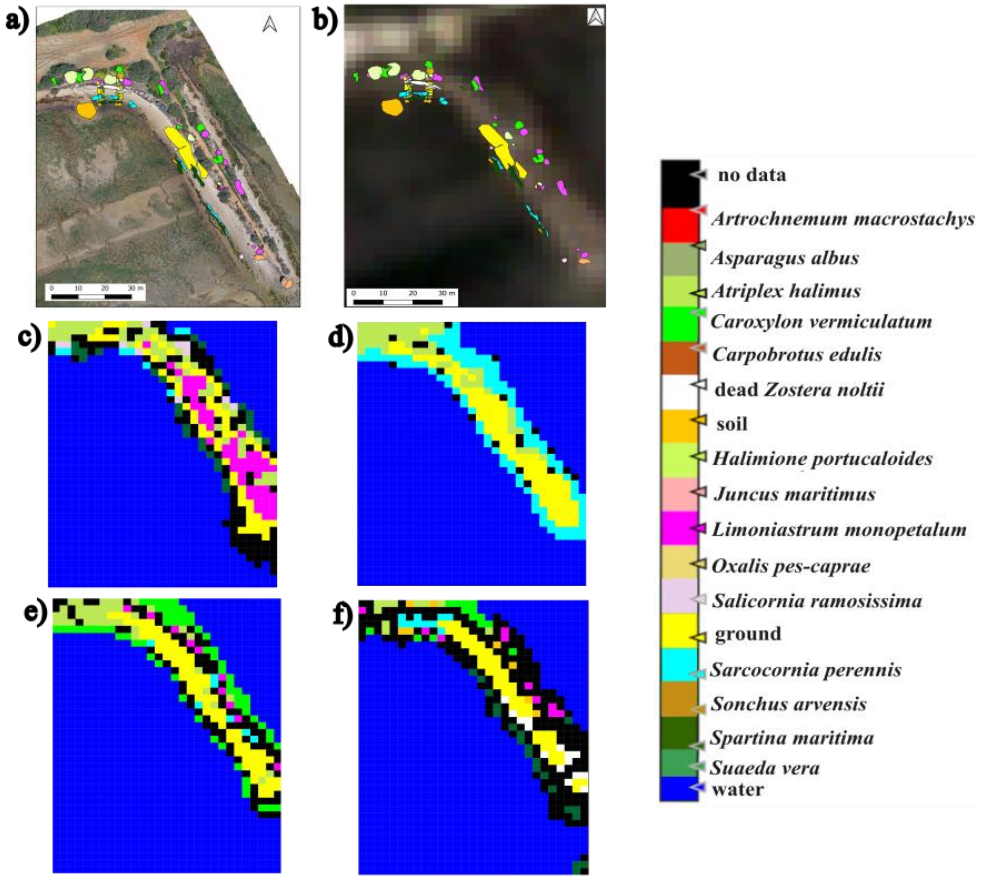

Figure 4.10. Supervised RF-PA classifications for the Olhão rewilded salt marsh. To facilitate comparison, panel **a)** presents a DJI P4 drone image, and panel **b)** displays the SuperDove satellite image from spring. The RF-PA classification outputs include the **c)** spring, **d)** summer, **e)** autumn, and **f)** winter images.

4.3.3. Random Forest imagery classification using the entire salt marsh area (RF-EA)

When applying the RF classification to the entire salt marsh area (RF-EA) at The Bias ROI, out of the 17 different plant species and other features encountered in the fieldwork campaigns, the resulting classifications produced eleven classes in spring (**Figure 4.11c**), twelve classes in summer (**Figure 4.11d**), eleven classes in autumn (**Figure 4.11e**), and eleven classes in winter (**Figure 4.11f**). Compared with the classification obtained using only the plot areas (RF-PA), RF-EA had an increase in the number of classes across all seasons. The RF-EA classification effectively discriminated several key features, including artificial walking paths in the upper part of the images, the flooding zone, and vegetated areas, with most plant species accurately classified within their respective marsh zonation (**Figure 4.11**). Seasonal variations can be seen in the classifications, such as the variations of *Limoniastrum monopetalum* (pink class), which

corresponds to its flowering season (**Appendix B, Table B1**), with a higher number of classes in spring (**Appendix C, Figure C1a**).

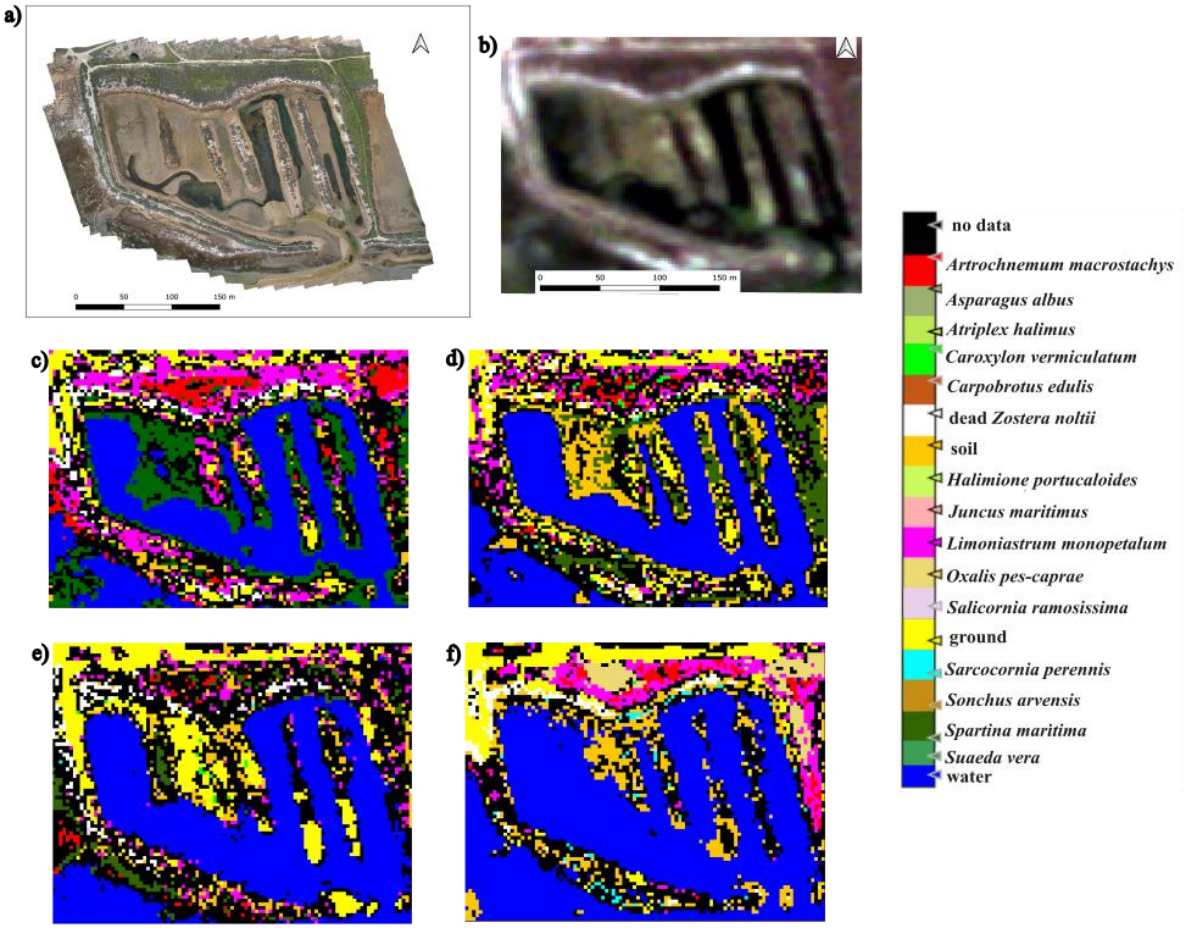

Figure 4.11. Supervised RF-EA classifications for the Bias rewilded salt marsh. To facilitate comparison, panel **a)** presents a DJI P4 drone image, and panel **b)** displays the SuperDove satellite image from spring. The RF-EA classification outputs include the **c)** spring, **d)** summer, **e)** autumn, and **f)** winter images.

In the Olhão ROI, the RF-EA classifications produced six classes in spring (**Figure 4.12c**), eight classes in summer (**Figure 4.12d**), seven classes in autumn (**Figure 4.12e**), and six classes in winter (**Figure 4.12f**). These results reflect an increase in the number of classes compared to the RF-PA imagery classifications (**Figure 19**). During the spring (**Figure 4.12c**) and summer (**Figure 4.12d**), the produced classification allows us to distinguish the primary features of the ROI, including artificial pathways, flooding areas, and vegetated zones. However, in autumn (**Figure 4.12e**) and winter (**Figure 4.12f**), significant misclassifications were observed, particularly in the depiction of ground in autumn and the classification of *Caroxylon vermiculatum* (green class) in winter.

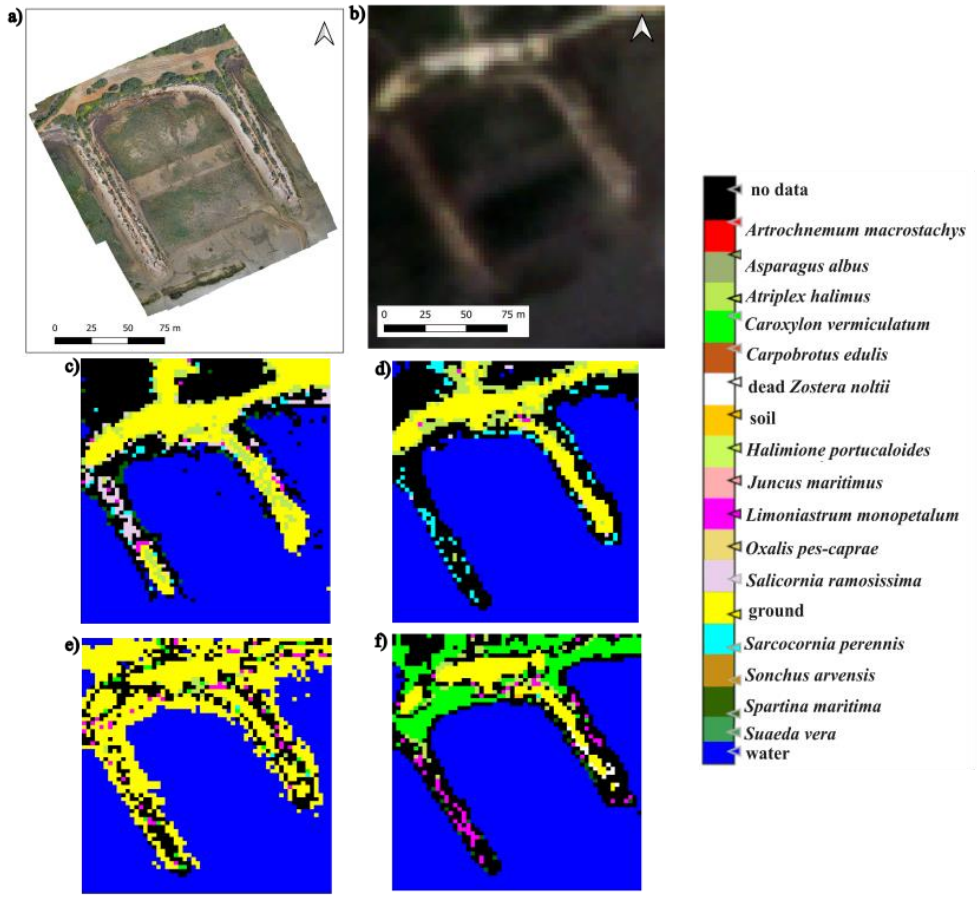

Figure 4.12. Supervised RF-EA classifications for the Olhão rewilded salt marsh. To facilitate comparison, panel **a)** presents a DJI P4 drone image, and panel **b)** displays the SuperDove satellite image from spring. The RF-EA classification outputs include the **c)** spring, **d)** summer, **e)** autumn, and **f)** winter images.

4.3.4. Random Forest imagery classification with a composite of data from all seasons, using the plot areas (RF-AC-PA)

The produced classifications close to the plot areas with a composite of the data acquired throughout the fieldwork campaigns (RF-AC-PA) in Bias resulted in nine classes in summer (**Figure 4.13c**), seven classes in autumn (**Figure 4.13d**), and ten classes in winter (**Figure 4.13e**). In Olhão, it resulted in seven classes in winter (**Figure 4.14c**), seven classes in spring (**Figure 4.14d**), and nine classes in summer (**Figure 4.14e**). Despite the increase in training samples, the classification images failed to accurately delineate the plant species zonation, having, in many cases, species from the high marsh in the low marsh, such as *Limoniastrum monopetalum* in autumn and winter from Bias (**Figure 4.13d** and **Figure 4.13e**, respectively).

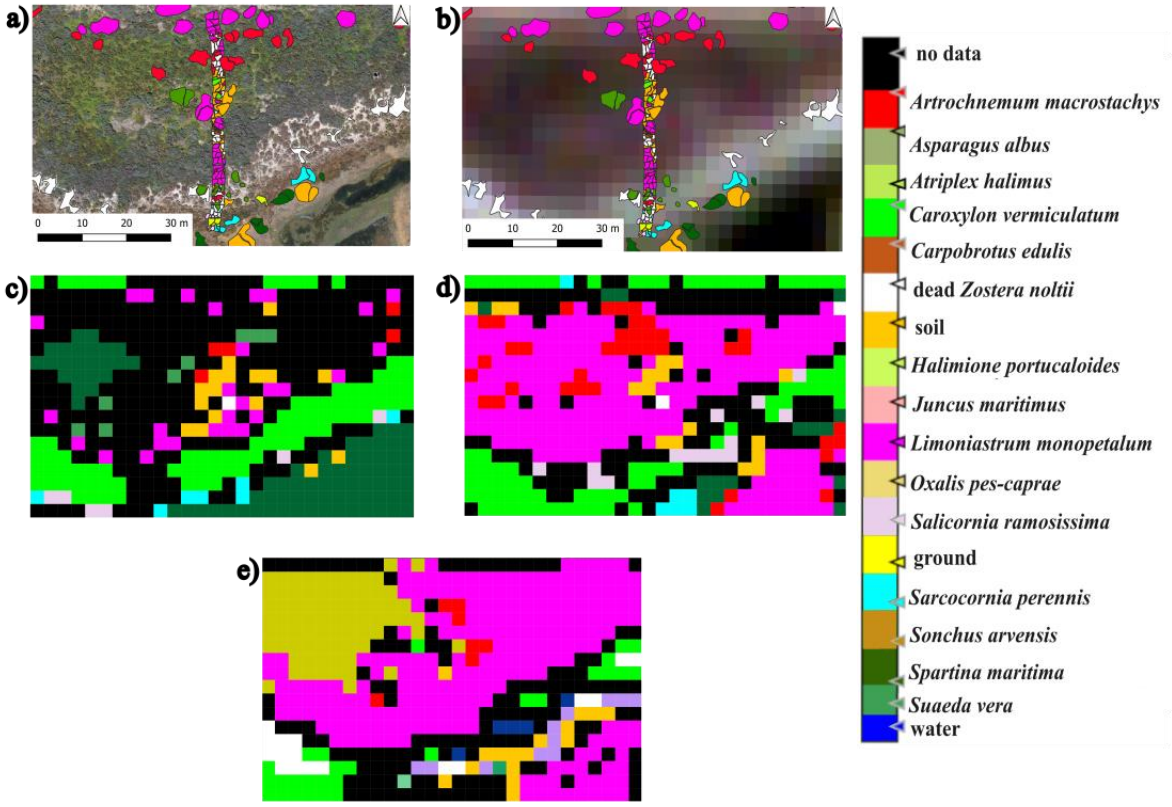

Figure 4.13. Supervised RF-AC-PA classifications for the Bias rewilded salt marsh. To facilitate comparison, panel **a)** presents a DJI P4 drone image, and panel **b)** displays the SuperDove satellite image from spring. The RF-AC-PA classification outputs include the **c)** summer, **d)** autumn, and **e)** winter images.

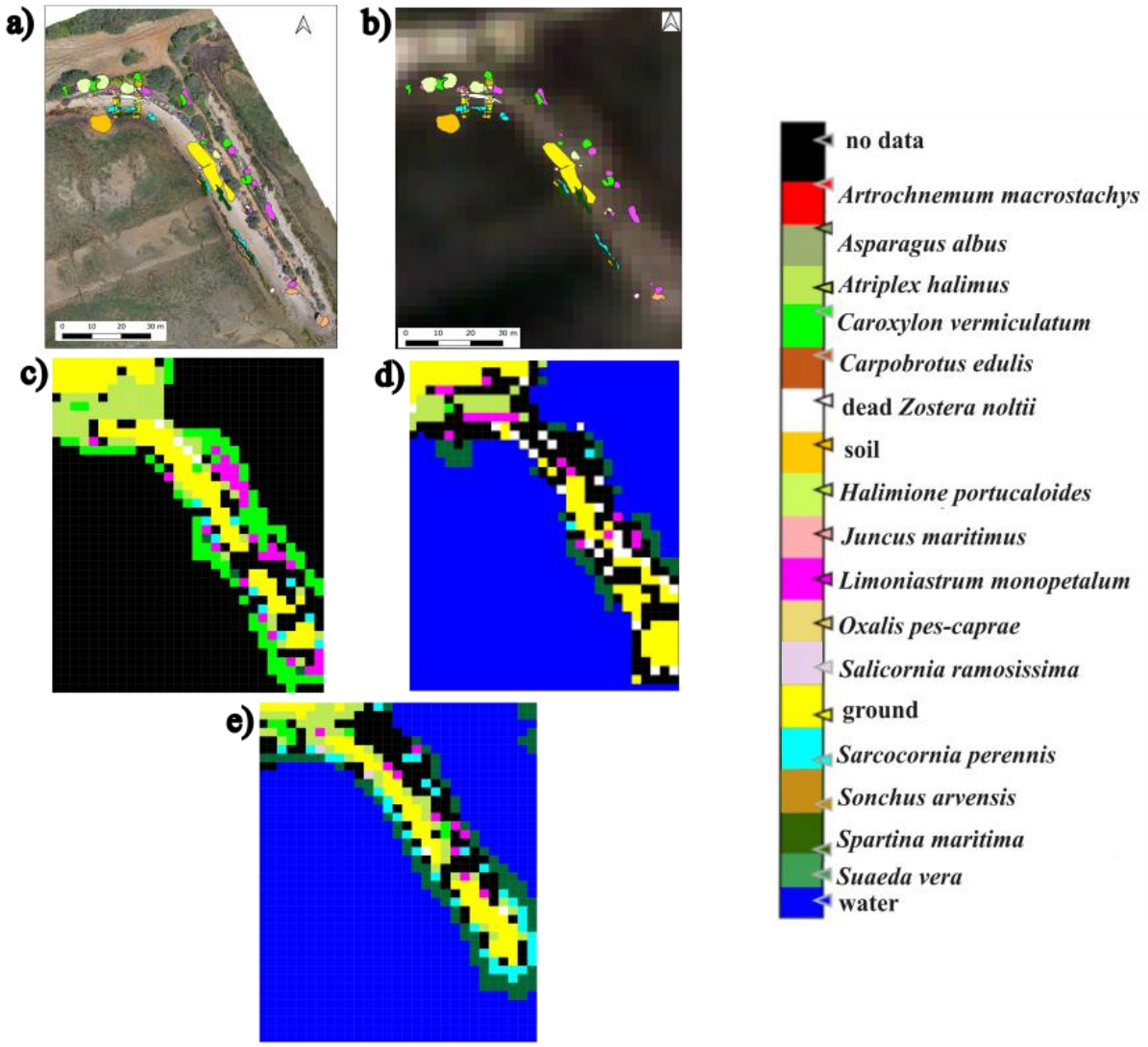

Figure 4.14. Supervised RF-AC-PA classifications for the Olhão rewilded salt marsh. To facilitate comparison, panel **a)** presents a DJI P4 drone image, and panel **b)** displays the SuperDove satellite image from spring. The RF-AC-PA classification outputs include the **c)** winter, **d)** spring, and **e)** summer images.

4.3.5. Random Forest imagery classification with a composite of data from all seasons, using the entire salt marsh area (RF-AC-EA)

The classifications of the entire ROIs using a composite of data (RF-AC-EA) had significantly improved results compared to the previous classifications, having a better distribution of the classes throughout the images. In Bias, the RF-AC-EA method produced ten classes in summer (**Figure 4.15c**), twelve classes in autumn (**Figure 4.15d**), and fourteen classes in winter (**Figure 4.15e**). In Olhão, the classifications identified six classes in winter (**Figure 4.16c**), eight classes in spring (**Figure 4.16d**), and nine classes in summer (**Figure 4.16e**). The RF-AC-EA method displayed improved classification

skills, effectively distinguishing the main features from the salt marshes and accurately displaying the correct zonation of most plant species. However, due to the composite nature of the data—incorporating information from multiple seasons—an analysis of seasonal variation is not feasible within this classification method.

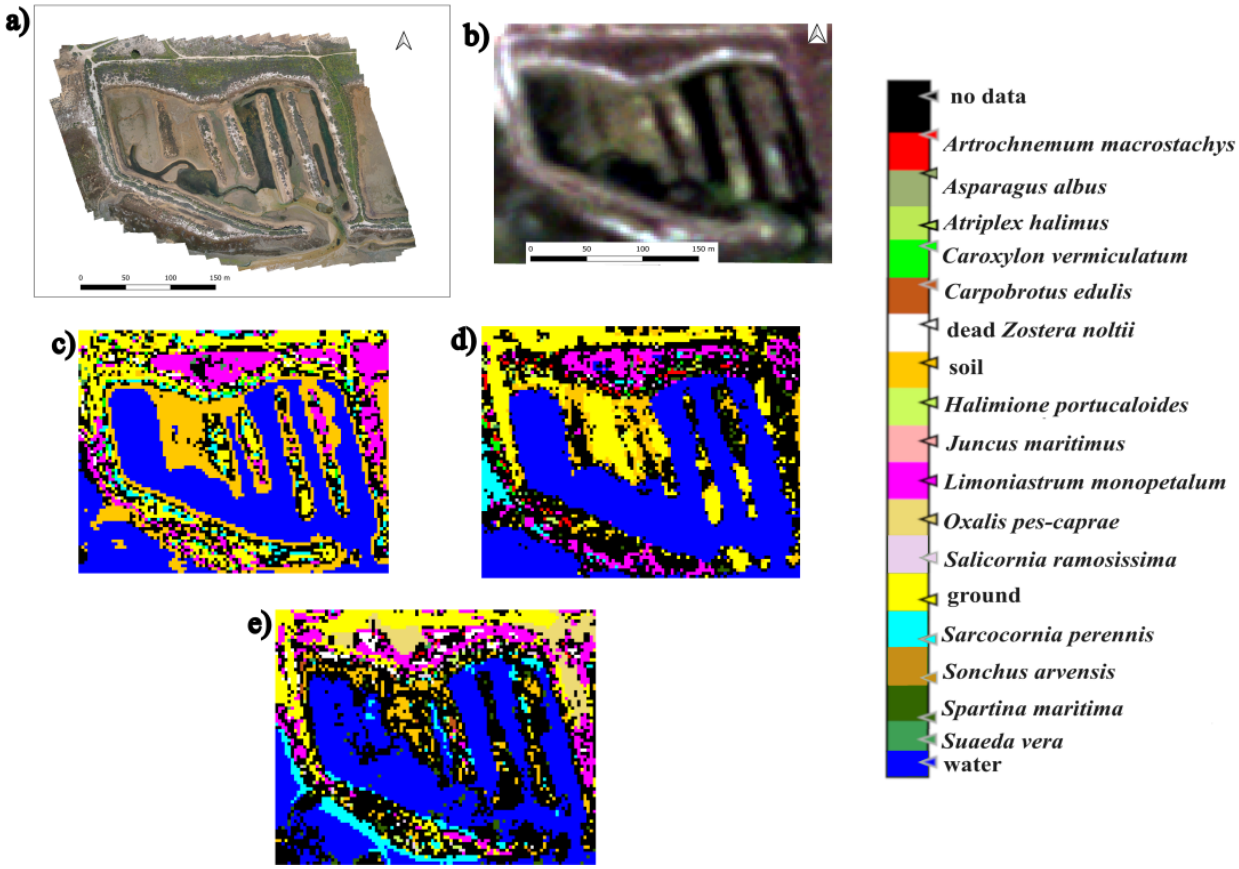

Figure 4.15. Supervised RF-AC-EA classifications for the Bias rewilded salt marsh. To facilitate comparison, panel **a)** presents a DJI P4 drone image, and panel **b)** displays the SuperDove satellite image from spring. The RF-AC-EA classification outputs include the **c)** summer, **d)** autumn, and **e)** winter images.

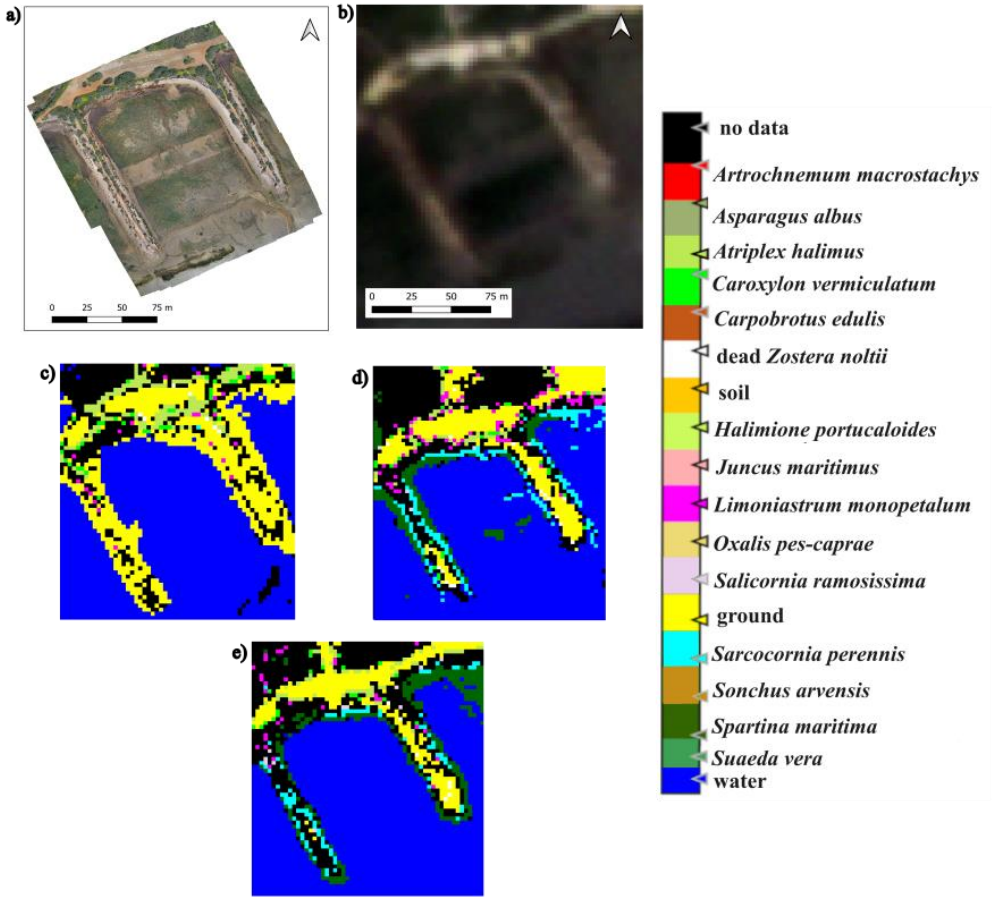

Figure 4.16. Supervised RF-AC-EA classifications for the Olhão rewilded salt marsh. To facilitate comparison, panel **a)** presents a DJI P4 drone image, and panel **b)** displays the SuperDove satellite image from spring. The RF-AC-EA classification outputs include the **c)** winter, **d)** spring, and **e)** summer images.

4.3.6. Accuracy of the applied models/algorithms of imagery classification

To better understand the results from the classification images, their accuracies and RMSEs were acquired. RF had the most satisfactory values in both ROIs, having the best agreement between what was observed in the field and what was predicted in the mapping. It yielded an average accuracy of 83.64% in Bias and 80.28% in Olhão, together with an average RMSE of 2.36 in Bias and 2.06 in Olhão (**Table 4.1**). In contrast, other supervised methods had much lower accuracies and RMSE values, with, on average, ML having 7.48% (Bias) and 9.09% (Olhão) accuracies and RMSE of 6.32 (Bias) and 6.11 (Olhão), MD with 17.64% (Bias) and 18.72% (Olhão) accuracies and RMSE of 11.26 (Bias) and 6.06, KNN 40.10% (Bias) and 41.18% (Olhão) accuracies and RMSE of 4.09 (Bias) and 4.79 (Olhão), and finally KD-KNN with of 43.85% (Bias) and 41.71% (Olhão) accuracies and RMSE of 3.83 (Bias) and 4.69 (Olhão) (**Table 4.1**).

The average accuracies and RMSEs from the RF classifications confirm the previous analysis, which shows that the best methodology was using a composite of data and the entire area of the salt marshes (RF-AC-EA) (**Table 4.2**). This methodology had the highest accuracy in both areas (average of 88.28% in Bias and 73.81% in Olhão) and low RMSE (average of 2.09 in Bias and 1.74 in Olhão (**Table 4.2**). In contrast, the methodology with the least satisfactory values was the RF-AC-PA, with an average accuracy of 27.86% in Bias and 51.71% in Olhão and low RMSE with 4.09 in Bias and 2.46 in Olhão (**Table 4.2**). Despite RF-AC-EA having the best average values, RF-EA still demonstrated satisfactory values, having accuracies above 50% and RMSEs close to 2. The average accuracies and RMSEs were similar to those achieved by RF-AC-EA. Even without the composite data, RF-PA generally showed, in general, slightly superior values than RF-AC-PA, even having satisfactory values (accuracy above 50% and RMSEs close to 2) in most classifications from Olhão (**Table 4.2**).

Table 4.1. Accuracy and RMSE for the applied supervised classification methods. The values presented are for both studied ROIs and from the spring campaign.

	Bias		**Olhão**	
Seasons	**Accuracy (%)**	**RMSE**	**Accuracy (%)**	**RMSE**
KNN	40.10	4.09	41.18	4.79
KD-KNN	43.85	3.83	41.71	4.69
MD	17.64	11.26	18.72	6.06
ML	7.48	6.32	9.09	6.11
RF	83.64	2.36	80.28	2.06

Table 4.2. Accuracy and RMSE for the applied classification methodologies using RF. The values presented are for both studied ROIs and all surveyed seasons.

		Bias		Olhão	
	Seasons	**Accuracy (%)**	**RMSE**	**Accuracy (%)**	**RMSE**
RF-PA	spring	47.61	3.01	54.16	3.58
	summer	20.00	4.52	67.85	1.34
	autumn	21.73	3.54	56.00	2.23
	winter	34.37	4.18	44.82	3.88
	Average	**30.93**	**3.81**	**55.71**	**2.76**
RF-EA	spring	83.64	2.36	80.28	2.06
	summer	83.69	2.12	82.60	1.04
	autumn	84.59	1.80	82.60	1.70
	winter	84.87	1.97	50.00	4.09
	Average	**84.20**	**2.06**	**73.87**	**2.22**
RF-AC-PA	spring	-	-	51.16	2.49
	summer	10.00	3.57	52.50	2.52
	autumn	30.00	4.33	-	-
	winter	43.59	4.38	51.51	2.36
	Average	**27.86**	**4.09**	**51.72**	**2.46**
RF-AC-EA	spring	-	-	74.79	1.93
	summer	90.54	1.54	69.56	1.71
	autumn	89.26	1.97	-	-
	winter	85.06	2.76	77.08	1.60
	Average	**88.28**	**2.09**	**73.81**	**1.74**

4.4. Analysis of the spectral signatures of the plots

For the initial analysis, three plots that represented each zonation of the salt marshes were chosen, more specifically, plots 1, 6, and 15 in Bias (**Table 4.3**) and plots 1, 3, and 6 in Olhão (**Table 4.4**). Throughout all the plots, the spectral signature shapes in both rewilded salt marshes vary considerably, not only due to the inter-species mixed communities inside them but also because of the seasonal variation of all the plants, such as plants drying in summer and flowering in spring.

In general, the spectral signatures had peaks close to the red edge and near infra-red (NIR) (between 705 nm and 865 nm), typical for plant species, and another peak in the yellow (610 nm) (**Table 4.3** and **Table 4.4**). In winter, the values in the near infra-red (865 nm) had a sudden peak compared to the other seasons, depicted as the blue lines in **Table 4.3** and **Table 4.4**. This increase in the NIR reflectance occurred due to the proliferation of the species *Oxalis pes-caprae* in the Bias rewilded salt marsh, appearing from plots 1 to 12 (**Appendix D, Table D1**). Since this species dominated in coverage and height compared to the other salt marsh species, reflectance during winter was more pronounced due to these species having a strong signal compared with the other vegetation, particularly the NIR bands. In Olhão (**Table 4.4** and **Appendix D, Table D2**), the reflectance values do not vary considerably, displaying peaks close to the red edge and NIR (between 705 nm and 865 nm).

In each fieldwork campaign, the composition of plant species within each plot changed (**Appendix D, Table D1** and **Table D2**). This occurred due to various factors such as plants dying, new growth overlapping existing species, or errors in the plot setup. However, the variations in the spectral signature do not follow a predictable pattern based on the percentage of plant species. This is evident when looking at **Table 4.3**, Plot 1, where similar percentages of *Artrochnemum macrostachys* and *Limoniastrum monopetalum* in different seasons (e.g., summer and autumn or spring and winter, respectively) have completely different reflectance values and patterns in the spectrum shape. Also, spring has a similar spectrum shape to summer despite the completely different plant percentages.

Table 4.3. Spectral signatures of plant species inside three plots of Bias in the high marsh (Plot 1), medium marsh (Plot 6), and low marsh (Plot 15). The wavelengths range from 443 nm (Blue) to 865 nm (Near-infrared). The percentages of plant species inside each plot for all seasons are shown with the spectral signature. The percentage of the plant species was calculated using the pixel where the spectral signature was extracted as the total area, using the contours of the plant species to calculate the percentage inside the pixel in QGIS.

Plot		Plant species	Spectral signatures
1	spring	*Limoniastrum monopetalum* (96.8%) Soil* (3.72%)	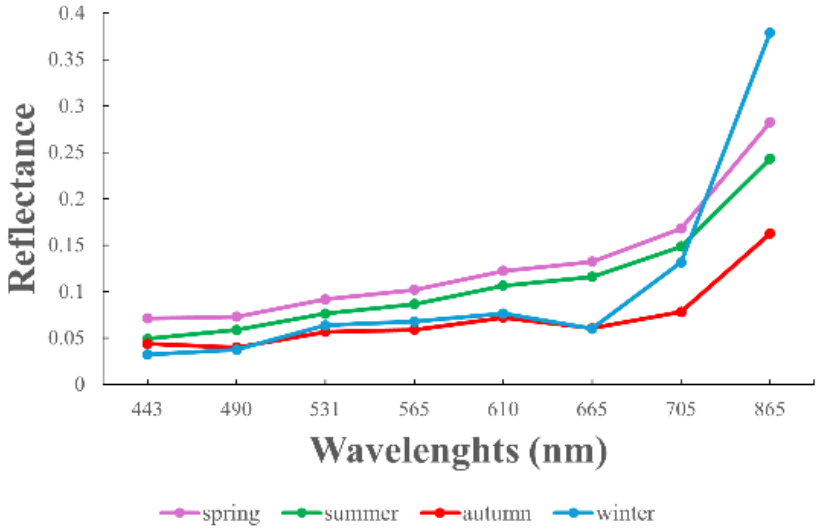
	summer	*Artrochnemum macrostachys* (68.71%) *Limoniastrum monopetalum* (25.64%) Soil* (5.65%)	
	autumn	*Artrochnemum macrostachys* (63.99%) *Limoniastrum monopetalum* (19.96%) Soil* (16.05%)	
	winter	*Limoniastrum monopetalum* (88.52%) *Oxalis pes-caprae* (11.48%)	

6	**spring**	*Artrochnemum macrostachys* (3.89%)
		Caroxylon vermiculatum (20%)
		Soil* (76.11%)
	summer	*Limoniastrum monopetalum* (17.61%)
		Caroxylon vermiculatum (0.66%)
		Soil* (81.74%)
	autumn	*Limoniastrum monopetalum* (1.19%)
		Caroxylon vermiculatum (1.85%)
		Soil* (96.96%)
	winter	*Artrochnemum macrostachys* (16.35%)
		Oxalis pes-caprae (83.65%)

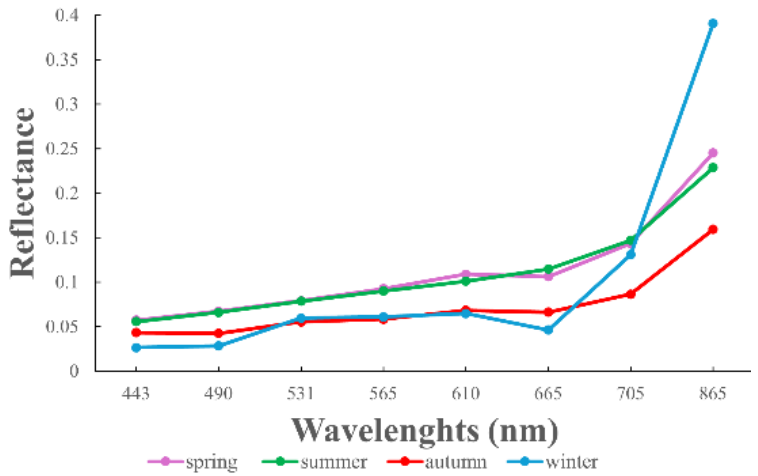

15	**spring**	*Suaeda vera* (12.42%)
		Sarcocornia perennis (4.49%)
		Halimione portucaloides (2.66%)
		Salicornia ramosissima (20.26%)
		Dead *Zostera noltii* (60.18%)
	summer	Soil* (55.65%)
		Sarcocornia perennis (42.68%)
		Spartina maritima (1.67%)
	autumn	Soil* (6.11%)
		Sarcocornia perennis (0.3%)
		Halimione portucaloides (3.16%)
		Salicornia ramosissima (90.43%)
	winter	Soil* (1.35%)
		Suaeda vera (8.11%)
		Sarcocornia perennis (11.97%)
		Salicornia ramosissima (20.76%)
		Dead *Zostera noltii* (57.81%)

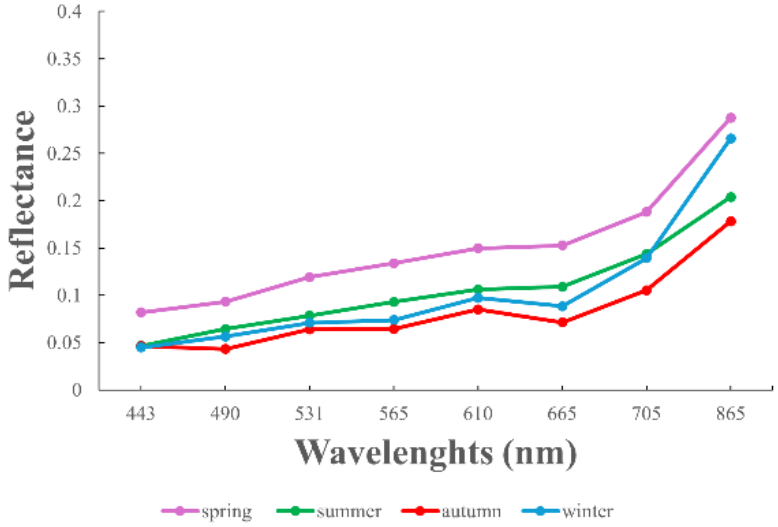

*Soil = General sediment **Ground = Artificial walking paths or sand

Table 4.4. Spectral signatures of plant species inside three plots of Olhão in the high marsh (Plot 1), medium marsh (Plot 6), and low marsh (Plot 15). The wavelengths range from 443 nm (Blue) to 865 nm (Near-infrared). The percentages of plant species inside each plot for all seasons are shown with the spectral signature. The percentage of the plant species was calculated using the pixel where the spectral signature was extracted as the total area, using the contours of the plant species to calculate the percentage inside the pixel in QGIS.

Plot		Plant species	Spectral signatures
1	**spring**	*Limoniastrum monopetalum* (17.45%) *Atriplex halimus* (71.36%) Ground** (11.19%)	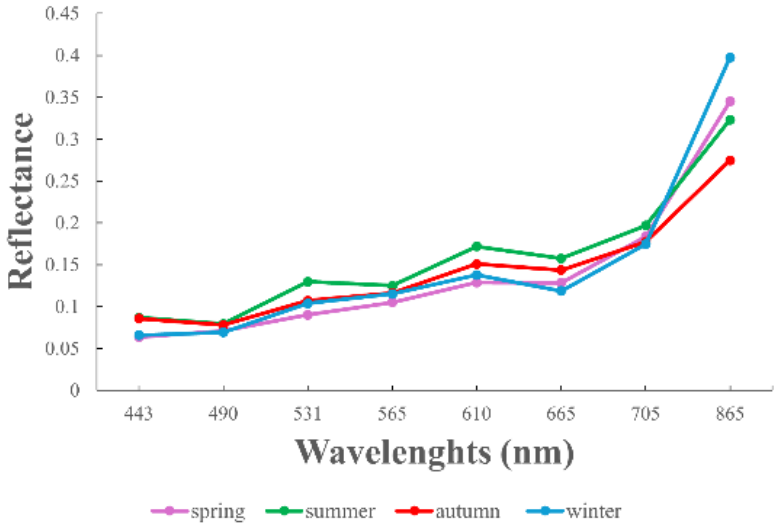
	summer	*Limoniastrum monopetalum* (36.03%) *Atriplex halimus* (36.31%) Ground** (27.66%)	
	autumn	*Limoniastrum monopetalum* (19.97%) *Caroxylon vermiculatum* (0.49%) *Atriplex halimus* (79.54%)	
	winter	*Limoniastrum monopetalum* (11.37%) Ground** (5.62%) *Atriplex halimus* (28.78%) *Oxalis pes-caprae* (54.23%)	

3	**spring**	Dead *Zostera noltii (66.56%)*
		Ground** (33.44%)
	summer	*Sarcocornia perennis* (15.49%)
		Salicornia ramosissima (0.43%)
		Dead *Zostera noltii* (75.21%)
		Ground** (8.87%)
	autumn	Dead *Zostera noltii (42.06%)*
		Ground** (57.94%)
	winter	Dead *Zostera noltii (77.45%)*
		Ground** (22.55%)

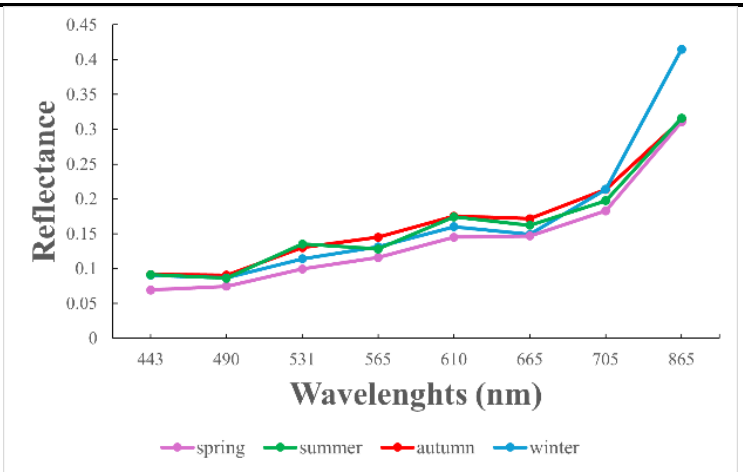

6	**spring**	Ground** (1.96%)
		Sarcocornia perennis (9.93%)
		Spartina maritima (74.38%)
		Soil* (13.73%)
	summer	Ground** (5.68%)
		Sarcocornia perennis (13.15%)
		Spartina maritima (51.18%)
		Soil* (29.99%)
	autumn	*Sarcocornia perennis* (52.66%)
		Salicornia ramosissima (4.17%)
		Ground** (43.17%)
		Spartina maritima (4.38%)
	winter	Soil* (27.51%)
		Ground** (4.15%)
		Sarcocornia perennis (5.88%)
		Spartina maritima (62.47%)

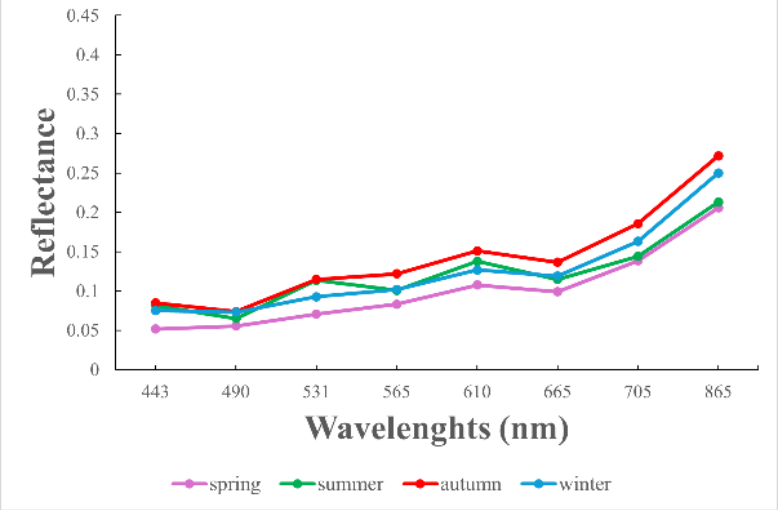

*Soil = General sediment **Ground = Artificial walking paths or sand

5. Discussion

5.1. Application of imagery classification methods to study rewilded salt marshes

Significant differences in characteristics are observed when comparing the salt marshes in this study, mainly in their vegetation density and sediment characteristics. The Bias rewilded salt marsh (**Figure 3.1c**) presents much denser and more diverse vegetation than Olhão (**Figure 3.1d**). The Olhão ROI has a vast portion of its area covered by sand and is in an earlier stage of the rewilding process (**Appendix A**, **Figure A2**). Even with those differences, the classifications in both rewilded salt marshes had similar behaviour, showing that this methodology can be used in different locations. The EM cluster unsupervised classification method managed to classify/reproduce the main features in the analysed salt marsh (**Figure 4.5** and **Figure 4.6**), as well as the seasonal variations. So, if a management project cannot have fieldwork campaigns, the EM cluster can be helpful in visualising general seasonal and zonation variations in rewilded salt marshes. The current study found that among the tested supervised classification methods, Random Forest (RF) was the most effective classification method (better model skill) when using 3m resolution SuperDove satellite images. KNN, KD-KNN, and MD portrayed multiple misclassifications, and ML only classified three features out of seventeen (ground, water, and *Limoniastrum monopetalum*). In contrast, RF correctly portrayed the main features of the salt marsh and classified most of the plant species. The robustness of RF outperformed other supervised classification methods and was consistent with findings from previous research (Belgiu & Drăgu, 2016; Breiman, 2001; Rodriguez-Galiano et al., 2012). RF classification can classify up to the species level, better displaying the zonation and seasonal variations in the areas than the EM cluster classification images (**Figure 4.5** and **Figure 4.6**).

Applying RF classification for the entire salt marsh area using the composite of training samples (RF-AC-EA) provided the best classification images compared to the other RF methods from this work. It denoted the most realistic distribution of the plant species' classes in each zone (**Figure 4.15** and **Figure 4.16**) and accuracies around 80%. However, because of the composite of data throughout the seasons, this method is not

ideal for the vegetation seasonal analysis. Creating a classification with a composite of data using only the area close to the plots (RF-AC-PA) gave unsatisfactory results (**Figure 4.13** and **Figure 4.14**). RF-AC-PA had, on average, the lowest accuracy in both ROIs, with accuracies close to 30% in Bias and 50% in Olhão (**Table 4.2**). When comparing the results between the ROIs, the RF classifications obtained for Olhão using the plot areas - RF-PA and RF-AC-PA - denoted higher accuracies and lower RMSEs than Bias (**Table 4.2**). This is due to the size of the area used for the classification. The area used to classify the RF-PA in Olhão is almost half the size used for the entire area, while in Bias, the area used for RF-PA is almost five times smaller than the entire area used. In Olhão, the classifications that did not use a composite of data - RF-PA and RF-EA - had slightly higher accuracy averages than those with a composite of data - RF-AC-PA and RF-AC-EA - (**Table 4.2**). Therefore, this study suggests that to classify plant species over a larger ROI, using composite data that covers the entire area will yield the most satisfactory images. For smaller ROIs, using composite data is unnecessary, as it produces results similar to classifications without it. Additionally, analysing the entire area still provides better results than focusing solely on the specific areas where data was initially collected.

Although the images were captured during low tide, the algorithm classified a substantial portion of the images as water, with over 60% of the identified classes being water in many instances (**Appendix C**, **Figure C1** for Bias and **Figure C2** for Olhão). This misclassification may have resulted from the quality of the images, where darker imagery potentially influenced the performance of the algorithm, leading to an overestimation of water classes due to errors in the RF algorithm. To mitigate such errors, additional training samples from the mudflat area should have been collected, or a mask should be created in these areas so that they would not be classified. Not all the plant species encountered in the fieldwork campaigns were classified by RF. *Asparagus albus*, *Juncus maritimus*, and *Sonchus arvenis* were not classified in both ROIs. This possibly occurred due to the small number of training samples collected for this plant species or due to the limitations of the resolution of the satellite images. Some of these species did not have the minimum patch size to allow for adequate classification, being smaller than the original imagery resolution from SuperDove (3m). Using other missions with higher resolution, such as WoldView-2 (1.84m) and QuickBird (0.65m), could mitigate this error, managing to classify this plant species.

The primary features from the salt marshes classified by the RF algorithm across all methods included ground, soil, water, *Spartina maritima*, *Limoniastrum monopetalum*, and *Artrochnemum macrostachys* in Bias, as well as *Atriplex halimus* in Olhão, which collectively accounted for more than 50% in all classifications (**Appendix C**, **Figure C1** for Bias and **Figure C2** for Olhão). This indicates that, aside from *Spartina maritima*, the majority of the identified features were either non-plant species or plant species from the high marsh. A possible explanation for this is the higher density of plant species in the high marsh, making them easier for the RF algorithm to classify. In contrast, plant species from the lower marsh, such as *Sarcocornia perennis*, *Salicornia ramosissima*, and *Halimione portucaloides*, were classified in fewer instances, likely due to their lower density. While high marsh plant species were generally classified within their correct zonation, *Spartina maritima* and *Sarcocornia perennis* experienced frequent misclassification, with both sometimes being incorrectly assigned to the high marsh. This could have occurred due to errors in the algorithm or these species having similar spectral signatures to plant species from the high marsh. Despite these misclassifications, RF was the most effective method for analysing rewilded salt marshes. For examining seasonal variations, the use of RF across the entire region of interest (RF-EA) was the most effective approach, while for analysing zonation variations, the use of RF with a composite of data from all seasons (RF-AC-EA) was preferred.

Rummel et al. (2022) analysed seasonal variations in a restored wetland in Australia, also using RF and high-resolution satellite imagery. However, unlike this study, it did not classify the plant species, only the main features from the wetland (such as mangroves, salt marsh, and exposed soil). Regardless, its results also show that increasing training samples generally increases the classification accuracy and that RF is a great classification algorithm for seasonal analyses. However, Rummel et al. (2022) used images from Worldview-2, which have a higher resolution than the SuperDove images used in this work.

Belluco et al. (2006) mapped the plant species from a natural salt marsh using multiple satellite missions, namely ROSIS, CASI, and MIVIS with hyperspectral images, and IKONOS and QuickBird with multispectral images. Like the current study, unsupervised and supervised methods were used to classify the plant species. Belluco et al. (2006) verified that spatial resolution affects classification accuracy much more significantly than spectral resolution. The coarsest multispectral data used in that work had a 3m

resolution, similar to SuperDove imagery. The K-means clustering algorithm was one of the employed classification methods to classify the plant species observed, being the colour manipulation of the labelled classes chosen through visual inspection of the generated map and comparison with reference data. However, this labelling of the classes could not be employed in this work due to the higher number of plant species analysed in the current study and the mixture of plant species being the focus of the analyses. The ML classification method was also applied by Belluco et al. (2006). However, contrary to the classifications achieved by Belluco et al. (2006), the ML classifications from the current study gave the most unsatisfactory results, only classifying 3 out of the 17 possible features. This might have occurred due to errors in the algorithm or its implementation.

5.2. Influence of mixture of plant species in the salt marsh spectral signature

The spectral signature of vegetation in each ROI is influenced by the plant mixture, as seen by the variations in the percentages of plant species giving various spectral signature shapes (**Appendix D, Table D1** and **Table D2**). However, in most plots where the composition of the plants inside of them was similar, the spectral shapes were completely different, sometimes having not only different peaks in the spectral signature but also higher or lower values compared to similar plots. These variations occurred mainly on the green I (531nm), Yellow (610nm), red (665nm), red-edge (705nm), and NIR (865nm). An example of this was in **Table 4.3**, Plot 1, where the spectral shapes from summer and spring in Bias are similar, even though their composition of plant species is entirely different (summer was mainly composed of *Artrochnemum macrostachys*, and spring was almost entirely composed of *Limoniastrum monopetalum*). One of the possible reasons for this is that despite having a mixture of different plant species, they may be plants with very similar spectral signatures, making it impossible to differentiate them from a spectral point of view. This similarity in the spectral signatures between different plant species may occur mainly due to similarities in the biochemical composition of the plant species (Sims & Gamon, 2002).

These results show that patterns in the spectral signature in relation to the different mixtures of plant species cannot be made. Other factors influenced the spectral signatures, such as each species' chemistry (with different proportions of pigments, such as chlorophyll and carotenoids, each with their own reflectance), age, and biomass (Adam

et al., 2010; Isacch et al., 2006; Rajakumari et al., 2022; Silvestri et al., 2005). With those factors influencing the spectral signature, the specific influence of the mixture of plant species could not be analysed. This study did not took into consideration these factors due to the time limitations, only focusing on the mixture of the plant species. The spectral signature differentiation between plant species occurs across a wide range of wavelengths, highlighting the desirability of using high-resolution hyperspectral instruments for accurate species classification (Schmidt & Skidmore, 2003; Gao & Zhang, 2006)

Even though the influence of each plant species in the spectral signature could not be found, the spectral signature could be used to make seasonal and zonation analyses of the rewilded salt marshes. The spectral signature shapes from spring and summer in the Bias rewilded salt marsh have higher reflectance values than in autumn and winter (**Appendix D, Table D1**). This mainly occurs because the accuracy in seasons with less rain (summer and spring) is higher since the presence of water can contaminate the spectral signatures (Liu et al., 2015; Sinha et al., 2012; Xu et al., 2019). However, in Olhão, the highest values tended to be in autumn and winter (**Appendix D, Table D2**). Regarding the zonation, in Bias, the low marsh had higher reflectance values, followed by the medium marsh, then the high marsh with lower values (**Figure 5.1**); the possible reason for this is that the low marsh is less dense in vegetation than the other areas in the zonation, where sediment can be more visible in the images. This can be seen by the plots in the low marsh, which had the highest percentages of soil, having up to 50% coverage (**Appendix D, Table D1** and **Table D2**). In Olhão, the medium marsh had the highest reflectance values, followed by the high marsh, then the low marsh with lower values (**Figure 5.2**). The medium marsh in Olhão had the highest values mainly due to this area being mostly composed of sand, which is a highly reflective surface (Streck et al., 2003; Viallefont-Robinet et al., 2019).

Rajakumari et al., 2022 managed to create a catalogue for salt marsh plant species, viewing the main variations in the spectral signature shape and the specific peaks of each salt marsh plant species, analysing plant species with the same genus as some found in this work, such as the genus *Suaeda sp.* and *Salicornia sp.* The authors did not analyse areas with a mixture of plant species but only analysed singular canopies. Field hyperspectral spectroscopy was used to achieve the spectral signature from these plant species, not satellite remote sensing images. In comparison with Rajakumari et al. (2022),

this study shows that to fully understand the mixture of the plant species using satellite imagery, first, the spectral signature shape of each species needs to be acquired through field hyperspectral spectroscopy so that the analysis of the mixture of plant species can be done.

Gao & Zhang (2006) analysed the variations in the spectral signature of salt marsh plant species throughout the seasons. Unlike the current study, Gao & Zhang (2006) used field hyperspectral spectroscopy to achieve the spectral signatures, only analysed singular plants (and not a mixture of plant species) and did not analyse the value in winter. When comparing the results from Gao & Zhang (2006) with the results obtained in this study, it can be seen that the main variations from the plant species occurred after the visible light spectrum (approximately after 700nm), showing that to fully differentiate plant species using spectral signature, hyperspectral data is necessary. Since Gao & Zhang (2006) did not analyse the mixture of plant species, nor the same species analysed in this work, a comparison between its results and the results from this work is not feasible. However, Gao & Zhang (2006) state that "the seasonal differences in the spectral characteristics among the four main salt marsh communities were quite clear, which can be attributed to the phenology of each community type". This shows that the spectral signature seasonal analysis of salt marsh plant species is feasible, but more studies are needed to test the feasibility of using high-resolution satellite imagery for this analysis.

In sum, the influence of the mixture of plant species was found in the analysed rewilded salt marshes, but specific patterns on the spectral signature shape due to this mixture of plant species were not evident in the results. However, the spectral signature was found to be a valuable tool for visualising seasonal and zonation variations in rewilded salt marshes because it can easily be used to visualise these variations, seeing which seasons and zonation have the highest values and the possible variations. More research using multispectral satellite images is necessary to confirm the feasibility of inferring the spectral signature of plant species, especially in salt marshes. There is currently an insufficient number of studies in this area, and more investigation is needed for this type of analysis in these ecosystems.

5.3. Influence of sediment characteristics in the salt marsh spectral signature

When analysing the results, the influence of OM in the spectral signature in the ROIs cannot be evaluated due to its low values (green bars in **Figure 4.1** and **Figure 4.2**). However, the influence of the d_{50} and H_2O% could be seen in the spectral signature, mainly their variations throughout the zonation of the salt marshes. The high marsh in both salt marshes had high d_{50} with low H_2O%, while the low marsh had lower d_{50} and high H_2O%, and these variations can be seen in the spectral signature (**Figure 5.1** and **Figure 5.2**). A comparison of the two rewilded salt marshes reveals a significant difference in their reflectance patterns (**Figure 5.1** and **Figure 5.2**). In the Bias rewilded salt marsh, the highest reflectance values predominantly originate from the low marsh, as indicated by the green lines in **Figure 5.1**. On the other hand, in the Olhão rewilded salt marsh, the medium marsh exhibits the highest reflectance values, represented by the blue lines in **Figure 5.2**. This distinctive behaviour can be attributed to the sediment composition of the medium marsh in Olhão, which is mainly sandy (a highly reflective surface), whereas in Bias, it remains vegetated. Also, the spectral signature shapes of the low marsh in Bias are consistently the highest, whereas in Olhão, they are the lowest. This observation underscores the influence of sediment characteristics on spectral signatures, showing that similar sediment types (in this case, mud) with variations in H_2O%, OM and d_{50} will have different spectral signatures (Ben-Dor et al., 1999; Sharma et al., 2022; Stoner & Baumgardner, 1981; Streck et al., 2003; Viallefont-Robinet et al., 2019). With this, future studies can use the satellite imagery from SuperDove to distinguish the sediment composition patterns in rewilded salt marshes. A rewilded salt marsh where the spectral signature has the highest values in the low marsh likely has dense vegetation with less content of sand, whereas a rewilded salt marsh where the medium marsh has the highest values likely has less dense vegetation with more sand.

Dube et al. (2013) used field hyperspectral radiometry to create a graph with the spectral signature from intertidal sediment properties (**Figure 5.3a**). When comparing the results from Dube et al. (2013) (**Figure 5.3a**) with the results from this work (**Figure 5.3b** and **Figure 5.3c**), the spectral signatures have similar shapes, confirming that using SuperDove imagery, the spectral signature from the sediment in salt marshes can be correctly created. Using satellite data and focusing more on the sediment properties, Marchetti et al. (2022) used Sentinel-2 data to create the spectral signature of various

sediment classes. Converting the values from the current work, the d_{50} values ranged between 0.016 and 0.455mm, falling into the 0.1-0.5 mm class from the graph (**Figure 5.4a**). When comparing the spectral signature shape in the visible spectra (from 443 to 865) from the 0.1-0.5 mm class (**Figure 5.4a**) and the results from this work (**Figure 5.4b** and **Figure 5.4c**), the shape of the spectral signature from this work is much different, being lower than the one from Marchetti et al. (2022). This mainly occurred due to the influence of the H_2O%. An increase in the H_2O% can reduce the reflectance values, especially in the NIR (Streck et al., 2003).

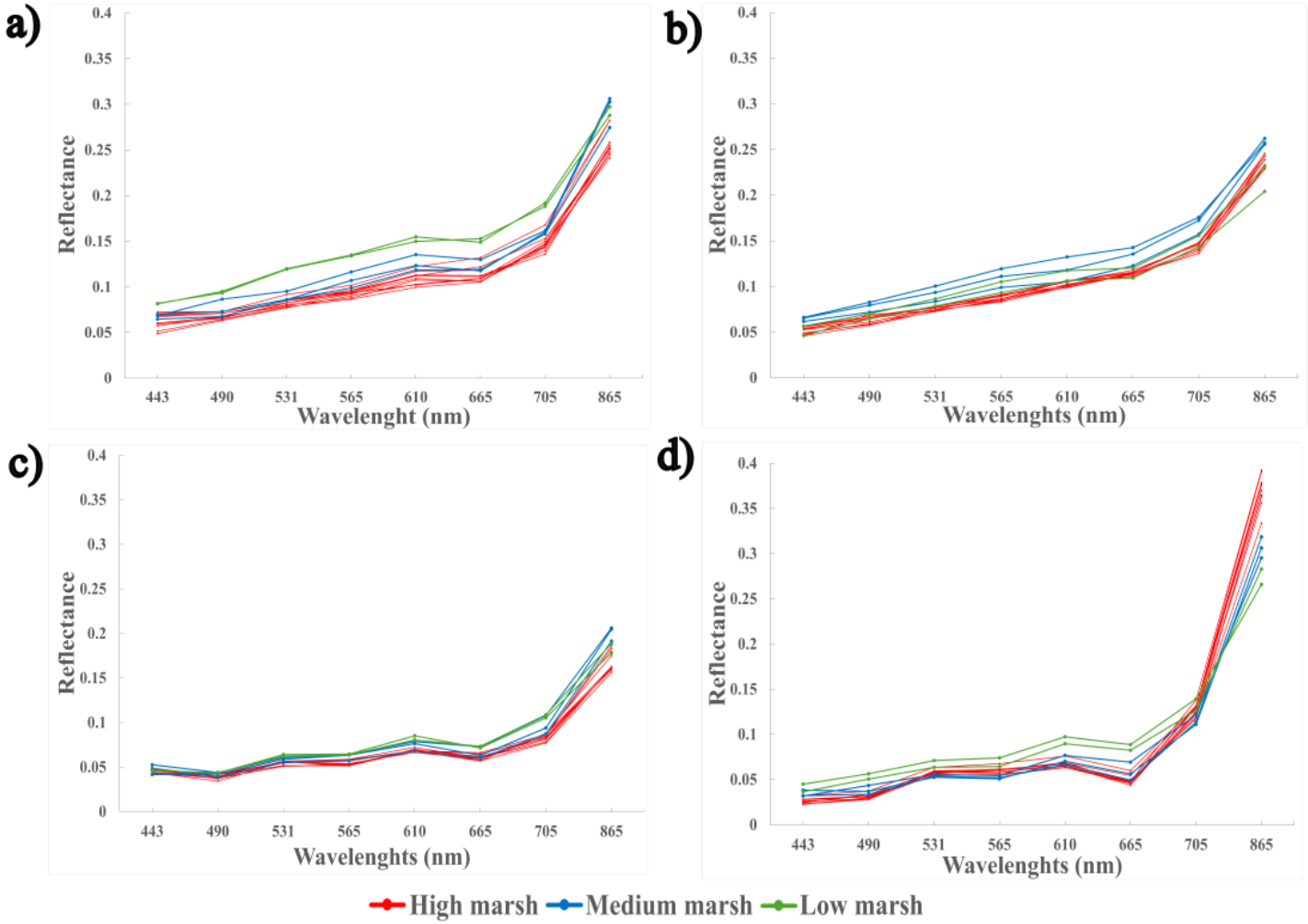

Figure 5.1. Spectral signature from all the plots of the Bias rewilded salt marsh in **a)** spring, **b)** summer, **c)** autumn, and **d)** winter, for the high marsh, medium marsh, and low marsh.

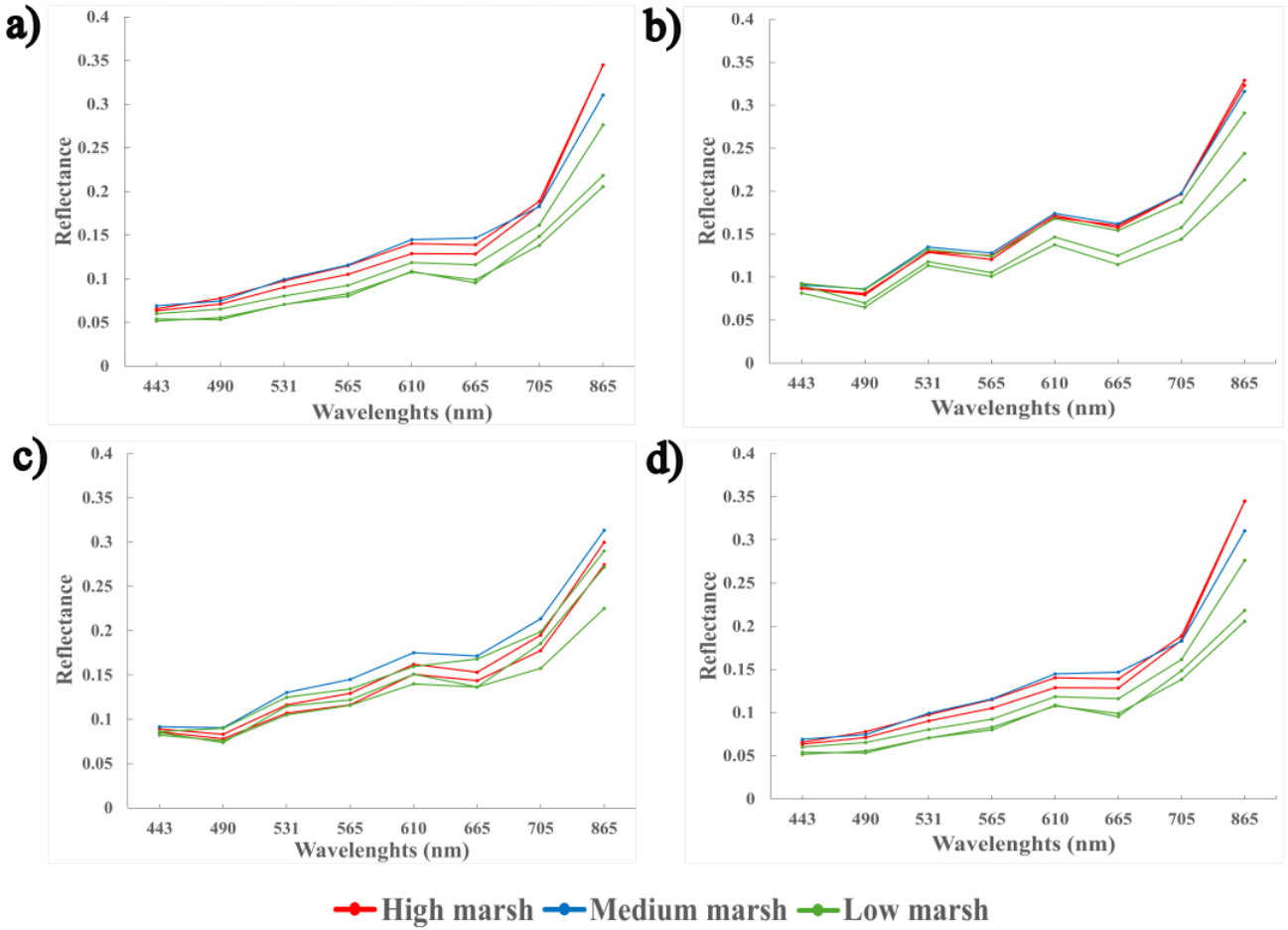

Figure 5.2. Spectral signature from all the plots of the Olhão rewilded salt marsh in **a)** spring, **b)** summer, **c)** autumn, and **d)** winter, for the high marsh, medium marsh, and low marsh.

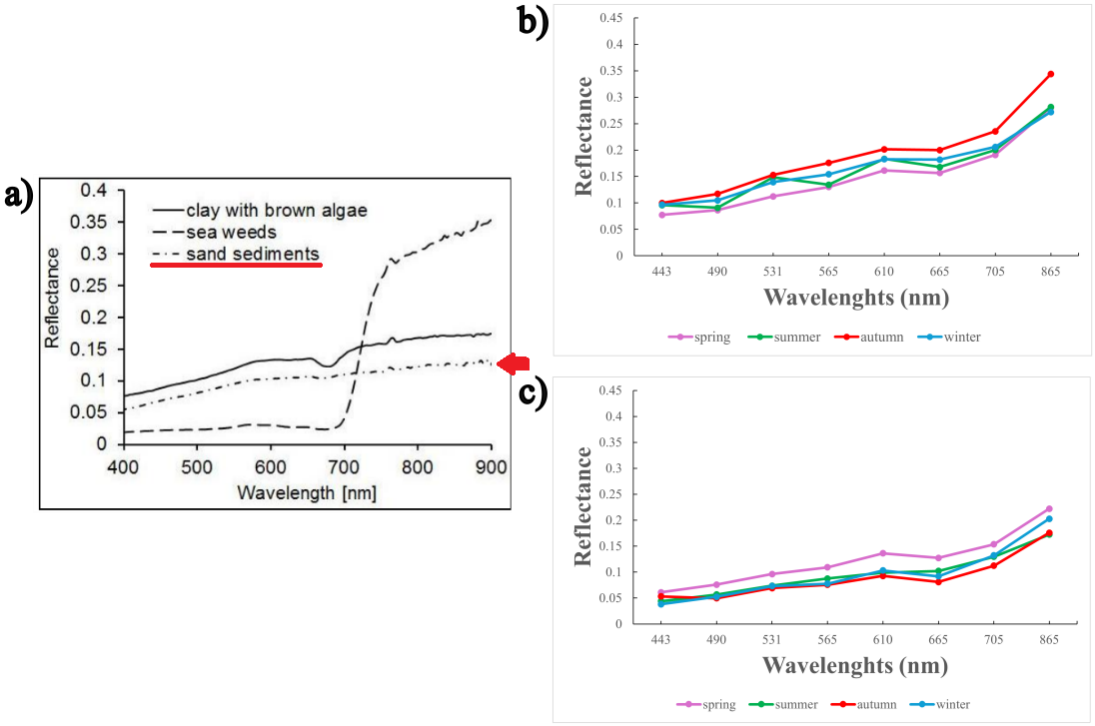

Figure 5.3. Spectral signatures **a)** derived from intertidal sediment properties by Dube et al. (2013), **b)** from the ground patch in Olhão and **c)** from the soil patch in Bias (**Appendix D**, **Table D3**).

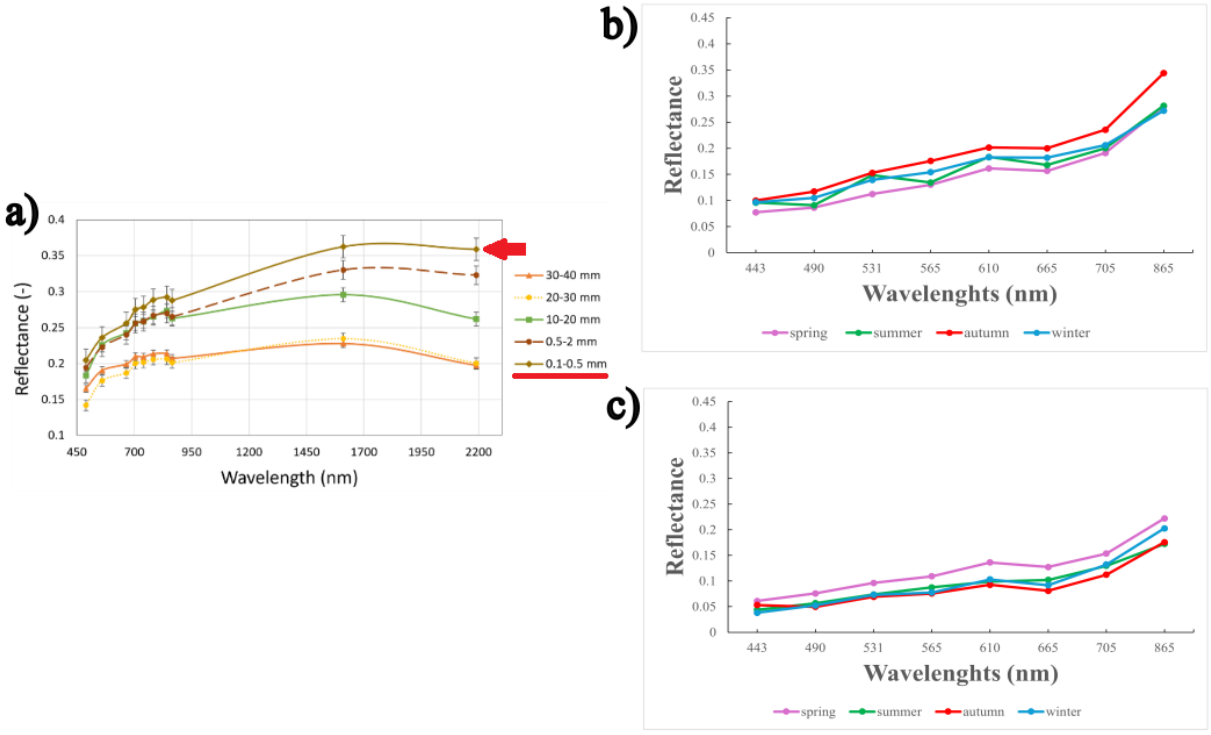

Figure 5.4. Spectral signatures **a)** of each sediment class by Marchetti et al. (2022), **b)** from the ground patch in Olhão and **c)** from the soil patch in Bias (**Appendix D**, **Table D3**).

5.4. The potential use of satellite remote sensing in rewilded salt marshes

This study successfully achieved its objective of identifying the most effective method for analysing seasonal and zonation variations in rewilded salt marshes, with RF emerging as the classification technique with the best skill. The image classification methodology with the best skill (RF-AC-EA) was proven to be feasible for monitoring rewilded salt marshes since the classification images showed seasonal and zonation variations, had high accuracies and was a much cheaper and less extensive method for monitoring these areas. However, this work did not manage to find an accurate connection between the variations in the mixture of plant species and the variations in the spectral signature shape, only finding its general influence. The influence of the sediment characteristics in the spectral signature was also found, mainly its influence regarding the zonation.

Being the first time that the SuperDove satellite images were used in rewilded salt marshes, the methodologies employed in this study proved effective in analysing and possibly used in monitoring rewilded salt marshes, having various advantages compared to other methods such as extensive fieldwork campaigns. First, RF classification images achieved images that could be used for a seasonal analysis of one year using less than 15 fieldwork campaigns. With a lower number of fieldwork campaigns, management projects will have significant reductions in expenses and will allow for more time to be used in the handling and analysis of data. Also, the current study showed that using multispectral satellite imagery from SuperDove, the supervised imagery classification denoted satisfactory results with high accuracies and low errors. The usage of the multispectral satellite imagery from Planet had the advantage of being cheaper than hyperspectral satellite imagery (Malerba et al., 2023), reducing the costs of a possible management project.

The results from this work have proven to be important in understanding how high-resolution satellite imagery can be applied to monitor rewilded salt marshes. By analysing two different salt marshes, it proves that the Random Forest image classification method can be applied in different areas since the results from both ROIs were, in general, similar. Together with that, the results from the sediment characteristics can be used as a basis for future studies. A monitoring project can acquire valuable information about a rewilded salt marsh without the necessity to go to the field. If the zonation of the rewilded salt marsh is known, the spectral signatures can be acquired crossing the zonation and using

the results from this work, see the characteristics from the area: if the spectral signature has the low marsh with the highest reflectance values, then it must be an area with more water content, less sand, and more vegetation; and if the spectral signature has the low marsh with the lowest reflectance values, then it must be an area with less water content, more sand, and less vegetation. Knowing these characteristics will help management projects acquire data from an area without needing to go there, thus reducing cost and reducing the interference in the area.

5.5. Limitations and future research

Regarding the limitations of this study, increasing the number of plots in each fieldwork campaign and replication over more years could have benefited the analysis. This would provide enough training samples for the imagery classification methods, possibly improving their quality even more. Another limitation of the study was the use of simpler equipment to create the plots. Using more sophisticated equipment to create the plots and more stable forms of acquiring the photos, such as an unmanned aerial vehicle (UAV), commonly known as a drone, would give more precise results and decrease the time of analysis, removing most or even completely, the editing of the photos. Also, an inter-annual analysis would have considerably improved the analysis of seasonal variations. Even though the SuperDove constellation of microsatellites from Planet has a wide range of spectral signature bands and high resolution, its data regarding the analyses of the spectral signature was insufficient. Using hyperspectral satellite images or field hyperspectral radiometers could have benefited the spectral analyses since the increased number of bands would give more precise results. Other studies confirm that analysing the spectral signature of plant species is best achieved by increasing the number of wavelength bands using hyperspectral data, more specifically, field hyperspectral radiometers (Awad, 2018; Carleer et al., 2005; Govender et al., 2008; Rajakumari et al., 2022; Warren et al., 2014). However, the downside of hyperspectral images is their cost since a hyperspectral mission can cost up to 250€/km^2 (Malerba et al., 2023).

Future research in rewilded salt marshes should prioritise increasing the number of training samples for image classification methods and conducting a more comprehensive analysis of factors influencing the spectral signature. This would provide a more detailed understanding of the impact of plant species variety on the spectral

signature, facilitating the analysis of variations in rewilded salt marshes. Another challenge that future studies need to address is that the use of satellite imagery remains inaccessible to many individuals with fewer financial resources. Therefore, efforts should be made to develop user-friendly platforms, reduce costs, ensure compatibility with existing tools, and utilise cloud-based storage and processing to make high-quality satellite data more accessible, especially for underfunded conservation initiatives.

6. Conclusions

The first objective of this study was to assess the effectiveness of different imagery classification methods to produce maps of vegetation zonation and seasonal variations in rewilded salt marshes using high-resolution satellite imagery (3m) from the SuperDove constellation of satellites. Multiple imagery classification methods were employed to assess their effectiveness in mapping two rewilded salt marshes in the Ria Formosa lagoon in Portugal. In addition to these classifications, the study also examined the influence of the mixture of plant species and sediment characteristics on the satellite bands' spectral signatures.

Unsupervised and supervised classification methods were applied in the ROIs, and Random Forest was chosen as the best image classification method when a composite of training samples was used during the classification process. This methodology demonstrated high accuracy in classifying the plant species identified during fieldwork within their respective zones. However, a seasonal analysis is not feasible when using a seasonal composite of data. The RF classifications using the entire area analyses yielded the best images for the seasonal analysis. The methods used in this work behaved similarly in the results from the two rewilded salt marshes, proving that their use is feasible and replicable in different rewilded salt marshes. Regarding the analysis of the spectral signature, the influence of the mixture of plant species was identified. However, specific patterns in the spectral signature shape in relation to the variations of plant species mixture were not found. The results obtained also denoted the influence of the sediment characteristics in the spectral signature. Locations with similar sediment classes had distinct spectral signatures due to the differences in the sediment characteristics, mainly d_{50}, H_2O%. In conclusion, more studies should analyse the influence of each plant

species on the spectral signature using multispectral satellite data, focusing on also analysing features such as the age, height, and chemical composition of the plant species, together with a more in-depth analysis of the influence of each sediment characteristic.

The study suggests that increasing the number of training samples and acquiring more stable manners of acquiring the fieldwork data could enhance the accuracy of Random Forest classifications when using the SuperDove satellite data. With these improvements, relevant governmental agencies could use multispectral satellite imagery more effectively, using the methodologies from this work to analyse the rewilded marsh ecological succession (zonation) patterns and assess its seasonal variations, thereby contributing to more successful restoration and improved management projects.

The thesis played an essential role in advancing future research by utilising SuperDove satellite imagery to find the methods with the best skill to analyse rewilded salt marshes. The SuperDove satellite constellation was also proven to be a great option for the analysis of rewilded salt marshes; its high resolution was proven to be enough to create highly accurate classification images. The analysis of the spectral signatures of various mixtures of plant species and sediment characteristics laid a foundation for more detailed and scalable environmental monitoring efforts. The approaches from this work established the groundwork for future studies to refine classification techniques, optimise spectral analysis, and apply these methods to a broader range of rewilded salt marshes worldwide.

References

Abbas, A. W., Minallh, N., Ahmad, N., Abid, S.A.R., & Khan, M.A.A. (2016). K-Means and ISODATA Clustering Algorithms for Landcover Classification Using Remote Sensing. Sindh University Research Journal (Science series) 28 (2), 315–318.

Adam, E., Mutanga, O., & Rugege, D. (2010). Multispectral and hyperspectral remote sensing for identification and mapping of wetland vegetation: A review. Wetlands Ecology and Management 18 (3), 281 – 296. https://doi.org/10.1007/s11273-009-9169-z

Agrawal, S., & Khairnar, G. B. (2019). A comparative assessment of remote sensing imaging techniques: Optical, sar and lidar. International Archives of the Photogrammetry, Remote Sensing and Spatial Information Sciences - ISPRS Archives, 42(5/W3), 1–6. https://doi.org/10.5194/isprs-archives-XLII-5-W3-1-2019

Allen, J. R. L., & Thomley, D. M. (2004). Laser granulometry of Holocene estuarine silts: effects of hydrogen peroxide treatment. The Holocene 14 (2), 290–295. https://doi.org/10.1191/0959683604hl681rr

Allen, T. R., Wang, Y., & Gore, B. (2013). Coastal wetland mapping combining multi-date SAR and LiDAR. Geocarto International, 28(7), 616–631. https://doi.org/10.1080/10106049.2013.768297

Alongi, D. M. (2020). Carbon balance in salt marsh and mangrove ecosystems: A global synthesis. Journal of Marine Science and Engineering 8 (10), 1–21. https://doi.org/10.3390/jmse8100767

Andrade, C., Freitas, M. C., Moreno, J., & Craveiro, S. C. (2004). Stratigraphical evidence of Late Holocene barrier breaching and extreme storms in lagoonal sediments of Ria Formosa, Algarve, Portugal. Marine Geology, 210(1–4), 339–362. https://doi.org/10.1016/j.margeo.2004.05.016

Andrade, C., Viegas, A., Tomé, A., & Romariz, C., (1989). Erosão do litoral cenozóico do Algarve. Geolis 3, 261–270. http://pascal-francis.inist.fr/vibad/index.php?action=getRecordDetail&idt=19449312

Arnaud-Fassetta, G., Bertrand, F., Costa, S., & Davidson, R., (2006). The western lagoon marshes of the Ria Formosa (Southern Portugal): sediment-vegetation dynamics, long-term to short-term changes and perspective. Continental Shelf Research 26, 363–384. https://doi.org/10.1016/j.csr.2005.12.008

Atkinson, P.M. & Curran, P.J. (1997). Choosing an appropriate spatial resolution for remote sensing investigations. Photogrammetric Engineering and Remote Sensing 63, 1345–1351. https://eprints.lancs.ac.uk/id/eprint/77075

Awad, M. M. (2018). Forest mapping: a comparison between hyperspectral and multispectral images and technologies. Journal of Forestry Research, 29(5), 1395–1405. https://doi.org/10.1007/s11676-017-0528-y

Balarabe, A. T., & Jordanov, I. (2024). A Deeper Look into Remote Sensing Scene Image Misclassification by CNNs. IEEE Access 12, 123078 - 123098. https://doi.org/10.1109/ACCESS.2024.3354976

Barbier, E. B., Hacker, S. D., Kennedy, C., Koch, E. W., Stier, A. C., & Silliman, B. R. (2011). The value of estuarine and coastal ecosystem services. Ecological Monographs 81(2), 169–193. https://doi.org/10.1890/10-1510.1

Beeftink, W. G. (1996). Vegetation and habitat of the salt marshes and beach plains in the south-western part of the Netherlands. Wentia 15(1), 83–108. https://doi.org/10.1111/j.1438-8677.1966.tb00021.x

Belgiu, M., & Drăgu, L. (2016). Random forest in remote sensing: A review of applications and future directions. ISPRS Journal of Photogrammetry and Remote Sensing 114, 24–31. https://doi.org/10.1016/j.isprsjprs.2016.01.011

Belluco, E., Camuffo, M., Ferrari, S., Modenese, L., Silvestri, S., Marani, A., & Marani, M. (2006). Mapping salt-marsh vegetation by multispectral and hyperspectral remote sensing. Remote Sensing of Environment 105(1), 54–67. https://doi.org/10.1016/j.rse.2006.06.006

Ben-Dor, E., Irons, J., & Epema, G.F. (1999). Soil Reflectance. Remote Sensing for the Earth Sciences: Manual of Remote Sensing 3(3), 111-188.

Bertrand F., Costa S., Arnaud-Fassetta G., Davidson R., Beltrando G., Goeldner-Giannela L., & Baron-Yélles, N. (2003). Dynamique des marais d'arrière-barrière associée à la passe de Barra Nova (Ria Formosa, Portugal méridional). Géomorphologie : relief, processus, environnement, 9, 3, 150–163. https://doi.org/10.3406/morfo.2003.1176

Billah, M. M., Bhuiyan, M. K. A., Islam, M. A., Das, J., & Hoque, A. R. (2022). Salt marsh restoration: an overview of techniques and success indicators. Environmental Science and Pollution Research 29 (11), 15347–15363. https://doi.org/10.1007/s11356-021-18305-5

Blott, S. J., & Pye, K. (2001). GRADISTAT: a grain size distribution and statistics package for the analysis of unconsolidated sediments. Earth Surface Processes and Landforms, 26, 1237–1248. https://doi.org/10.1002/esp.261

Blount, T. R., Carrasco, A. R., Cristina, S., & Silvestri, S. (2022). Exploring open-source multispectral satellite remote sensing as a tool to map long-term evolution of salt marsh shorelines. Estuarine, Coastal and Shelf Science, 266. https://doi.org/10.1016/j.ecss.2021.107664

Bouma, T. J., van Belzen, J., Balke, T., Zhu, Z., Airoldi, L., Blight, A. J., Davies, A. J., Galvan, C., Hawkins, S.J., Hoggart, S. P. G., Lara, J. L., Losada, I. J., Maza, M., Ondiviela, B., Skov, M. W., Strain, E.M., Thompson, R.C., Yang, S., Zanuttigh, B., Zhang, L., & Herman, P. M. J. (2014). Identifying knowledge gaps hampering application of intertidal habitats in coastal protection: opportunities & steps to take. Coastal Engineering 87, 147–157. https://doi.org/10.1016/j.coastaleng.2013.11.014

Breiman, L. (2001). Random forest. Machine Learning 45, 5–32. https://doi.org/10.1023/A:1010933404324

Burden, A., Garbutt, A., & Evans, C. D. (2019). Effect of restoration on saltmarsh carbon composite in Eastern England. Biology Letters, 15(1). https://doi.org/10.1098/rsbl.2018.0773

Burden, A., Garbutt, R. A., Evans, C. D., Jones, D. L., & Cooper, D. M. (2013). Carbon sequestration and biogeochemical cycling in a saltmarsh subject to coastal managed realignment. Estuarine, Coastal and Shelf Science, 120, 12–20. https://doi.org/10.1016/j.ecss.2013.01.014

Caçador, I., Tibério, S., & Cabral, H. N. (2007). Species zonation in Corroios salt marsh in the Tagus estuary (Portugal) and its dynamics in the past fifty years. Hydrobiologia 587(1), 205–211. https://doi.org/10.1007/s10750-007-0681-y

Carey, J. C., Moran, S. B., Kelly, R. P., Kolker, A. S., & Fulweiler, R. W. (2017). The Declining Role of Organic Matter in New England Salt Marshes. Estuaries and Coasts 40(3), 626–639. https://doi.org/10.1007/s12237-015-9971-1

Carleer, A., Debeir, O., & Wolff, E. (2005). Assessment of Very High Spatial Resolution Satellite Image Segmentations. Photogrammetric Engineering & Remote Sensing, 71, 1285–1294. https://doi.org/10.14358/PERS.71.11.1285

Carrasco, A. R., Kombiadou, K., Amado, M., & Matias, A. (2021). Past and future marsh adaptation: Lessons learned from the Ria Formosa lagoon. Science of the Total Environment, 790. https://doi.org/10.1016/j.scitotenv.2021.148082

Castillo, J. M., Ayres, D. R., Leira-Doce, P., Bailey, J., Blum, M., Strong, D. R., Luque, T., & Figueroa, E. (2010). The production of hybrids with high ecological amplitude between exotic Spartina densiflora and native S. maritima in the Iberian Peninsula. Diversity and Distributions, 16(4), 547–558. https://doi.org/10.1111/j.1472-4642.2010.00673.x

Cheng, Z., Denby, B., McCleary, K., & Lucia, B. (2024). EagleEye: Nanosatellite constellation design for high-coverage, high-resolution sensing. International Conference on Architectural Support for Programming Languages and Operating Systems - ASPLOS 1, 117–132. https://doi.org/10.1145/3617232.3624851

Chmura, G.L., Anisfeld, S.C., Cahoon, D.R., & Lynch, J.C. (2003). Global carbon sequestration in tidal, saline wetland soils. Glob. Biogeochem. Cycles 17, 1111. https://doi.org/10.1029/2002GB001917

Contreras-Cruzado, I., Infante-Izquierdo, M. D., Márquez-García, B., Hermoso-López, V., Polo, A., Nieva, F. J. J., Cartes-Barroso, J. B., Castillo, J. M., & Muñoz-Rodríguez, A. (2017). Relationships between spatio-temporal changes in the sedimentary environment and halophytes zonation in salt marshes. Geoderma, 305, 173–187. https://doi.org/10.1016/j.geoderma.2017.05.037

Costa, J.C., Lousã, M., & Espírito-Santo, M.D. (1996). A vegetação do Parque Natural da Ria Formosa/The vegetation of "Parque Natural da Ria Formosa" (Algarve, Portugal). Studia Botanica 15, 69–157. http://hdl.handle.net/10400.5/14986

Craft, C., Megonigal, P., Broome, S., Stevenson, J., Freese, R., Cornell, J., Zheng, L., & Sacco, J. (2003). The Pace of Ecosystem Development of Constructed *Spartina alterniflora* Marshes. Ecological Applications 13(5). https://www.jstor.org/stable/4134723

Craft, C. B., Seneca, E. D., & Broome, S. W. (1991). Loss on Ignition and Kjeldahl Digestion for Estimating Organic Carbon and Total Nitrogen in Estuarine Marsh Soils: Calibration with Dry Combustion. Estuaries 14 (2), 175–179. https://doi.org/10.2307/1351691

Cristina, S., Icely, J., & Newton, A. (2019). The application of remote sensing for monitoring the Ria Formosa: the sentinel missions. Ria Formosa eBook chapter 10. http://hdl.handle.net/10400.1/14038

Crooks, S., Schutten, J., Sheern, G. D., Pye, K., & Davy, A. J. (2002). Drainage and elevation as factors in the restoration of salt marsh in Britain. Restoration Ecology, 10(3), 591–602. https://doi.org/10.1046/j.1526-100X.2002.t01-1-02036.x

Cunningham, P., & Delany, S.J., (2021). k-Nearest Neighbour Classifiers - A Tutorial. ACM Comput. Surv. 54, 6, Article 128. https://doi.org/10.1145/3459665

D'Alpaos, A. (2011). The mutual influence of biotic and abiotic components on the long-term ecomorphodynamic evolution of salt-marsh ecosystems. Geomorphology 126, 269–278. https://doi.org/10.1016/j.geomorph.2010.04.027

D'Alpaos, A., & Marani, M. (2016). Reading the signatures of biologic–geomorphic feedbacks in salt-marsh landscapes. Advances in Water Resources 93, 265–275. https://doi.org/10.1016/j.advwatres.2015.09.004

Dame, R. F., & Kenny, P. D. (1986). Variability of Spartina alterniflora primary production in the euhaline North Inlet estuary. Marine Ecology Progress Series 32 (1). https://doi.org/10.3354/meps032071

Dat Pham, T., Xia, J., Thang Ha, N., Tien Bui, D., Nhu Le, N., & Tekeuchi, W. (2019). A review of remote sensing approaches for monitoring blue carbon ecosystems: Mangroves, sea grasses and salt marshes during 2010–2018. Sensors (Switzerland) 19(8). https://doi.org/10.3390/s19081933

De los Santos, C. B., Lahuna, F., Silva, A., Freitas, C., Martins, M., Carrasco, A. R., & Santos, R. (2022). Vertical intertidal variation of organic matter stocks and patterns of sediment deposition in a mesotidal coastal wetland. Estuarine, Coastal and Shelf Science, 272. https://doi.org/10.1016/j.ecss.2022.107896

Dempster, A. P., Laird, N M, & Rubin, D B. (1977). Maximum Likelihood from Incomplete Data via the EM Algorithm. Journal of the Royal Statistical Society. Series B (Methodological) 39(1), 1–38. https://doi.org/10.1111/j.2517-6161.1977.tb01600.x

Dias, J.M., & Sousa, M.C., (2009). Numerical modelling of Ria Formosa tidal dynamics. Journal of Coastal Research 56(56), 1345–1349.

Dos Santos, G. M., Meléndez-Pastor, I., Navarro-Pedreño, J., & Lucas, I. G. (2019). A Review of Landsat TM/ETM based Vegetation Indices as Applied to Wetland Ecosystems. Journal of Geographical Research, 2(1), 34–48. https://doi.org/10.30564/jgr.v2i1.499

Dronova, I., Taddeo, S., Hemes, K. S., Knox, S. H., Valach, A., Oikawa, P. Y., Kasak, K., & Baldocchi, D. D. (2021). Remotely sensed phenological heterogeneity of restored wetlands: linking vegetation structure and function. Agricultural and Forest Meteorology, 296. https://doi.org/10.1016/j.agrformet.2020.108215

Du, J., Kimball, J. S., Bindlish, R., Walker, J. P., & Watts, J. D. (2022). Local Scale (3-m) Soil Moisture Mapping Using SMAP and Planet SuperDove. Remote Sensing, 14(15). https://doi.org/10.3390/rs14153812

Duarte, C. M., Middelburg, J. J., & Caraco, N. (2005). Major role of marine vegetation on the oceanic carbon cycle. Biogeosciences 2, 1– 8. https://doi.org/10.5194/bg-2-1-2005

Duarte, C.M., Losada, I.J., Hendriks, I.E., Mazarrasa, I., & Marbà, N. (2013). The role of coastal plant communities for climate change mitigation and adaptation. Nature Climate Change 3, 961–968. https://doi.org/10.1038/nclimate1970

Dube, T., Gara, T. W., Gumindoga, W., Chivhenge, E., & Chinembiri, T. S. (2013). Characterization of the top sediment layer in coastal intertidal mudflats from medium-to-coarse resolution satellite imagery and field measurements. International journal of water resources and environmental engineering, 5(12), 676-686. https://doi.org/10.5897/IJWREE2013.0417

Eastwood, J. A., Yates, M. G., Thomson, A. G., & Fuller, R. M. (1997). The reliability of vegetation indices for monitoring salt marsh vegetation cover. International Journal of Remote Sensing 18(18), 3901–3907. https://doi.org/10.1080/014311697216739

Eleuterius, L. N., & Eleuterius, C. K. (1979). Tide Levels and Salt Marsh. Bulletin of Marine Science 29(3), 394–400.

Farris, A. S., Defne, Z., & Ganju, N. K. (2019). Identifying salt marsh shorelines from remotely sensed elevation data and imagery. Remote Sensing 11(15). https://doi.org/10.3390/rs11151795

Ferreira, Ó., Matias, A., & Pacheco, A. (2016). The east coast of Algarve: A Barrier island dominated coast. Thalassas 32(2), 75–85. https://doi.org/10.1007/s41208-016-0010-1

French, J. R. (2006). Tidal marsh sedimentation and resilience to environmental change: Exploratory modelling of tidal, sea-level and sediment supply forcing in predominantly allochthonous systems. Marine Geology 235(1-4 SPEC. ISS.), 119–136. https://doi.org/10.1016/j.margeo.2006.10.009

French, J. R., Benson, T., & Burningham, H. (2007). Morphodynamics and Sediment Flux in the Blyth Estuary, Suffolk, UK. High Resolution Morphodynamics and Sedimentary Evolution of Estuaries, 143–171. https://doi.org/10.1007/1-4020-3296-x_8

Gao, Z. G., & Zhang, L.Q. (2006). Multi-seasonal spectral characteristics analysis of coastal salt marsh vegetation in Shanghai, China. Estuarine, Coastal and Shelf Science 69(1-2), 217-224. https://doi.org/10.1016/j.ecss.2006.04.016

Gesch, D. B. (2009). Analysis of Lidar elevation data for improved identification and delineation of lands vulnerable to sea-level rise. Journal of Coastal Research 53, 49–58. https://doi.org/10.2112/SI53-006.1

Ghassemian, H. (2016). A review of remote sensing image fusion methods. Information Fusion 32, 75 – 89. https://doi.org/10.1016/j.inffus.2016.03.003

Gonzalez, R. C. & Woods, R.E. (2018). Digital Image Processing. 4th Edition, Pearson Education, New York, pp. 770.

Goodwin, G. C. H., Mudd, S. M., & Clubb, F. J. (2018). Unsupervised detection of salt marsh platforms: A topographic method. Earth Surface Dynamics 6(1), 239–255. https://doi.org/10.5194/esurf-6-239-2018

Google Earth Pro, 7.3.6 (2023a). Iberic peninsula, Europe. 40°07’27.81’’ N, 4°37’37.38’’ W, 14 of December 2015 Eye alt. 1160.20km. SIO, NOAA, U.S. Navy, NGA, GEBCO. Landsat/Copernicus.

Google Earth Pro, 7.3.6 (2023b). Ria Formosa, Algarve, Portugal. 36°59’26.21’’ N, 7°53’35.62’’ W, 14 of April 2022. Eye alt. 19.5km. SIO, NOAA, U.S. Navy, NGA, GEBCO. TerraMetrics 2023.

Google Earth Pro, 7.3.6 (2023c). Olhão, Portugal. 37°01’20.33’’ N, 7°51’04.81’’ W, 14 of April 2022. Eye alt. 563m. SIO, NOAA, U.S. Navy, NGA, GEBCO.

Google Earth Pro, 7.3.6 (2023d). Bias, Olhão, Portugal. 37°02’16.73’’ N, 7°46’38.49’’ W, 14 of April 2022. Eye alt. 1.13km. SIO, NOAA, U.S. Navy, NGA, GEBCO.

Govender, M., Chetty, K., Naiken, V., & Bulcock, H. (2008). A comparison of satellite hyperspectral and multispectral remote sensing imagery for improved classification and mapping of vegetation. Water SA, 34(2), 147–154. https://doi.org/10.4314/wsa.v34i2.183634

Goward, S. N., Masek, J. G., Williams, D. L., Irons, J. R., & Thompson, R. J. (2000). The Landsat 7 mission Terrestrial research and applications for the 21st century. Remote Sensing of Environment 78(1-2), 3–12. https://doi.org/10.1016/S0034-4257(01)00262-0

Gray, A. B., Pasternack, G. B., & Watson, E. B. (2010). Hydrogen peroxide treatment effects on the particle size distribution of alluvial and marsh sediments. Holocene 20(2), 293–301. https://doi.org/10.1177/0959683609350390

Grings, F., Salvia, M., Karszenbaum, H., Ferrazzoli, P., Kandus, P., & Perna, P. (2009). Exploring the capacity of radar remote sensing to estimate wetland marshes water storage. Journal of Environmental Management, 90(7), 2189–2198. https://doi.org/10.1016/j.jenvman.2007.06.029

Gu, J., Luo, M., Zhang, X., Christakos, G., Agusti, S., Duarte, C. M., & Wu, J. (2018). Losses of salt marsh in China: Trends, threats and management. Estuarine, Coastal and Shelf Science 214, 98–109. https://doi.org/10.1016/j.ecss.2018.09.015

Guisado-Pintado, E., & Jackson, D. W. T. (2020). Monitoring Cross-shore Intertidal Beach Dynamics using Oblique Time-lapse Photography. Journal of Coastal Research 95(sp1), 1106–1110. https://doi.org/10.2112/SI95-215.1

Guo, M., Li, J., Sheng, C., Xu, J., & Wu, L. (2017). A review of wetland remote sensing. Sensors 17(4), 777. https://doi.org/10.3390/s17040777

Haffar, R., Jebreel, N.M., Domingo-Ferrer, J., & Sánchez, D. (2021). Explaining Image Misclassification in Deep Learning via Adversarial Examples. Modeling Decisions for Artificial Intelligence: 18th International Conference, MDAI 2021, Umeå, Sweden, September 27–30, 2021, Proceedings, 323–334. https://doi.org/10.1007/978-3-030-85529-1_26

Hansen, M. C., & Loveland, T. R. (2012). A review of large area monitoring of land cover change using Landsat data. Remote Sensing of Environment 122, 66–74. https://doi.org/10.1016/j.rse.2011.08.024

Hart, E. E., Haigh, A., & Ciuti, S. (2023). A scoping review of the scientific evidence base for rewilding in Europe. Biological Conservation 285. https://doi.org/10.1016/j.biocon.2023.110243

Heiri, O., Lotter, A. F., & Lemcke, G. (2001). Loss on ignition as a method for estimating organic and carbonate content in sediments: Reproducibility and comparability of results. Journal of Paleolimnology, 25(1). https://doi.org/101–110. 10.1023/A:1008119611481

Himes-Cornell, A., Pendleton, L., & Atiyah, P. (2018). Valuing ecosystem services from blue forests: A systematic review of the valuation of salt marshes, sea grass beds and mangrove forests. Ecosystem Services 30, 36–48. https://doi.org/10.1016/j.ecoser.2018.01.006

Hood, W. G. (2014). Differences in tidal channel network geometry between reference marshes and marshes restored by historical dike breaching. Ecological Engineering 71, 563–573. https://doi.org/10.1016/j.ecoleng.2014.07.076

Hou, W., Li, D., Xu, C., Zhang, H., Li, T., (2018). An Advanced K Nearest Neighbour Classification Algorithm Based on KD-tree. IEEE International Conference of Safety Produce Informatization (IICSPI), Chongqing, China, 902–905. https://doi.org/10.1109/IICSPI.2018.8690508.

Huabin, W., Gangjun, L., Weiya, X., & Gonghui, W., (2005). GIS-based landslide hazard assessment: An overview. Progress in Physical Geography 29 (4), 548–567. https://doi.org/10.1191/0309133305pp462ra

Huete, A. & Justice, C. (1999) MODIS Vegetation Index (MOD 13) Algorithm Theoretical Basis Document. https://modis.gsfc.nasa.gov/data/atbd/atbd_mod13.pdf

Hyland, S. J. (2002). An Investigation of the Impacts of Ponded Pastures on Barramundi and Other Finfish Populations in Tropical Coastal Salt marsh. Project Report. FRDC. https://www.frdc.com.au/project/1997-201

Irmler, U., Heller, K., Meyer, H., & Reinke, H.D. (2002). Zonation of spiders and carabid beetles (Araneida, Coleoptera: Carabidae) in an inundation gradient of salt marshes at the North and Baltic Sea. Biodiversity & Conservation 11, 1129–1147. https://doi.org/10.1023/A:1016018021533

Isacch, J. P., Costa, C. S. B., Rodríguez-Gallego, L., Conde, D., Escapa, M., Gagliardini, D. A., & Iribarne, O. O. (2006). Distribution of saltmarsh plant communities associated with environmental factors along a latitudinal gradient on the south-west Atlantic coast. Journal of Biogeography 33(5), 888–900. https://doi.org/10.1111/j.1365-2699.2006.01461.x

Iverson, L.R., Prasad, A.M., & Matthews, S.N. (2008). Estimating potential habitat for 134 eastern US tree species under six climate scenarios. Forest Ecology and Management 254(3), 390–406. https://doi.org/10.1016/j.foreco.2007.07.023

Jena, R., Pradhan, B., Beydoun, G., Al-Amri, A., & Sofyan, H. (2020). Seismic hazard and risk assessment: a review of state-of-the-art traditional and GIS models. Arabian Journal of Geosciences 13(2). https://doi.org/10.1007/s12517-019-5012-x

Jiang, D., Huang, Y., Zhuang, D., Zhu, Y., Xu, X., & Ren, H. (2012). A Simple Semi-Automatic Approach for Land Cover Classification from Multispectral Remote Sensing Imagery. PLoS ONE 7(9). https://doi.org/10.1371/journal.pone.0045889

Jung, Y. G., Kang, M. S., & Heo, J. (2014). Clustering performance comparison using K-means and expectation maximization algorithms. Biotechnology and Biotechnological Equipment 28, S44–S48. https://doi.org/10.1080/13102818.2014.949045

Klemas, V. (2013). Remote sensing of emergent and submerged wetlands: an overview. International Journal of Remote Sensing 34(18), 6286–6320. https://doi.org/10.1080/01431161.2013.800656

Krause, J. R., Oczkowski, A. J., & Watson, E. B. (2023). Improved mapping of coastal salt marsh habitat change at Barnegat Bay (NJ, USA) using object-based image analysis of high-resolution aerial imagery. Remote Sensing Applications: Society and Environment 29. https://doi.org/10.1016/j.rsase.2022.100910

Kumar, L., Sinha, P., & Taylor, S. (2014). Improving image classification in a complex wetland ecosystem through image fusion techniques. Journal of Applied Remote Sensing, 8(1), 083616. https://doi.org/10.1117/1.jrs.8.083616

Laengner, M.L., Siteur, K., & van der Wal, D. (2019). Trends in the seaward extent of salt marshes across europe from long-term satellite data. Remote Sensing 11, 1653. https://doi.org/10.3390/rs11141653

Leachtenauer, J., Daniel, K., & Vogl, T. (1998). Digitizing Satellite Imagery: Quality and Cost Considerations Digitizing Satellite Imagery: Quality and Cost Considerations. Photogrammetric Engineering & Remote Sensing 64(1), 29–34. https://doi.org/10.14358/PERS.77.12.1257

Lee, H., Yuan, T., Yu, H., & Jung, H. C. (2020). Interferometric SAR for Wetland Hydrology: An Overview of Methods, Challenges, and Trends. IEEE Geoscience and Remote Sensing Magazine 8(1), 120–135. https://doi.org/10.1109/MGRS.2019.2958653

Leistner, C., Saffari, A., Santner, J., & Bischof, H. (2009). Semi-Supervised Random Forests. IEEE 12th International Conference on Computer Vision, 506–513. https://doi.org/10.1109/ICCV.2009.5459198

Li, Z., Shen, H., Weng, Q., Zhang, Y., Dou, P., & Zhang, L. (2022). Cloud and cloud shadow detection for optical satellite imagery: Features, algorithms, validation, and prospects. ISPRS Journal of Photogrammetry and Remote Sensing 188, 89–108. https://doi.org/10.1016/j.isprsjprs.2022.03.020

Liu, J., Heiskanen, J., Aynekulu, E., & Pellikka, P. K. E. (2015). Seasonal variation of land cover classification accuracy of Landsat 8 images in Burkina Faso. International Archives of the Photogrammetry, Remote Sensing and Spatial Information Sciences - ISPRS Archives, 40(7W3), 455–460. https://doi.org/10.5194/isprsarchives-XL-7-W3-455-2015

Lowe, B. E., (2015). The Random Forest Algorithm with Application to Multispectral Image Analysis. Computer Science Theses, Paper 5. http://hdl.handle.net/10950/260

Lu, D., & Weng, Q. (2007). A survey of image classification methods and techniques for improving classification performance. International Journal of Remote Sensing 28(5), 823–870). https://doi.org/10.1080/01431160600746456

Macreadie, P. I., Hughes, A. R., & Kimbro, D. L. (2013). Loss of "Blue Carbon" from Coastal Salt Marshes Following Habitat Disturbance. PLoS ONE 8(7). https://doi.org/10.1371/journal.pone.0069244

Malczewski, J. (2004). GIS-based land-use suitability analysis: A critical overview. Progress in Planning 62(1), 3–65. https://doi.org/10.1016/j.progress.2003.09.002

Malerba, M. E., Duarte de Paula Costa, M., Friess, D. A., Schuster, L., Young, M. A., Lagomasino, D., Serrano, O., Hickey, S. M., York, P. H., Rasheed, M., Lefcheck, J. S., Radford, B., Atwood, T. B., Ierodiaconou, D., & Macreadie, P. I., (2023). Remote sensing for cost-effective blue carbon accounting. Earth-Science Reviews 238, 104337 https://doi.org/10.1016/j.earscirev.2023.104337

Marani, M., Silvestri, S., Belluco, E., Ursino, N., Comerlati, A., Tosatto, O., & Putti, M. (2006). Spatial organization and ecohydrological interactions in oxygen-limited vegetation ecosystems. Water Resources Research 42, 1–12. https://doi.org/10.1029/2005WR004582

Marchetti, G., Bizzi, S., Belletti, B., Lastoria, B., Comiti, F., & Carbonneau, P. E. (2022). Mapping riverbed sediment size from Sentinel-2 satellite data. Earth Surface Processes and Landforms, 47(10), 2544–2559. https://doi.org/10.1002/esp.5394

Mauchamp, A., Chauvelon, P., & Grillas, P. (2002). Restoration of floodplain salt marsh: Opening polders along a coastal river in Mediterranean France, Vistre marshes. Ecological Engineering 18(5), 619-632. https://doi.org/10.1016/S0925-8574(02)00024-1

McDonald, T., Gann, G. D., Jonson, J., & Dixon, K. W. (2016) International standards for the practice of ecological restoration-including principles and key concepts. Society for Ecological Restoration: Washington, DC, USA. Soil-Tec, Inc. Marcel Huijser, Bethanie Walder, 1–48.

McLeod, E., Chmura, G. L., Bouillon, S., Salm, R., Björk, M., Duarte, C. M., Lovelock, C. E., Schlesinger, W. H., & Silliman, B. R. (2011). A blueprint for blue carbon: Toward an improved understanding of the role of vegetated coastal habitats in sequestering CO2. Frontiers in Ecology and the Environment 9(10), 552–560. https://doi.org/10.1890/110004

Mcowen, C., Weatherdon, L., Bochove, J.-W., Sullivan, E., Blyth, S., Zockler, C., Stanwell Smith, D., Kingston, N., Martin, C., Spalding, M., & Fletcher, S. (2017). A global map of salt marshes. Biodiversity Data Journal 5, e11764 https://doi.org/10.3897/BDJ.5.e11764

Meiman, S., Civco, D., Holsinger, K., & Elphick, C. S. (2012). Comparing habitat models using ground-based and remote sensing data: Salt marsh sparrow presence versus nesting. Salt marsh 32(4), 725–736. https://doi.org/10.1007/s13157-012-0306-8

Mitsch, W. J., & Gosselink, J. G. (2015). Wetlands (5th ed.). John Wiley & Sons, Inc. https://archive.org/details/Wetlands_5th_Edition_by_William_J._Mitsch_James_G._Gosselink

Moffett, K. B., Gorelick, S. M., McLaren, R. G., & Sudicky, E. A. (2012). Salt marsh ecohydrological zonation due to heterogeneous vegetation-groundwater-surface water interactions. Water Resources Research 48(2). https://doi.org/10.1029/2011WR010874

Morris, R. K. A., Reach, I. S., Duffy, M. J., Collins, T. S., & Leafe, R. N. (2004). On the Loss of Salt marshes in South-East England and the Relationship with Nereis diversicolor. Journal of Applied Ecology 41(4), 787–791. https://www.jstor.org/stable/3505709

Mudd, S. M., D'Alpaos, A., & Morris, J. T. (2010). How does vegetation affect sedimentation on tidal marshes? Investigating particle capture and hydrodynamic controls on biologically mediated sedimentation. Journal of Geophysical Research: Earth Surface 115(3). https://doi.org/10.1029/2009JF001566

Muench, A., & Elsey-Quirk, T. (2019). Competitive reversal between plant species is driven by species-specific tolerance to flooding stress and nutrient acquisition during early marsh succession. Journal of Applied Ecology 56(9), 2236–2247. https://doi.org/10.1111/1365-2664.13458

Nelson, J. L., & Zavaleta, E. S. (2012). Salt marsh as a coastal filter for the oceans: changes in function with experimental increases in nitrogen loading and sea-level rise. PLoS One 7. https://doi.org/10.1371/journal.pone.0038558

Newton, A., Icely, J., Cristina, S., Perillo, G. M. E., Turner, R. E., Ashan, D., Cragg, S., Luo, Y., Tu, C., Li, Y., Zhang, H., Ramesh, R., Forbes, D. L., Solidoro, C., Béjaoui, B., Gao, S., Pastres, R., Kelsey, H., Taillie, D., Nhan, N., Brito, A., de Lima, R., & Kuenzer, C. (2020). Anthropogenic, Direct Pressures on Coastal Salt marsh. Frontiers in Ecology and Evolution 8. https://doi.org/10.3389/fevo.2020.00144

Newton, A., Icely, J. D., Falcao, M., Nobre, A., Nunes, J. P., Ferreira, J. G., & Vale, C. (2003). Evaluation of eutrophication in the Ria Formosa coastal lagoon, Portugal. Continental Shelf Research 23(17–19), 1945–1961. https://doi.org/10.1016/j.csr.2003.06.008

Niroumand-Jadidi, M., Legleiter, C. J., & Bovolo, F. (2022). River Bathymetry Retrieval from Landsat-9 Images Based on Neural Networks and Comparison to SuperDove and Sentinel-2. IEEE Journal of Selected Topics in Applied Earth Observations and Remote Sensing 15, 5250–5260. https://doi.org/10.1109/JSTARS.2022.3187179

Nordström, M. C., Currin, C. A., Talley, T. S., Whitcraft, C. R., & Levin, L. A. (2014). Benthic food-web succession in a developing salt marsh. Marine Ecology Progress Series 500, 43–55. https://doi.org/10.3354/meps10686

Olaode, A., Naghdy, G. A., Todd, C., & Naghdy, G. (2014). Unsupervised Classification of Images: A Review. International Journal of Image Processing 8(5).

Orson, R., Panageotou, W., & Leatherman, S. P. (1985). Response of Tidal Salt Marshes of the U.S. Atlantic and Gulf Coasts to Rising Sea Levels. Journal of Coastal Research 1(1), 29–37 https://www.jstor.org/sTable/4297007?seq=1&cid=pdf-

Pacheco, A., Ferreira, Ó., Williams, J. J., Garel, E., Vila-Concejo, A., & Dias, J. A. (2010). Hydrodynamics and equilibrium of a multiple-inlet system. Marine Geology 274(1–4), 32–42. https://doi.org/10.1016/j.margeo.2010.03.003

Perino, A., Pereira, H. M., Navarro, L. M., Fernández, N., Bullock, J. M., Ceauşu, S., Cortés-Avizanda, A., Van Klink, R., Kuemmerle, T., Lomba, A., Pe'er, G., Plieninger, T., Benayas, J. M. R., Sandom, C. J., Svenning, J. C., & Wheeler, H. C. (2019). Rewilding complex ecosystems. Science 364 (6438). https://doi.org/10.1126/science.aav5570

Perumal, K., & Bhaskaran, R. (2010). Supervised Classification Performance of Multispectral Images. Journal of Computing 2(2). https://doi.org/10.48550/arXiv.1002.4046

Phiri, D., & Morgenroth, J. (2017). Developments in Landsat land cover classification methods: A review. Remote Sensing 9(9). https://doi.org/10.3390/rs9090967

Phiri, D., Simwanda, M., Salekin, S., Nyirenda, V. R., Murayama, Y., & Ranagalage, M. (2020). Sentinel-2 data for land cover/use mapping: A review. Remote Sensing 12(14). https://doi.org/10.3390/rs12142291

PictureThis (2015). PictureThis website, accessed on 23/09/2023, <https://www.picturethisai.com/>

Pinton, D., Canestrelli, A., Wilkinson, B., Ifju, P., & Ortega, A. (2021). Estimating ground elevation and vegetation characteristics in coastal salt marshes using UAV-based lidar and digital aerial photogrammetry. Remote Sensing 13(22). https://doi.org/10.3390/rs13224506

Planet 2023a, Planet developers website, accessed on 07/01/2024, <https://developers.planet.com/docs/data/udm-2/>

Planet Labs PBC (2023). Image © 2023 Planet Labs PBC. https://api.planet.com

Poppe, K. L., & Rybczyk, J. M. (2021). Tidal marsh restoration enhances sediment accretion and carbon composite in the Stillaguamish River estuary, Washington. PLoS ONE 16. https://doi.org/10.1371/journal.pone.0257244

Potts, T., Burdon, D., Jackson, E., Atkins, J., Saunders, J., Hastings, E., & Langmead, O. (2014). Do marine protected areas deliver flows of ecosystem services to support human welfare? Marine Policy 44, 139–148. https://doi.org/10.1016/j.marpol.2013.08.011

Qian, Y., Qiu, F., Chang, J., & Zhang, K. (2008). Visualization-informed noise elimination and its application in processing high-spatial-resolution remote sensing imagery. Computers and Geosciences, 34(1), 35–52. https://doi.org/10.1016/j.cageo.2007.02.006

Raber, G., Jensen, J.R., Hodgson, M.E., Tullis, J.A., Davis, B.A., & Berglund, J. (2007). Impact of Lidar Nominal Post-spacing on DEM Accuracy and Flood Zone Delineation. Photogrammetric Engineering and Remote Sensing 73, 793-804.

Rajakumari, S., Mahesh, R., Sarunjith, K. J., & Ramesh, R. (2022). Building spectral catalogue for salt marsh vegetation, hyperspectral and multispectral remote sensing. Regional Studies in Marine Science 53. https://doi.org/10.1016/j.rsma.2022.102435

Reed, D. J., Spencer, T., Murray, A. L., French, J. R., & Leonard, L. (1999). Marsh surface sediment deposition and the role of tidal creeks: Implications for created and managed coastal marshes. Journal of Coastal Conservation 5(1), 81–90. https://doi.org/10.1007/BF02802742

Reschke, J., & Hüttich, C. (2014). Continuous field mapping of Mediterranean salt marsh using sub-pixel spectral signatures and multi-temporal Landsat data. International Journal of Applied Earth Observation and Geoinformation 28, 220–229. https://doi.org/10.1016/j.jag.2013.12.014

Richard, G. A. (1978). Seasonal and Environmental in Sediment Accretion in a Variations Long Island Salt Marsh. Estuaries and Coasts: J ERF 1, 29–35. https://doi.org/10.2307/1351647

Rodriguez-Galiano, V. F., Ghimire, B., Rogan, J., Chica-Olmo, M., & Rigol-Sanchez, J. P. (2012). An assessment of the effectiveness of a random forest classifier for land-cover classification. ISPRS Journal of Photogrammetry and Remote Sensing 67(1), 93–104. https://doi.org/10.1016/j.isprsjprs.2011.11.002

Roner, M., D'Alpaos, A., Ghinassi, M., Marani, M., Silvestri, S., Franceschinis, E., & Realdon, N. (2016). Spatial variation of salt-marsh organic and inorganic deposition and organic carbon composite: Inferences from the Venice lagoon, Italy. Advances in Water Resources 93, 276–287. https://doi.org/10.1016/j.advwatres.2015.11.011

Rouse, J.W., Haas, R.H., Schell, J.A. & Deering, D.W. (1974) Monitoring Vegetation Systems in the Great Plains with ERTS. Third ERTS-1 Symposium NASA, NASA SP-351, Washington DC, 309-317.

Rummell, A. J., Leon, J. X., Borland, H. P., Elliott, B. B., Gilby, B. L., Henderson, C. J., & Olds, A. D. (2022). Watching the Saltmarsh Grow: A High-Resolution Remote Sensing Approach to Quantify the Effects of Wetland Restoration. Remote Sensing 14(18). https://doi.org/10.3390/rs14184559

Salles, P., Voulgaris, G., & Aubrey, D. G. (2005). Contribution of nonlinear mechanisms in the persistence of multiple tidal inlet systems. Estuarine, Coastal and Shelf Science 65(3), 475–491. https://doi.org/10.1016/j.ecss.2005.06.018

Sathya, P., & Deepa, V. B. (2017). Analysis of Supervised Image Classification Method for Satellite Images. International Journal of Computer Science Research 5(2), 16–19. ID: IJCSR-050204.

Schmidt, K. S., & Skidmore, A. K. (2003). Spectral discrimination of vegetation types in a coastal wetland. Remote Sensing of Environment 85(1), 92–108. https://doi.org/10.1016/S0034-4257(02)00196-7

Schrift, A. M., Mendelssohn, I. A., & Materne, M. D. (2008). Salt marsh restoration with sediment-slurry amendments following a drought-induced large-scale disturbance. Wetlands 28, 1071–1085. https://doi.org/10.1672/07-78.1

Sharma, R., Mishra, D. R., Levi, M. R., & Sutter, L. A. (2022). Remote Sensing of Surface and Subsurface Soil Organic Carbon in Tidal Wetlands: A Review and Ideas for Future Research. Remote Sensing 14(12). https://doi.org/10.3390/rs14122940

Shen, H., Li, X., Cheng, Q., Zeng, C., Yang, G., Li, H., & Zhang, L. (2015). Missing information reconstruction of remote sensing data: a technical review. IEEE Geoscience and Remote Sensing Magazine 3, 61–85. https://doi.org/10.1109/MGRS.2015.2441912.

Shepard, C. C., Crain, C. M., & Beck, M. W. (2011). The protective role of coastal marshes: A systematic review and meta-analysis. PLoS ONE 6(11). https://doi.org/10.1371/journal.pone.0027374

Showstack, R. (2014). Sentinel Satellites Initiate New Era in Earth Observation. Eos, Transactions American Geophysical Union 95(26), 239–240. https://doi.org/10.1002/2014eo260003

Silvestri, S., Defina, A., & Marani, M. (2005). Tidal regime, salinity and salt marsh plant zonation. Estuarine, Coastal and Shelf Science 62(1–2), 119–130. https://doi.org/10.1016/j.ecss.2004.08.010

Silvestri, S., & Marani, M. (2004). Salt-Marsh Vegetation and Morphology: Basic Physiology, Modelling and Remote Sensing Observations. The ecogeomorphology of tidal marshes, 59, 5-25. https://doi.org/10.1029/CE059p0005

Simenstad, C., Reed, D., & Ford, M. (2006). When is restoration not? Incorporating landscape-scale processes to restore self-sustaining ecosystems in coastal wetland restoration. Ecological Engineering 26(1), 27–39. https://doi.org/10.1016/j.ecoleng.2005.09.007

Sims, D. A., & Gamon, J. A. (2002). Relationships between leaf pigment content and spectral reflectance across a wide range of species, leaf structures and developmental stages. Remote Sensing of Environment 81(2-3), 337 – 354. https://doi.org/10.1016/S0034-4257(02)00010-X

Singh, P., Diwakar, M., Shankar, A., Shree, R., & Kumar, M. (2021). A Review on SAR Image and its Despeckling. Archives of Computational Methods in Engineering 28(7), 4633–4653. https://doi.org/10.1007/s11831-021-09548-z

Sinha, P., Kumar, L., & Reid, N. (2012). Seasonal Variation in Land-Cover Classification Accuracy in a Diverse Region. Photogrammetric Engineering and Remote Sensing, 78(3), p. 271-280. https://doi.org/ 10.14358/PERS.78.3.271

Slocum, M. G., Mendelssohn, I. A. & Kuhn, N. L. (2005). Effects of sediment slurry enrichment on salt marsh rehabilitation: Plant and soil responses over seven years. Estuaries 28, 519–528. https://doi.org/10.1007/BF02696063

Spencer, K. L., & Harvey, G. L. (2012). Understanding system disturbance and ecosystem services in restored saltmarshes: Integrating physical and biogeochemical processes. Estuarine, Coastal and Shelf Science 106, 23–32. https://doi.org/10.1016/j.ecss.2012.04.020

Stoner, E. R., & Baumgardner, M. F. (1981). Characteristic variations in reflectance of surface soils. Soil Science Society of America Proceedings 45(6), 1161-1165, 1981. https://doi.org/10.2136/SSSAJ1981.03615995004500060031X

Streck, N. A., Rundquist, D., & Connot, J. (2003). Spectral signature of selected soils. Revista Brasileira de Agrometeorologia, Santa Maria 11(1), 181-184.

Taddeo, S. (2022). Leveraging time series of satellite and aerial images to promote the long-term monitoring of restored plant communities. Applied Vegetation Science 25(2). https://doi.org/10.1111/avsc.12664

Tang, Y., Shao, Q., Liu, J., Zhang, H., Yang, F., Cao, W., Wu, D., & Gong, G. (2019). Did ecological restoration hit its mark? Monitoring and assessing ecological changes in the grain for green program region using multi-source satellite images. Remote Sensing 11(3). https://doi.org/10.3390/rs11030358

Tatem, A. J., Goetz, S. J., & Hay, S. I. (2008). Fifty years of earth-observation satellites. American Scientist 96(5), 390–398. https://doi.org/10.1511/2008.74.390

Temmerman, S., Meire, P., Bouma, T. J., Herman, P. M. J., Ysebaert, T., & De Vriend, H. J. (2013). Ecosystem-based coastal defense in the face of global change. Nature 504, 79–83. https://doi.org/10.1038/nature12859

Townend, I., Fletcher, C., Knappen, M., & Rossington, K. (2011). A review of salt marsh dynamics. Water and Environment Journal 25(4), 477–488. https://doi.org/10.1111/j.1747-6593.2010.00243.x

Turner, R. E. (1990). Landscape Development and Coastal Wetland Losses in the Northern Gulf of Mexico 30(1), 89-105. https://doi.org/10.1093/icb/30.1.89

Vazir, K. (2021). Planet Imagery and Color Correction. Support Planet. Accessed on 20/07/2024, <https://support.planet.com/hc/en-us/articles/4404691539857-Planet-Imagery-and-Color-Correction>

Vernberg, F. J. (1993). Salt-marsh processes: A Review. Environmental Toxicology and Chemistry 12(12), 2167–2195. https://doi.org/10.1002/etc.5620121203

Viallefont-Robinet, F., Bacour, C., Bouvet, M., Kheireddine, M., Ouhssain, M., Idoughi, R., Grignon, L., Munesa, E., Lemaître, F., & Rivière, T. (2019). Contribution to sandy site characterization: Spectro-directional signature, grain size distribution and mineralogy extracted from sand samples. Remote Sensing 11(20). https://doi.org/10.3390/rs11202446

Vila-Concejo, A., Ferreira, Ó., Ciavola, P., Matias, A., & Dias, J. M. A. (2004). Tracer studies on the updrift margin of a complex inlet system. Marine Geology 208(1), 43–72. https://doi.org/10.1016/j.margeo.2004.04.020

Vila-Concejo, A., Matias, A., Ferreira, O., Duarte, C., & Dias, J. M. A. (2002). Recent Evolution of the Natural Inlets of a Barrier Island System in Southern Portugal. Journal of Coastal Research 36, 741–752. https://doi.org/10.2112/1551-5036-36.sp1.741

Vuik, V., Jonkman, S.N., Borsje, B.W., & Suzuki, T. (2016). Nature-based flood protection: the efficiency of vegetated foreshores for reducing wave loads on coastal dikes. Coastal Engineering 116, 42–56. https://doi.org/10.1016/j.coastaleng.2016.06.001

Warren, S. D., Alt, M., Olson, K. D., Irl, S. D. H., Steinbauer, M. J., & Jentsch, A. (2014). The relationship between the spectral diversity of satellite imagery, habitat heterogeneity, and plant species richness. Ecological Informatics 24, 160–168. https://doi.org/10.1016/j.ecoinf.2014.08.006

Wei, C., Guo, B., Fan, Y., Zang, W., & Ji, J. (2022). The Change Pattern and Its Dominant Driving Factors of Wetlands in the Yellow River Delta Based on Sentinel-2 Images. Remote Sensing 14(17). https://doi.org/10.3390/rs14174388

Woerner, L. S., & Hackney, C. T. (1997). Distribution of *Juncus roemerianus* in North Carolina tidal marshes: The importance of physical and biotic variables. Salt marsh 17(2), 284–291. https://doi.org/10.1007/BF03161416

Wolfe, R., Tan, B., & Lin, G. (2021). PlanetScope Imagery Geolocation Accuracy Assessment. AGU Fall Meeting 2021, New Orleans, LA, 13-17 December 2021. Bibcode: 2021AGUFM.B15I1545T

Wolters, M., Garbutt, A., & Bakker, J. P. (2005). Salt-marsh restoration: Evaluating the success of de-embankments in north-west Europe. Biological Conservation 123(2), 249–268. https://doi.org/10.1016/j.biocon.2004.11.013

Wu, Q. (2018). GIS and remote sensing applications in wetland mapping and monitoring. Comprehensive Geographic Information Systems. Elsevier, 140–157. https://doi.org/10.20944/preprints201709.0058.v1

Wulder, M. A., Roy, D. P., Radeloff, V. C., Loveland, T. R., Anderson, M. C., Johnson, D. M., Healey, S., Zhu, Z., Scambos, T. A., Pahlevan, N., Hansen, M., Gorelick, N., Crawford, C. J., Masek, J. G., Hermosilla, T., White, J. C., Belward, A. S., Schaaf, C., Woodcock, C. E., Huntington J. L., Lymburner, L., Hostert, P., Gao, G., Lyapustin, A., Pekel, J. F., Strobl, P., & Cook, B. D. (2022). Fifty years of Landsat science and impacts. Remote Sensing of Environment 280. https://doi.org/10.1016/j.rse.2022.113195

Xie, Y., Sha, Z., & Yu, M. (2008). Remote sensing imagery in vegetation mapping: a review. Journal of Plant Ecology 1(1), 9–23. https://doi.org/10.1093/jpe/rtm005

Xu, Y., Yu, L., Cai, Z., Zhao, J., Peng, D., Li, C., Lu, H., Yu, C., & Gong, P. (2019). Exploring intra-annual variation in cropland classification accuracy using monthly, seasonal, and yearly sample set. International Journal of Remote Sensing 40(23), 8748–8763. https://doi.org/10.1080/01431161.2019.1620377

Yang, H. L., Peng, J. H., Xia, B. R., & Zhang, D. X. (2013). An improved EM algorithm for remote sensing classification. Chinese Science Bulletin 58(9), 1060–1071. https://doi.org/10.1007/s11434-012-5485-4

Yeh, A.G.O., (1999). Urban planning and GIS. The University of Edinburgh.

Zhang, S., Li, X., Zong, M., Zhu, X., & Cheng, D. (2017). Learning k for kNN Classification. ACM Transactions on Intelligent Systems and Technology 8(3). https://doi.org/10.1145/2990508

Zhang, S., Hu, C., Barnes, B. B., & Harrison, T. N. (2022). Monitoring Sargassum Inundation on Beaches and Nearshore Waters Using PlanetScope/Dove Observations. IEEE Geoscience and Remote Sensing Letters 19, 1–5. https://doi.org/10.1109/LGRS.2022.3148

Appendixes

Appendix A: Maps of the evolution in time of the rewilded salt marshes

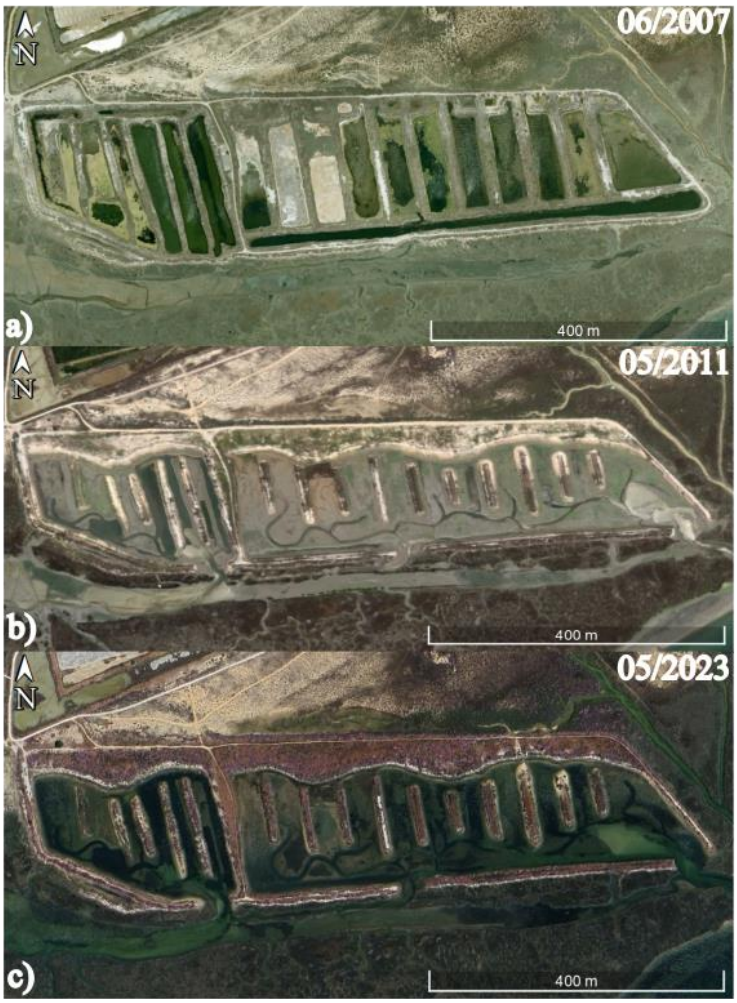

Figure A1. Maps showing three different periods of the restored salt marsh in Bias, Olhão: a) in 2007, still being closed; b) in 2011, already opened; and **c)** in 2023, the latest image. (Google Earth PRO, 2023).

Figure A2. Maps showing three different periods of the restored salt marsh in Olhão: a) in 2015, still being closed; b) in 2017, already opened; and **c)** in 2023, the latest image. (Google Earth PRO, 2023).

Appendix B: Plant species encountered in the salt marshes

Table B1. List of plant species encountered in Bias and Olhão in the fieldwork campaigns.

Species	Photos	Elevation in relation to Mean Sea Level (cm)	Flowering season	Life cycle	Salt marsh zonation	Online sources
Arthrocnemum macrostachyum*		0 – 228	April-September	Perennial	High and medium	https://www.llifle.com/Encyclopedia/SUCCULENTS/Family/Chenopodiaceae/34212/Arthrocnemum_macrostachyum#:~:text=Description%3A%20Arthrocnemum%20macrostachyum%20is%20a,ascending%2C%20sometimes%20rooting%20at%20base https://flora-on.pt/?q=Arthrocnemum
Atriplex halimus**		0 – 106	August – October	Perennial	High	https://landscapeplants.aub.edu.lb/Plants/GetPDF/17b22b59-5508-478b-ab6e-ccd38d139bd8 https://flora-on.pt/?q=Atriplex+halimus

Asparagus albus**	 https://flora-on.pt/#/hDlTD	0-125	June - October	Perennial	Non-natural to salt marshes	https://flora-on.pt/?q=Asparagus+albus https://worldspecies.org/ntaxa/1208905
Caroxylon vermiculatum* (Salsola vermiculata)		0 – 106	April – June Mid-July – mid-September October	Perennial	High	https://www.cabidigitallibrary.org/doi/10.1079/cabicompendium.48244
Carpobrotus edulis***		0 - 66	January - July	Perennial	Non-natural to salt marshes	https://www.cabidigitallibrary.org/doi/10.1079/cabicompendium.48244 https://floraveg.eu/taxon/overview/Carpobrotus%20edulis

Halimione portucaloides***		0 - 21	April - September	Perennial	Low	https://flora-on.pt/?q=Halimione https://cantuesoseeds.com/en/shop/bulk-seeds/halimione-portulacoides/
Juncus maritimus***	 https://flora-on.pt/#/hrtzy	0 - 141	June – mid-July	Perennial	High	https://flora-on.pt/?q=Juncus+maritimus https://www.shootgardening.com/plants/juncus-maritimus
Limoniastrum monopetalum*		0 – 43	March - September	Perennial	High - medium	https://flora-on.pt/?q=Limoniastrum https://floraveg.eu/taxon/overview/Limoniastrum%20monopetalum

Oxalis pes-caprae*	 https://flora-on.pt/#/htACM	0 - 92	November - April	Perennial	Non-natural to salt marshes	https://flora-on.pt/?q=Oxalis+pes-caprae https://weeds.org.au/profiles/soursob-bermuda-buttercup/#:~:text=What%20is%20it%3F-,Soursob%20(Oxalis%20pes-caprae)%20is%20a%20small%2C%20upright,markings%20on%20the%20upper%20surface https://invasoras.pt/en/invasive-plant/oxalis-pes-caprae
Salicornia ramosissima*		0 - 18	May - November	Annual	Low	https://flora-on.pt/?q=Salicornia http://almargem.org/biodiv/especie/salicornia-ramosissima/

Sarcocornia perennis*		0 - 20	August - November	Perennial	Low	https://flora-on.pt/?q=Sarcocornia+perennis https://www.wildflowersofireland.net/plant_detail.php?id_flower=474&wildflower=Glasswort,%20Perennial
Sonchus arvensis**  https://identify.plantnet.org/pt-br/k-world-flora/observations/1021163669		0 - 2000	March - October	Perennial	Non-natural to salt marshes	https://identify.plantnet.org/pt/k-world-flora/species/Sonchus%20arvensis%20L./data https://www.worldfloraonline.org/taxon/wfo-0000092611
Spartina maritima*		0 - 20	May – Mid-June Mid-July - September	Perennial	Low	https://flora-on.pt/?q=Spartina+maritima https://www.gbif.org/species/5290044~

Suaeda Maritima***	 https://jb.utad.pt/multimedia/24722#imagem-24722	0 - 65	July - September	Annual	Medium - High	https://jb.utad.pt/especie/Suaeda_maritima
Suaeda vera*		0 - 65	March – July Mid-July – Mid-August October	Perennial	High	https://flora-on.pt/?q=Suaeda+vera https://www.picturethisai.com/wiki/Suaeda_vera.html

* Encountered in Bias and Olhão. ** Encountered only in Bias. *** Encountered only in Olhão

Appendix C: Graphical analysis of image classification methods

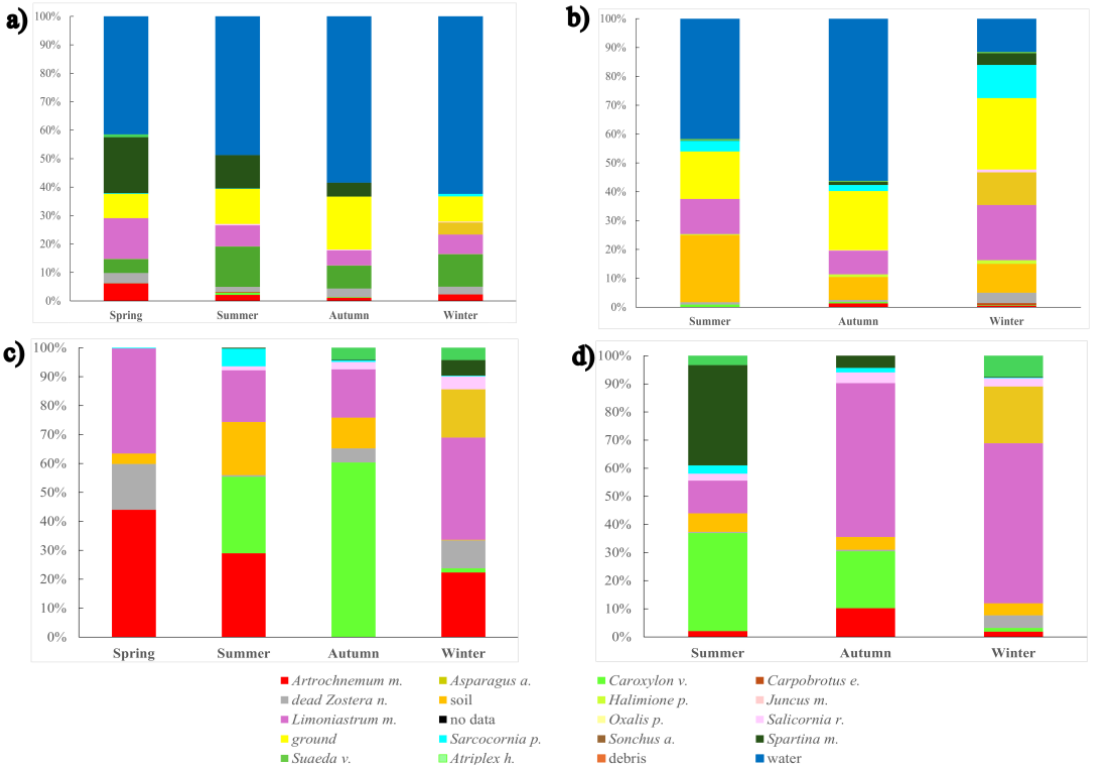

Figure C1. Percentages of plant species classified using RF for **a)** RF-EA, **b)** RF-AC-EA, **c)** RF-PA, and **d)** RF-AC-PA in Bias. Each graph shows the values for all seasons analysed.

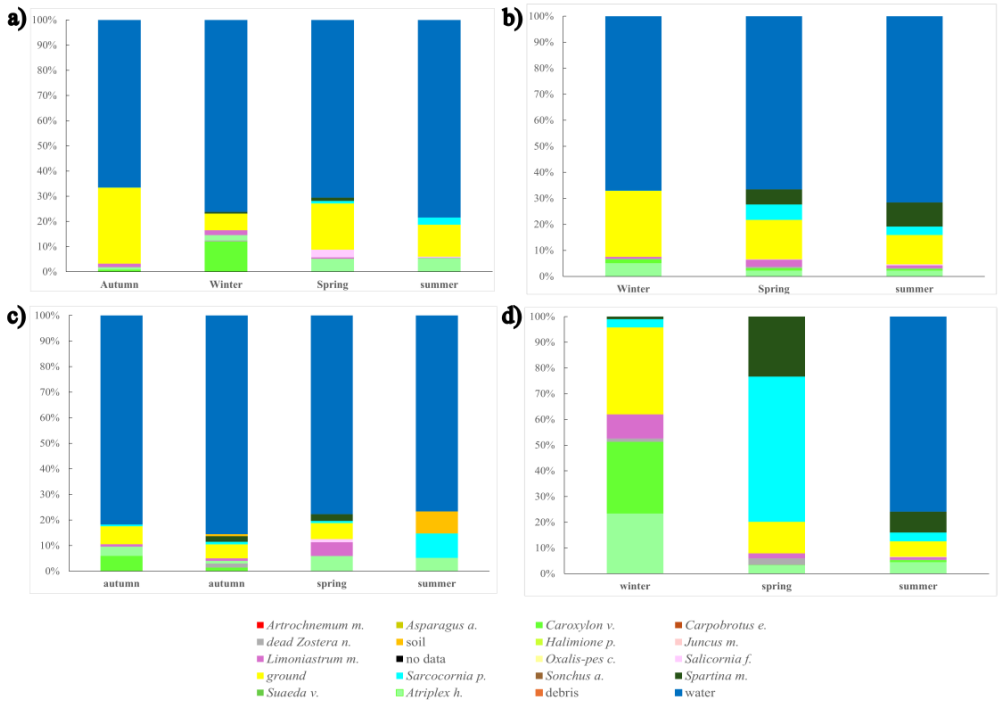

Figure C2. Percentages of plant species classified using RF for **a)** RF-EA, **b)** RF-AC-EA, **c)** RF-PA, and **d)** RF-AC-PA in Olhão. Each graph shows the values for all seasons analysed.

Appendix D: Entire spectral signature of plots and patches

Table D1. Spectral signature of plant species inside the plots in Bias. The wavelengths range from 443 nm (Blue) to 865 nm (Near-infrared). Together with the spectral signature, the percentages of plant species inside each plot for all seasons. The percentage of the plant species was calculated using the pixel where the spectral signature was extracted as the total area, using the contours of the plant species to calculate the percentage inside the pixel in QGIS.

Plot	Plant species and coverage percentage		Spectral signatures
1	**spring**	*Limoniastrum monopetalum* (96.8%) Soil (3.72%)	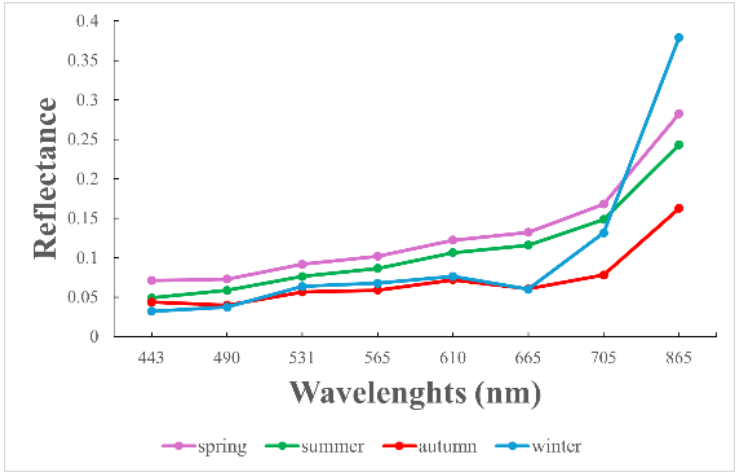
	summer	*Artrochnemum macrostachys (*8.71%) *Limoniastrum monopetalum* (25.64%) Soil* (5.65%)	
	autumn	*Artrochnemum macrostachys* (63.99%) *Limoniastrum monopetalum* (19.96%) Soil* (16.05%)	
	winter	*Limoniastrum monopetalum* (88.52%) *Oxalis pes-caprae* (11.48%)	

2	**spring**	*Artrochnemum macrostachys* (22.65%) *Limoniastrum monopetalum* (44.42%) Soil* (32.93%)
	summer	*Limoniastrum monopetalum* (100%)
	autumn	*Artrochnemum macrostachys* (10.65%) *Limoniastrum monopetalum* (88.77%) Soil* (0.58%)
	winter	*Artrochnemum macrostachys* (2.36%) *Limoniastrum monopetalum* (83.49%) *Oxalis pes-caprae* (14.15%)

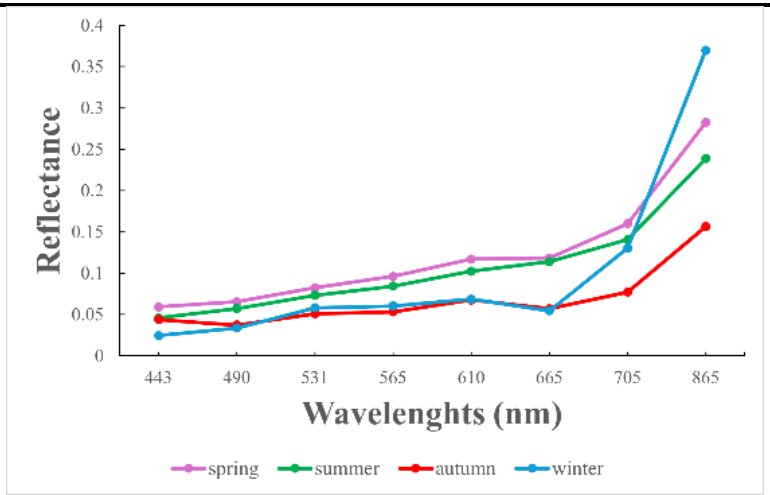

3	**spring**	*Artrochnemum macrostachys* (32.4%) *Limoniastrum monopetalum* (18.67%) Soil* (48.92%)
	summer	*Artrochnemum macrostachys* (99.8%) Soil* (0.2%)
	autumn	*Artrochnemum macrostachys* (97.99%) Soil* (2.01%)
	winter	*Artrochnemum macrostachys* (34.04%) *Limoniastrum monopetalum* (8.45%) *Oxalis pes-caprae* (57.51%)

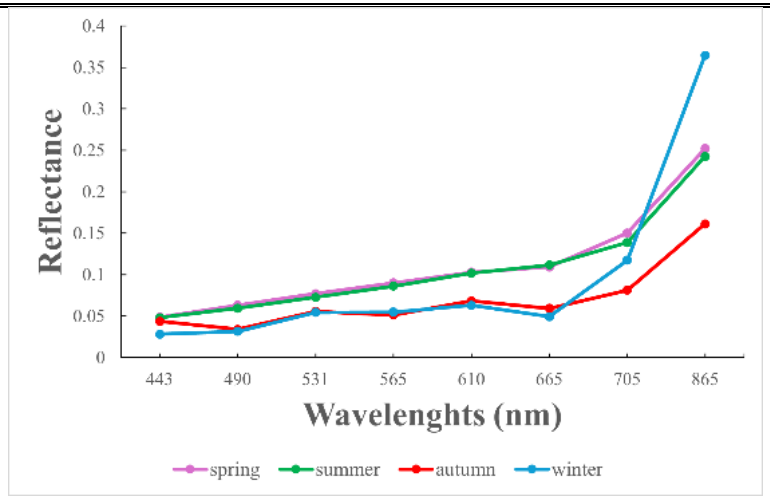

4	**spring**	*Artrochnemum macrostachys* (38.53%) Soil* (61.47%)
	summer	*Artrochnemum macrostachys* (87.6%) Soil* (12.4%)
	autumn	*Artrochnemum macrostachys* (68.52%) Soil* (31.48%)
	winter	*Artrochnemum macrostachys* (7.93%) *Limoniastrum monopetalum* (66.41%) *Oxalis pes-caprae* (25.65%)

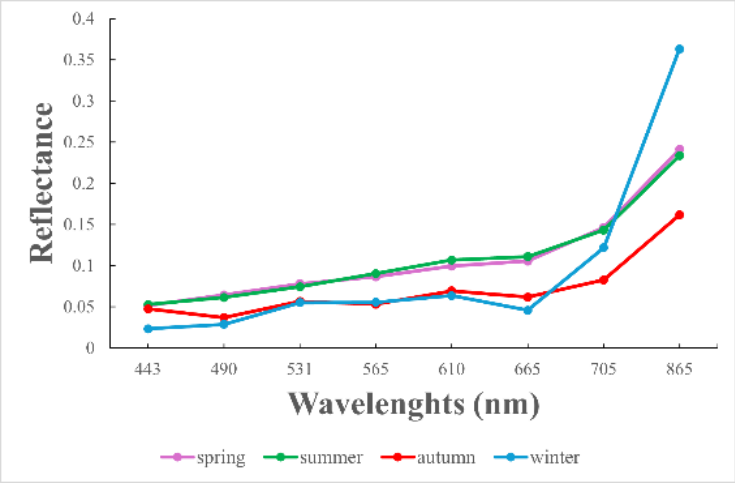

5	**spring**	*Artrochnemum macrostachys* (7.63%) *Caroxylon vermiculatum* (40.74%) Soil* (51.63%)
	summer	*Artrochnemum macrostachys* (12.6%) *Limoniastrum monopetalum* (3.1%) *Caroxylon vermiculatum* (5.4%) Soil* (78.9%)
	autumn	*Artrochnemum macrostachys* (5.22%) *Caroxylon vermiculatum* (2.61%) Soil* (92.17%)
	winter	*Artrochnemum macrostachys* (97.84%) *Oxalis pes-caprae* (2.16%)

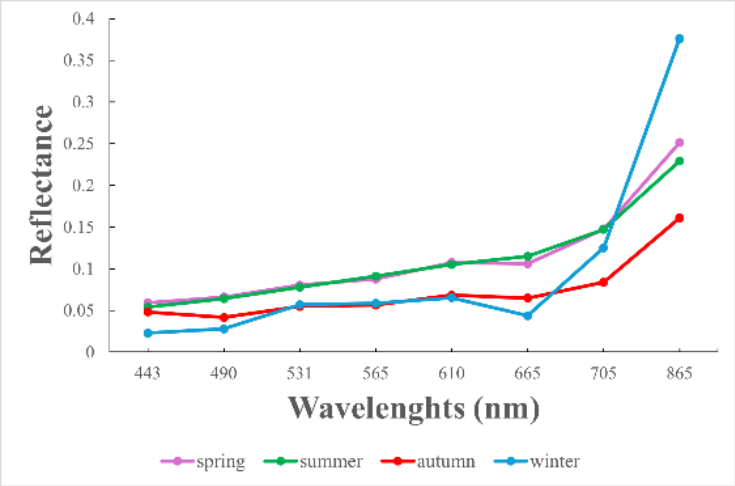

6	**spring**	*Artrochnemum macrostachys* (3.89%) *Caroxylon vermiculatum* (20%) Soil* (76.11%)
	summer	*Limoniastrum monopetalum* (17.61%) *Caroxylon vermiculatum* (0.66%) Soil* (81.74%)
	autumn	*Limoniastrum monopetalum* (1.19%) *Caroxylon vermiculatum* (1.85%) Soil* (96.96%)
	winter	*Artrochnemum macrostachys* (16.35%) *Oxalis pes-caprae* (83.65%)

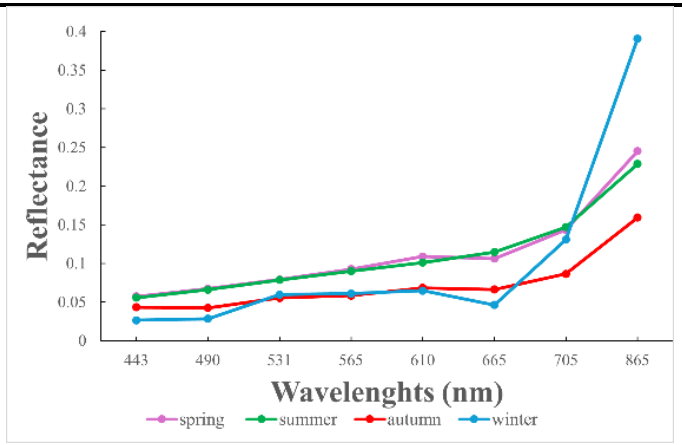

7	**spring**	*Limoniastrum monopetalum* (13.86%) *Caroxylon vermiculatum* (3.48%) Soil* (82.66%)
	summer	*Limoniastrum monopetalum* (84.6%) Soil* (15.4%)
	autumn	*Limoniastrum monopetalum* (76%) Soil* (24%)
	winter	*Artrochnemum macrostachys* (2.37%) *Caroxylon vermiculatum* (2.06%) *Oxalis pes-caprae* (95.57%)

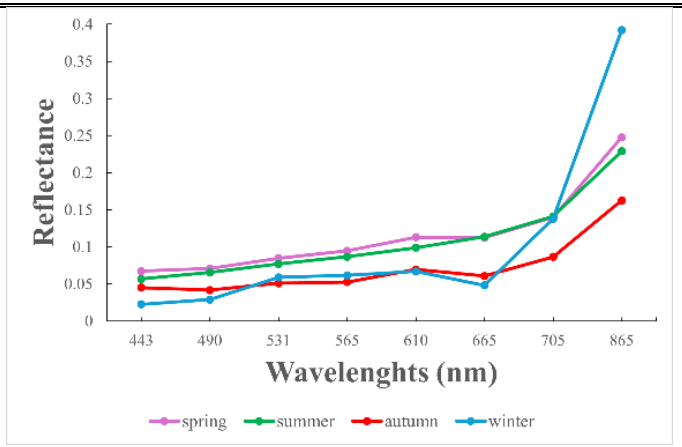

8	**spring**	*Limoniastrum monopetalum* (40.11%)
		Soil* (59.89%)
	summer	*Limoniastrum monopetalum* (59.47%)
		Caroxylon vermiculatum (0.83%)
		Soil* (12%)
		Carpobrotus edilus (27.7%)
	autumn	*Limoniastrum monopetalum* (83.89%)
		Caroxylon vermiculatum (0.63%)
		Soil* (11.62%)
		Carpobrotus edilus (3.86%)
	winter	*Caroxylon vermiculatum* (0.37%)
		Oxalis pes-caprae (99.63%)

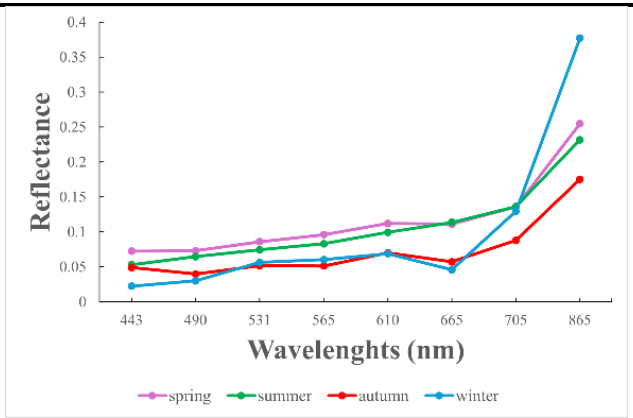

9	**spring**	*Limoniastrum monopetalum* (20.93%)
		Soil* (44.46%)
		Carpobrotus edilus (34.61%)
	summer	*Limoniastrum monopetalum* (46.65%)
		Caroxylon vermiculatum (4.11%)
		Soil* (40.49%)
		Carpobrotus edilus (8.75%)
	autumn	*Limoniastrum monopetalum* (30.57%)
		Caroxylon vermiculatum (2.58%)
		Soil* (66.82%)
		Carpobrotus edilus (0.83%)
	winter	*Limoniastrum monopetalum* (42.57%)
		Oxalis pes-caprae (57.43%)

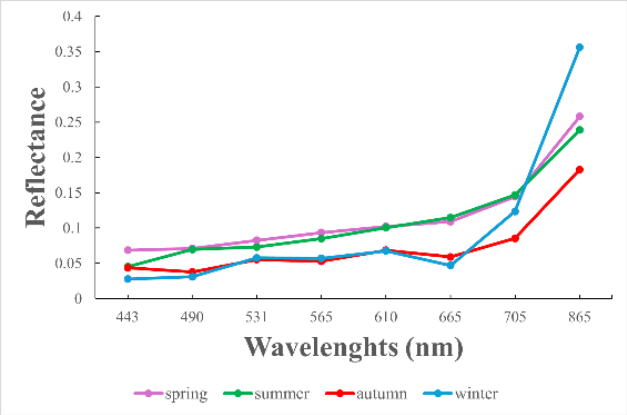

10	**spring**	*Limoniastrum monopetalum* (46.4%)
		Soil* (53.39%)
		Carpobrotus edilus (0.21%)
	summer	*Limoniastrum monopetalum* (65.52%)
		Caroxylon vermiculatum (18.73%)
		Soil* (15.75%)
	autumn	*Limoniastrum monopetalum* (45.5%)
		Caroxylon vermiculatum (38.79%)
		Soil* (15.71%)
	winter	*Limoniastrum monopetalum* (56.35%)
		Soil* (1.01%)
		Oxalis pes-caprae (42.63%)

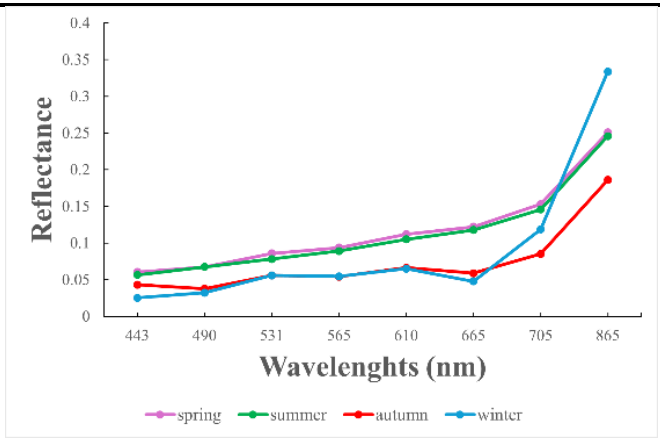

11	**spring**	*Limoniastrum monopetalum* (100%)
	summer	*Limoniastrum monopetalum* (64.77%)
		Caroxylon vermiculatum (14.34%)
		Soil* (6.97%)
		Suaeda vera (13.92%)
	autumn	*Artrochnemum macrostachys* (29.85%)
		Limoniastrum monopetalum (46.59%)
		Soil* (2.53%)
		Suaeda vera (21.03%)
	winter	*Limoniastrum monopetalum* (38.25%)
		Caroxylon vermiculatum (0.56%)
		Soil* (23.57%)
		Oxalis pes-caprae (37.62%)

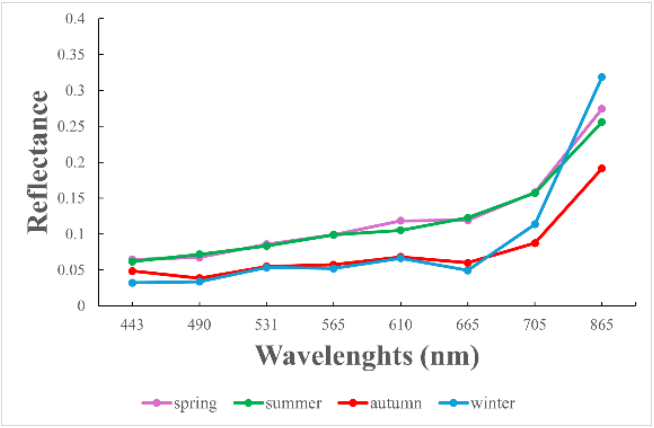

12	**spring**	*Artrochnemum macrostachys* (7.54%)
		Limoniastrum monopetalum (92.46%)
	summer	*Artrochnemum macrostachys* (58.4%)
		Limoniastrum monopetalum (14.2%)
		Caroxylon vermiculatum (16.1%)
		Soil* (3.4%)
		Suaeda vera (2%)
		Dead *Zostera noltii* (5.9%)
	autumn	*Artrochnemum macrostachys* (27.49%)
		Limoniastrum monopetalum (47.84%)
		Suaeda vera (15.15%)
		Dead *Zostera noltii* (9.53%)
	winter	*Limoniastrum monopetalum* (64.91%)
		Caroxylon vermiculatum (11.46%)
		Soil* (15.62%)
		Oxalis pes-caprae (8.01%)

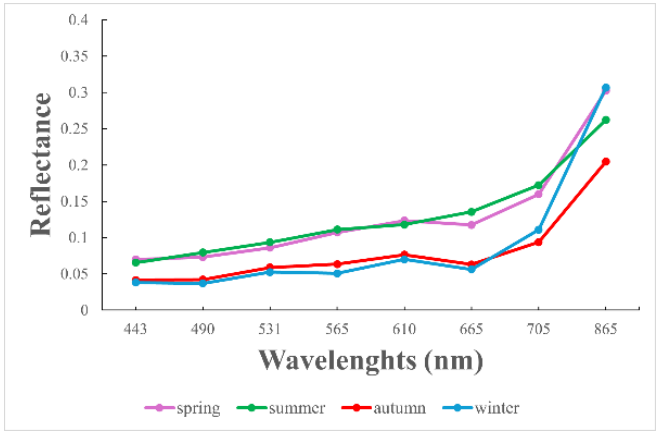

13	**spring**	*Limoniastrum monopetalum* (45.57%)
		Soil* (10.55%)
		Suaeda vera (29.71%)
		Dead *Zostera noltii* (14.17%)
	summer	*Artrochnemum macrostachys* (57%)
		Caroxylon vermiculatum (6.5%)
		Soil* (0.9%)
		Suaeda vera (8%)
		Sarcocornia perennis (0.8%)
		Dead *Zostera noltii* (26.8%)
	autumn	*Artrochnemum macrostachys* (10.09%)
		Soil* (21.46%)
		Suaeda vera (14.86%)
		Dead *Zostera noltii* (53.59%)

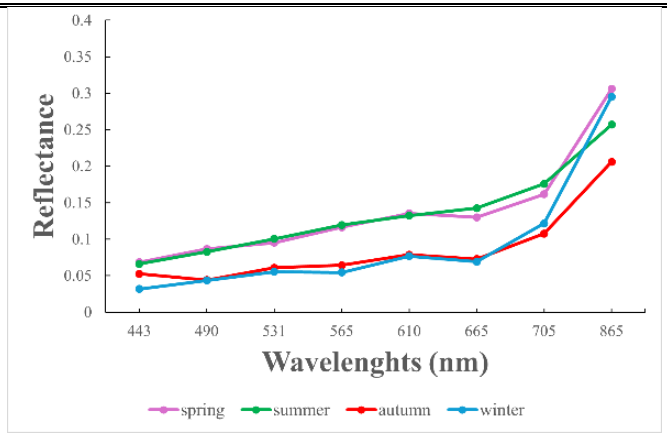

	winter	*Artrochnemum macrostachys* (2.19%)
		Limoniastrum monopetalum (55.97%)
		Soil* (11.95%)
		Suaeda vera (29.89%)
14	**spring**	*Artrochnemum macrostachys* (30.11%)
		Suaeda vera (26.66%)
		Sarcocornia perennis (0.14%)
		Dead *Zostera noltii* (43.09%)
	summer	*Artrochnemum macrostachys* (40.4%)
		Soil* (1.6%)
		Sarcocornia perennis (42%)
		Halimione portucaloides (8.1%)
		Dead *Zostera noltii* (7.9%)
	autumn	*Artrochnemum macrostachys* (9.87%)
		Soil* (33.61%)
		Suaeda vera (6.49%)
		Salicornia ramosissima (49.70%)
		Dead *Zostera noltii* (0.34%)
	winter	*Limoniastrum monopetalum* (39.72%)
		Soil* (2.34%)
		Suaeda vera (36.63%)
		Halimione portucaloides (6.17%)
		Dead *Zostera noltii* (15.14%)

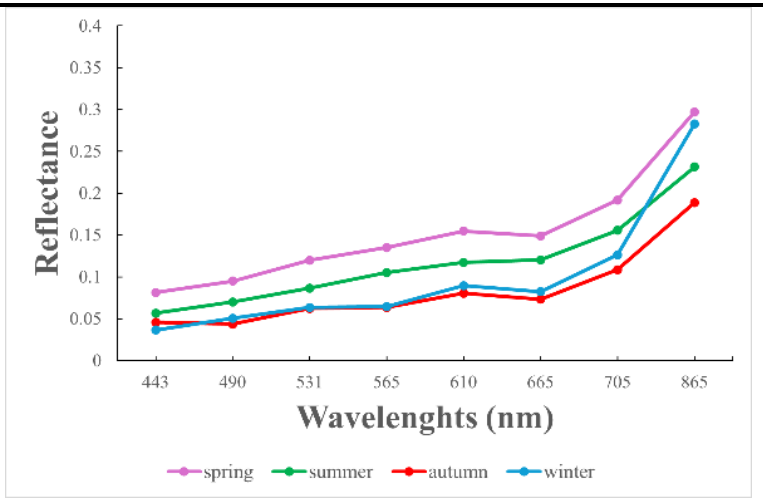

15	**spring**	*Suaeda vera* (12.42%)
		Sarcocornia perennis (4.49%)
		Halimione portucaloides (2.66%)
		Salicornia ramosissima (20.26%)
		Dead *Zostera noltii* (60.18%)
	summer	Soil* (55.65%)
		Sarcocornia perennis (42.68%)
		Spartina maritima (1.67%)
	autumn	Soil* (6.11%)
		Sarcocornia perennis (0.3%)
		Halimione portucaloides (3.16%)
		Salicornia ramosissima (90.43%)
	winter	Soil* (1.35%)
		Suaeda vera (8.11%)
		Sarcocornia perennis (11.97%)
		Salicornia ramosissima (20.76%)
		Dead *Zostera noltii* (57.81%)

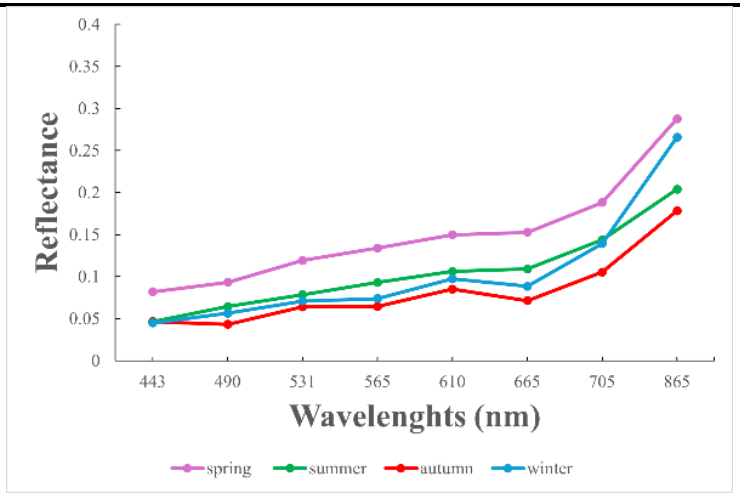

*Soil = General sediment **Ground = Artificial walking paths or sand

Table D2. Spectral signature of plant species inside the plots in Olhão. The wavelengths range from 443 nm (Blue) to 865 nm (Near-infrared). Together with the spectral signature, the percentages of plant species inside each plot for all seasons. The percentage of the plant species was calculated using the pixel where the spectral signature was extracted as the total area, using the contours of the plant species to calculate the percentage inside the pixel in QGIS.

Plot		Plant species	Spectral signatures
1	**spring**	*Limoniastrum monopetalum* (17.45%)	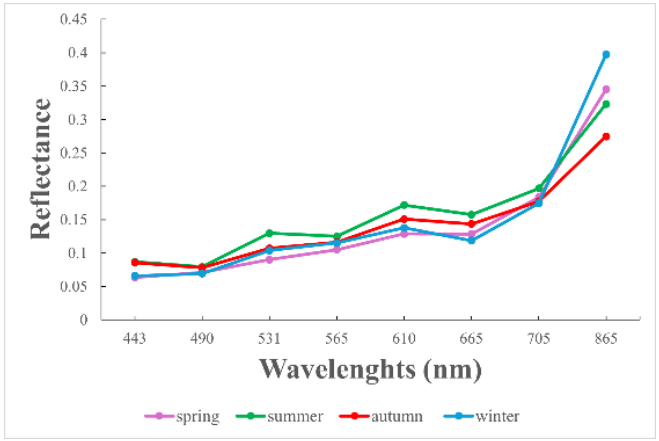
		Atriplex halimus (71.36%)	
		Ground** (11.19%)	
	summer	*Limoniastrum monopetalum* (36.03%)	
		Atriplex halimus (36.31%)	
		Ground** (27.66%)	
	autumn	*Limoniastrum monopetalum* (19.97%)	
		Caroxylon vermiculatum (0.49%)	
		Atriplex halimus (79.54%)	
	winter	*Limoniastrum monopetalum* (11.37%)	
		Ground** (5.62%)	
		Atriplex halimus (28.78%)	
		Oxalis pes-caprae (54.23%)	

2	**spring**	*Limoniastrum monopetalum* (42.15%)
		Atriplex halimus (19.98%)
		Dead *Zostera noltii* (14.01%)
		Ground** (23.87%)
	summer	*Limoniastrum monopetalum* (42.15%)
		Dead *Zostera noltii* (14.01%)
		Ground** (23.87%)
	autumn	*Limoniastrum monopetalum* (51.26%)
		Atriplex halimus (19.98%)
		Dead *Zostera noltii* (35.88%)
		Ground** (0.1%)
	winter	*Limoniastrum monopetalum* (48.51%)
		Soil* (2.67%)
		Ground** (19.55%)
		Atriplex halimus (18.59%)
		Dead *Zostera noltii* (10.68%)

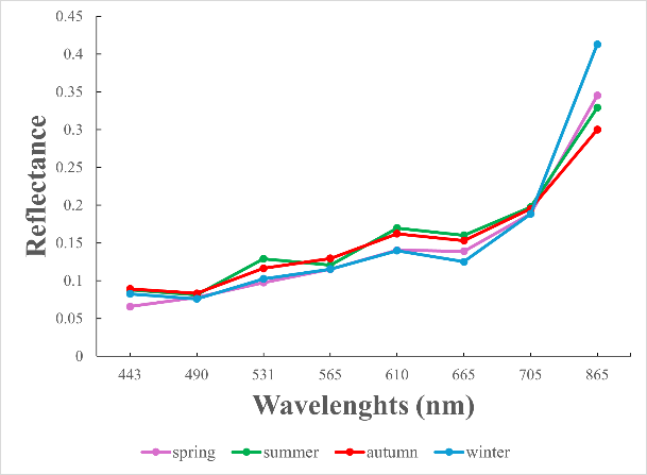

3	**spring**	Dead *Zostera noltii* (66.56%)
		Ground** (33.44%)
	summer	*Sarcocornia perennis* (15.49%)
		Salicornia ramosissima (0.43%)
		Dead *Zostera noltii* (75.21%)
		Ground** (8.87%)
	autumn	Dead *Zostera noltii* (42.06%)
		Ground** (57.94%)
	winter	Dead *Zostera noltii* (77.45%)
		Ground** (22.55%)

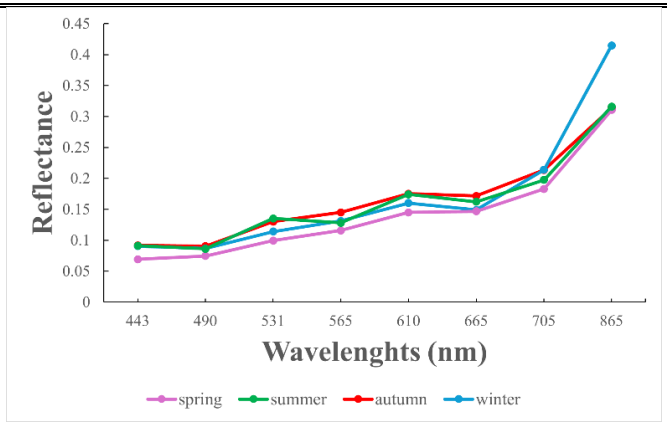

4	**spring**	*Sarcocornia perennis* (19.15%)
		Dead *Zostera noltii* (1.01%)
		Ground** (79.83%)
	summer	Ground** (33.20 %)
		Sarcocornia perennis (30.52 %)
		Salicornia ramosissima (2.27 %)
		Soil* (34.01 %)
	autumn	*Sarcocornia perennis* (42.52%)
		Salicornia ramosissima (32.14%)
		Dead *Zostera noltii* (24.88%)
		Ground** (0.46%)
	winter	*Sarcocornia perennis* (18.52%)
		Dead *Zostera noltii* (0.7%)
		Ground** (80.78%)

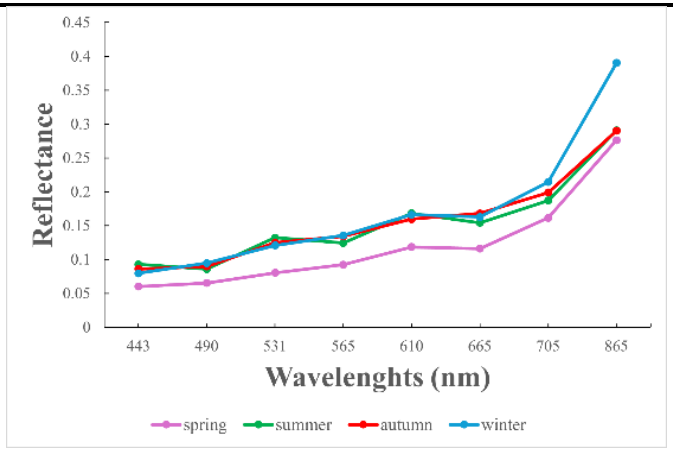

5	**spring**	*Sarcocornia perennis* (26.29%)
		Salicornia ramosissima (4.43%)
		Ground** (0.54%)
		Spartina maritima (68.74%)
	summer	*Sarcocornia perennis* (29.46%)
		Salicornia ramosissima (8.29%)
		Spartina maritima (31.62%)
		Soil* (8.47%)
		Ground** (22.15%)
	autumn	*Sarcocornia perennis* (75.78%)
		Salicornia ramosissima (24.22%)
		Spartina maritima (78.79%)
	winter	Soil* (31.07%)
		Sarcocornia perennis (18%)
		Spartina maritima (50.93%)

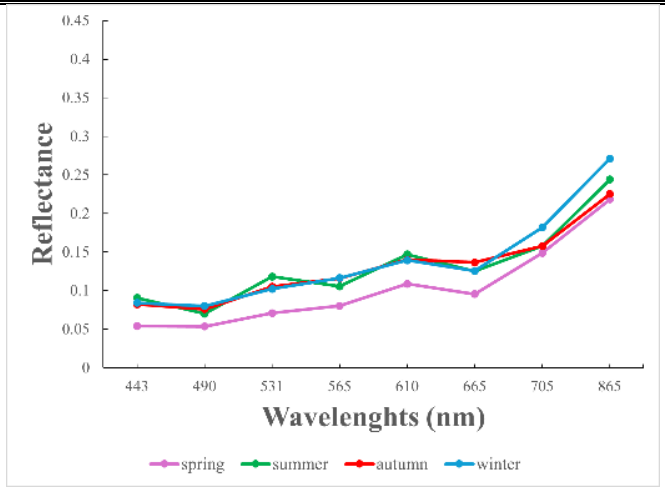

6

spring	Ground** (1.96%)
	Sarcocornia perennis (9.93%)
	Spartina maritima (74.38%)
	Soil* (13.73%)
summer	Ground** (5.68%)
	Sarcocornia perennis (13.15%)
	Spartina maritima (51.18%)
	Soil* (29.99%)
autumn	*Sarcocornia perennis* (52.66%)
	Salicornia ramosissima (4.17%)
	Ground** (43.17%)
	Spartina maritima (4.38%)
winter	Soil* (27.51%)
	Ground** (4.15%)
	Sarcocornia perennis (5.88%)
	Spartina maritima (62.47%)

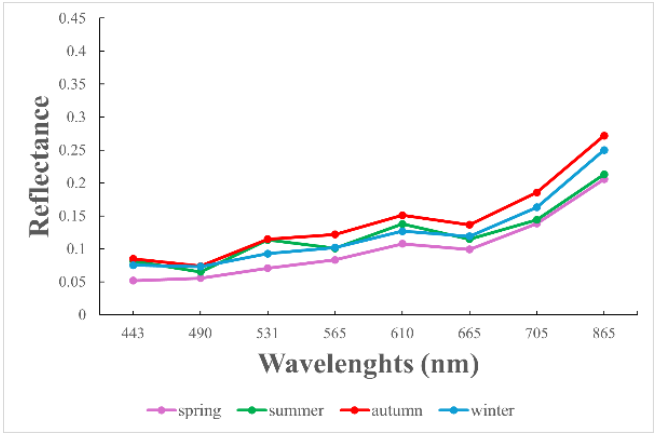

*Soil = General sediment **Ground = Artificial walking paths or sand

Table D3. Spectral signature of plant species patches and other features from the salt marsh in both ROIs. The wavelengths range from 443 nm (Blue) to 865 nm (Near-infrared). Together with the spectral signature, photos from each plant species taken in the fieldwork are also shown as a reference.

Species	Photo	Spectral signature
Limoniastrum monopetalum		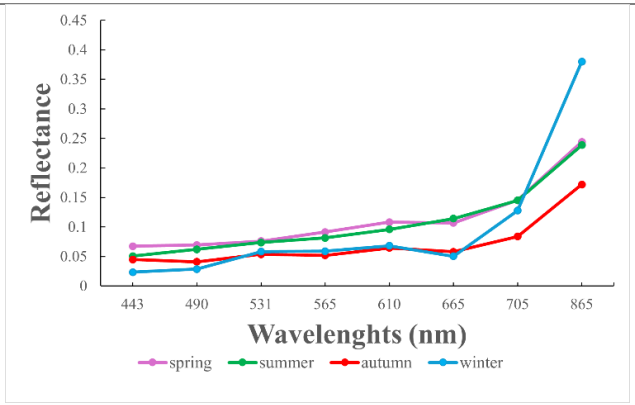
Caroxylon vermiculatum		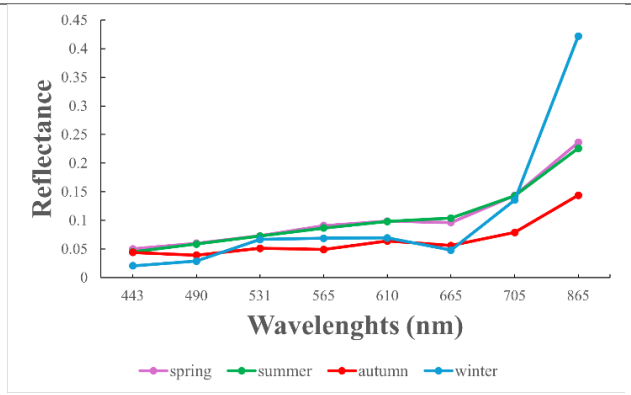

Artrochnemum macrostachys		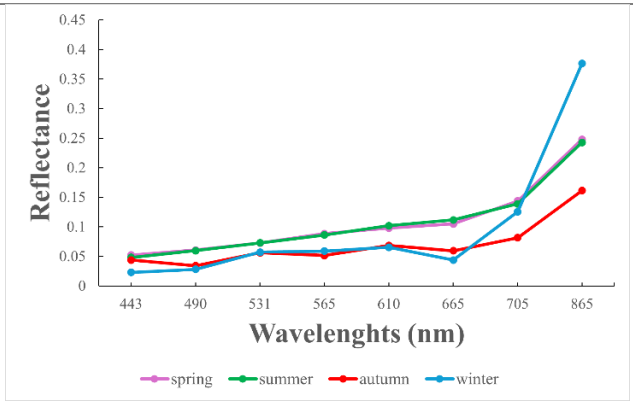
Carpobrotus edilus		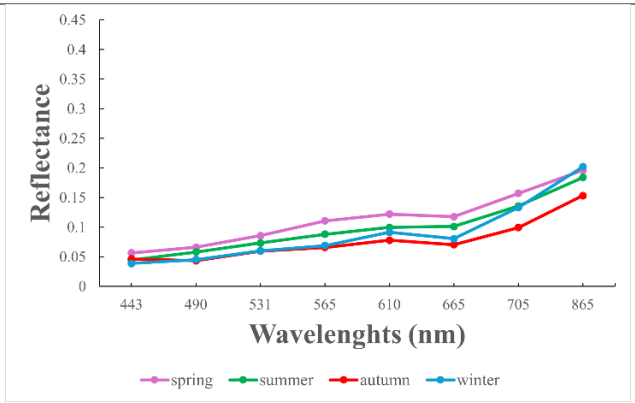

Suaeda vera		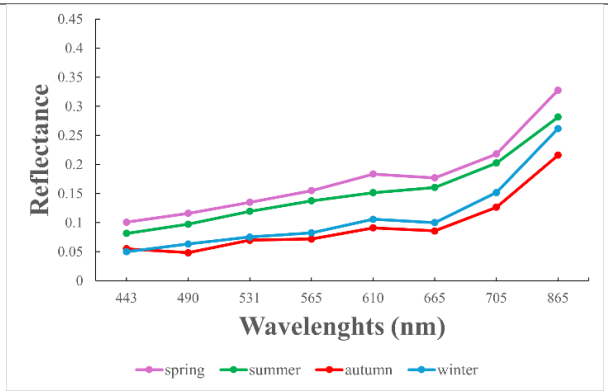
Dead *Zostera noltii*		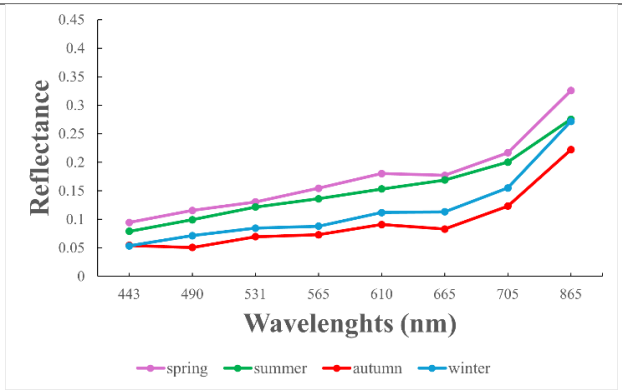

Soil*		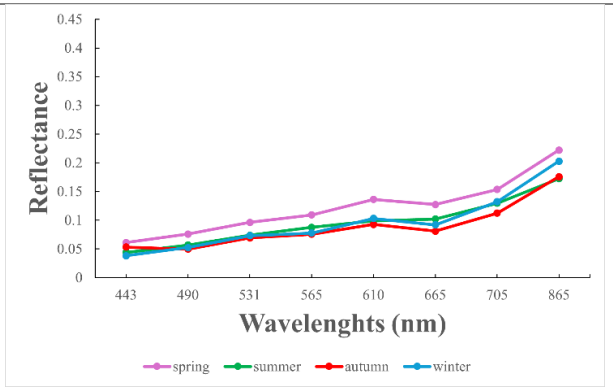
Sarcocornia perennis		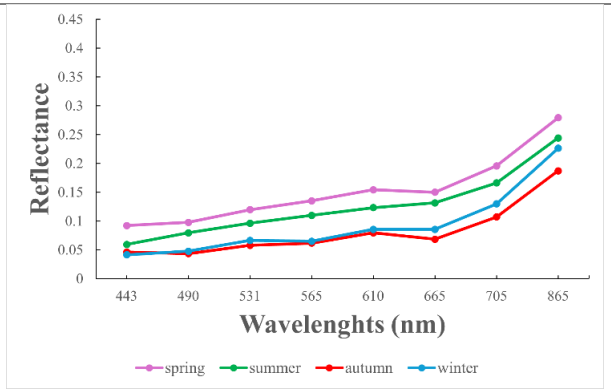

Spartina maritima		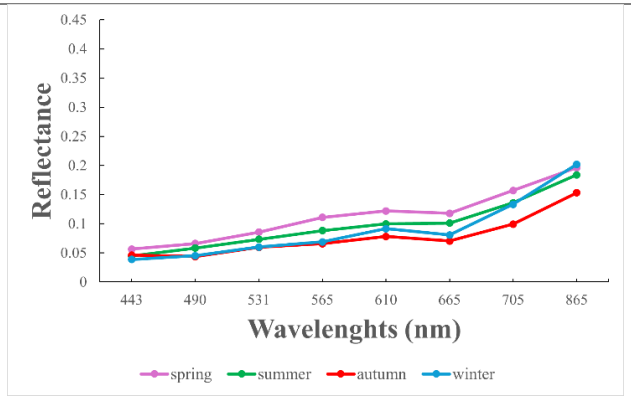
Halimione portucaloides		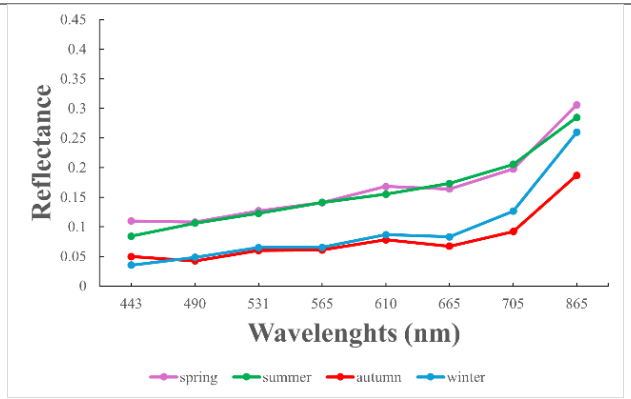

Ground**		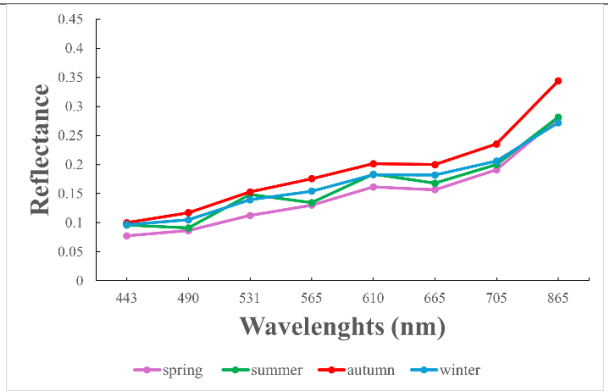
Atriplex halimus	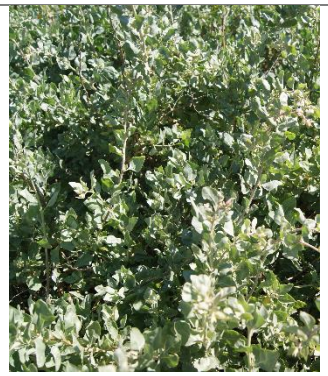	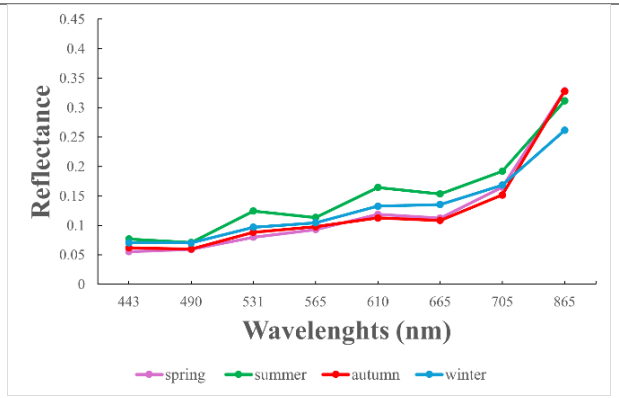

Salicornia ramosissima